INFLUENCE OF HUDSON BAY ON THE CARBON DYNAMICS OF THE HUDSON BAY LOWLANDS

KRISTINA DELIDJAKOVA

A THESIS SUBMITTED TO

THE FACULTY OF GRADUATE STUDIES

IN PARTIAL FULFILLMENT OF THE REQUIREMENTS

FOR THE DEGREE OF

MASTER OF SCIENCE

GRADUATE PROGRAM IN GEOGRAPHY

YORK UNIVERSITY

TORONTO, ONTARIO

OCTOBER, 2013

Abstract

This research serves as the first experimental study to assess the advective influence of Hudson Bay (HB) on the carbon dioxide dynamics of the Hudson Bay Lowlands (HBL). The HBL are extensive peatlands along the coast of HB, which sustains ice for most of the year, creating strong advective influence on the surrounding ecosystems. Changing synoptic-scale atmospheric variability under a warming climate has the potential to decrease the strength of the carbon sink in the HBL, by reducing the advective influence of HB. Its increasing ice-free season and decreasing onshore wind regimes will play a major role in the changing hydrologic, photosynthetic and ecological functioning of the adjacent ecosystems, which are likely to behave as carbon sources under such changes. These wind regime shifts and warming temperatures will increase ground heating, resulting in the degradation and aeration of permafrost soils. This, in turn, is expected to result in their enhanced melting and decomposition rates, creating a strong positive feedback process into the greenhouse gas effect.

ACKNOWLEDGEMENTS

I find it hard to believe that the time has come to write the Acknowledgments section. Thank you Dr. Bello for taking me on as a student in the first place, and believing that I can take on such a project. Your vast amount of knowledge and passion for all aspects of environmental science and the North motivated me throughout my entire degree and helped me appreciate the importance and need for research. Thank you for your patience, direction, inspiration and advice, which I will carry forward beyond this degree. Thank you Dr. Higuchi for being part of my supervisory committee and for your great interest in this project. Your insight, passion and dedication are reflected within these pages. Dr. Douglas Chan, thank you for taking interest and taking time to be part of my examining committee. Hopefully this will be worthwhile.

Without the support of Masaō Ashtine and Monica Vaswani, this experience would have been quite different. You were part of my mini graduate school family at York and gave me some of the best advice on both professional and personal levels. I hope that you remain my mini graduate school family well beyond this chapter of life. Thank you mom and dad for being understanding, supportive and being excited for me during these busy times. Last but not least, Jacob Kahan's encouragement was the reason why I am writing this now and not months later. He made sure I worked on my thesis and made no room for excuses, which was very difficult with a Netflix account.

In addition, I would like to acknowledge York University for providing the resources for this thesis and Northern Studies Training Program for providing the funding necessary to complete this project. Large amounts of the data presented here were collected by Bipin Pokharel and Sarah Verma.

TABLE OF CONTENTS

LIST OF FIGURES

$$y = y_0 + a * EXP(-0.5\left(\frac{ln\left(\frac{x}{x_0}\right)}{b}\right)^2)x$$

LIST OF TABLES

NOMENCLATURE

Symbol	Description	Units
C	Carbon	
HBL	Hudson Bay Lowlands	
EC	Eddy Covariance	
ER	Ecosystem Respiration	$\mu mol/m^2/s$
CH_4	Methane	$\mu mol/m^2/s$
H_2O	Water Vapour	$\mu mol/m^2/s$
CO_2	Carbon Dioxide	$\mu mol/m^2/s$
GDD	Growing Degree Days	
NEE	Net Ecosystem Exchange	$\mu mol/m^2/s$
PAR	Photosynthetically Active Radiation	$\mu mol/m^2/s$
E	Evaporation	mm
P	Precipitation	mm
Q*	Net Radiation	W/m^2
Q_E	Latent Heat Flux	W/m^2
Q_G	Ground Heat Flux	W/m^2
Q_H	Sensible Heat Flux	W/m^2
Rg	Incoming Solar Radiation	W/m^2
T	Air Temperature	°C
u_*	Friction Velocity	m/s
VPD	Vapour Pressure Deficit	kPa
T_{ref}	Reference temperature	°C
ER_{ref}	Respiration rate at reference temperature	$\mu mol/m^2/s$
T_0	Regression parameter	- 46.02 °C
E_0	Activation Energy	K

1.0 INTRODUCTION

1.1 Global Warming and Hudson Bay

The understanding of biochemical processes of different types of ecosystems, whether influenced by natural or anthropogenic forces, has been the central focus of micrometeorological studies. The concern over global warming has prompted such research to focus on the role of greenhouse gases on ecosystem balance and budgets. The solar radiative forcing at the top of the atmosphere drives the global climate system, which consists of myriad interactions between various components of the Earth. As a time average over a few years, the incoming solar and outgoing infrared radiative fluxes are in balance at the top of the atmosphere to maintain an average global temperature of 14.8°C (Oke, 1987). With increasing greenhouse gas concentrations (IPCC, 2012), some of the outgoing longwave energy emitted from the surface of the Earth is radiatively "trapped" and results in the warming of the atmosphere. Carbon dioxide (CO_2) in the atmosphere has been exponentially increasing since the start of the Industrial Revolution, and its trend is expected to go uncurtailed with the present state of economic growth and political focus (IPCC, 2012). Although oceanic and terrestrial ecosystems have been characterized as CO_2 sinks (Tans *et al.*, 1990), their role as such is uncertain in the future (Armentano and Menges, 1986). Thus, it is important to investigate the roles that these greenhouse gases play through a deeper understanding of the feedback processes involved in driving the climate system.

The ice-albedo and CO_2-peatland feedback processes are the main catalysts of the enhanced warming in northern regions. The continual and accelerated burning of fossil fuels and deforestation has released large amounts of CO_2 into the atmosphere, thereby warming

atmospheric temperatures. This, in turn, is contributing to melting of snow, ice and permafrost soils in the north, which results in the release of more greenhouse gases and more absorption of energy. In addition, changing vegetation structure due to changing climate will have an effect on the surface albedo, whereby taller and denser vegetation will result in lower albedo during winter and summer, resulting in an increased absorption of solar radiation. In this context, the role of Hudson Bay in climate moderation and ecological significance needs to be considered with respect to future warming in this region. It is a strong feature of central Canada and the low Arctic, as it exerts a substantial influence on the climate, energy balance and vegetative composition of adjacent areas (Rouse, 1991) through atmospheric and oceanic circulation systems. It acts as an extension of the Arctic Ocean into central parts of Canada and influences the length of the growing season due to the presence of ice on the western coast much of the year except for the period from late July to September when the Bay becomes ice-free (Danielson, 1969). The summer position of North America's Arctic Front is forced south by the cold Hudson Bay (Bryson, 1966), which generates persistent onshore summer winds and land-sea breezes that lower temperatures, increase fog and reduce evapotranspiration rates. The geographical situation of the world's peatlands at high latitudes makes them more prone to the effects of global warming than wetlands at lower latitudes (Roulet *et al.*, 1997; Tarnocai, 2006). The Hudson Bay Lowlands (HBL) are particularly susceptible to climate warming, as they extend far within mid-latitudes and are dependent on the presence of Hudson Bay and its arctic sea state. Northern regions are expected to undergo the greatest temperature increase as a result of global warming in comparison to the rest of the Earth (Schlesinger and Mitchell, 1987), raising critical questions as to exactly how the Arctic and Subarctic environments will respond.

Northern peatlands such as the HBL represent dynamic ecosystems which could play a dual role in the regional carbon budget. The HBL are unique in North America's high latitudes, in forming a very large area which is uniformly flat and very wet, classifying them as substantial carbon-storing peatlands. It is the second largest continuous peatland in the world, spanning 250,000 km^2 and comprising 25% of all of Canada's wetlands and contains about 25% of the world's soil organic carbon stock (Gorham, 1991). These wetlands include populations of tamarack and black spruce forests, sedges, grasses, shrubs, mosses and lichens, found over landcover types such as bog, fen, swamp, marsh and shallow open water (Desjardins *et al.,* 1994). The location of a wetland is related to regional climate controls on precipitation and evapotranspiration and is hence controlled by the water balance. The most important variable is the position of the water table because it controls the depths of the aerobic and anaerobic layers, and thus biomass productivity and decomposition, and ultimately the production rate of organic soils (Rouse, 2000). Peat accumulation occurs under conditions favouring litter input as opposed to litter output through enhanced carbon sequestration and low respiration rates (Gorham, 1991; Rouse, 1991; Vitt *et al.,* 2009). As a result, peatlands have low rates of decomposition which are maintained through cold temperatures that prolong the existence of permafrost (Clymo, 1998; Rouse, 2000; Corradi *et al.,* 2005; Moore *et al.,* 2007). As an annual average, the world's peatlands consume 28 g C m^{-2} yr^{-1} of atmospheric CO_2 (Gorham, 1991); the large amount of stored carbon will likely make a significant contribution to its continual release in the near future under climate warming. At least about 2% of the increases in atmospheric CO_2 observed in the last 100 years is attributable to the oxidation of peat from drained wetlands (Armentano and Menges, 1986) where litter outputs exceeded litter inputs. As permafrost begins to melt with increasing air temperatures, the impediment to water drainage by an otherwise frozen soil will be

removed, thereby lowering the water table to never before seen levels (Roulet, 1990; Eugster *et al.*, 2000). As a result of this better drainage, climate warming would be expected to result in changes in the vegetation composition, and more aerobic conditions within the peatlands, with warmer and drier soils and less ponded water.

Due to the above properties, peatlands are known to sequester large amounts of carbon within peat that is 3-4 m thick (Tans *et al.*, 1990; Ciais *et al.*, 1995; Griffis *et al.*, 2000; Aurela *et al.*, 2002; Corradi *et al.*, 2005; Roulet *et al.*, 2007; Cai *et al.,* 2010). However, as a result of the aforementioned feedback effects, subarctic wetlands are expected to undergo pronounced changes in climate (Tarnocai, 2006) and have the potential to become non-negligible carbon sources (Armaneto and Menges, 1986; Zimov *et al.*, 1999; Aurela *et al.*, 2002; Cai *et al.*, 2010). Even in their present state, some studies report northern peatlands as sources (Griffis *et al.*, 2000; Rouse *et al.*, 2002), which brings to question the amount of carbon they would release and how the vegetation structure may change under increasing temperatures. The southern boundaries of the continuous permafrost regions are most susceptible to climate warming, as regions that are overlain by air temperatures of more than 6°C and a mean ground temperature of around 0°C are more likely to rapidly respond to increasing temperatures (Woo *et al,.* 1992). Thus, wetland and peatland degradation is likely to occur in the near future as a result of an increase in the snow-free period and summer temperatures which will drive evapotranspiration rates higher and will dry up the water-logged wetlands (Rouse *et al.,* 1992; Eugster *et al.*, 2000; Rouse, 2000). Peatlands have the distinguishing physical features of extremely large water content when wet, and equally large air content when dry (Rouse, 2000), which makes them more vulnerable to increasing evapotranspiration rates. The frozen subsurface exerts a direct thermal regulation on wetland plants and impedes root development and drainage, thus promoting wetland and

peatland development, dominated by non-vascular plants. This plays a major role in their moisture and thermal regulation and feeds back to the plant-atmosphere system.

Rouse and Bello (1985) were the first to quantify the effect of Hudson Bay on the HBL in terms of its impact on ground heating, atmospheric warming and evaporation. They quantified the effects of Hudson Bay on the HBL through measurements obtained by three Bowen Ratio energy balance systems positioned at varying distances away from the Hudson Bay coast. They found significant differences in the energy balance partitioning between onshore and offshore wind regimes, whereby onshore regimes were characterized by enhanced sensible heat flux, and subdued latent and ground heat fluxes. Their results indicate that the sea ice present over Hudson Bay plays a major role in the partitioning of the available energy and is thus a potential, but not yet quantified, factor in evapotranspiration and photosynthesis. The study suggests that there would be a progressive shift from the frequency of onshore to offshore winds as a result of earlier sea ice melt. Due to this increase in the frequency of warm winds, the permafrost active layer will be melted earlier and deepened further, allowing for a longer growing season. With increasing air temperatures, and assuming no compensation in the form of rainfall, the greater evaporation due to higher temperatures would lead to the drying out of very shallow lakes earlier in the summer and a decrease in the surface moisture content of the ground. The permafrost active layer would thus be deepened owing to large ground heat flux early in the melt season, affecting human-made features, such as the railways and buildings. Subsequently, processes and ecosystems that are present at the current latitude of the HBL would be shifted to higher latitudes, placing such locations as Churchill, MB in a discontinuous permafrost zone and into the main boreal forest region. Since any long-term climate warming or cooling will have pronounced impact on the longevity of sea ice, it is useful to understand the interactions between

sea ice, the energy balance, air temperature and photosynthesis, in order to make scientific predictions of the likely impact on the landscape, particularly with respect to permafrost and vegetation.

Other studies have been conducted within the HBL that have applied both the Bowen Ratio energy balance and eddy covariance systems (Hamilton *et al.*, 1994; Burton *et al.*, 1996; Waddington and Roulet, 1996, Griffis *et al.*, 2000; Eaton et al., 2001; Griffis and Rouse, 2001; Lafleur and Humphreys, 2007; Roulet *et al.*, 2007). In addition, it is well known that the presence of Hudson Bay moderates the climate of the HBL through its southern extent of cold or frozen water (Danielson, 1969; Rouse, 1991; Gough and Leung, 2002; Rouse, 2000; Cai *et al.,* 2008) and that coastal areas in general play an important role in carbon sequestration (Borges *et al.,* 2005; Cai *et al.,* 2006). However, the advective influence of Hudson Bay on the carbon dioxide dynamics has not been investigated, while the Rouse and Bello (1985) investigation stands as the only such energy balance study for this region. In order to enhance our understanding of the possible shift in the impact of changing Hudson Bay under climate warming on the adjacent peatland formation, carbon and energy flux data from the ecosystems on the western coast of Hudson Bay have been analysed. The EC method was used to measure these fluxes to obtain a more accurate characterization of the ecosystem response to the presence and fluctuation of onshore and offshore wind dynamics and resultant temperature influences on the decomposition and growth processes. Under a changing climate, the vegetation structure is expected to change (Callaghan *et al.,* 2004), whereby mosses, lichens, vascular plants and shrubs will change in their abundance relative to each other. This shift is expected to have a direct influence on the permafrost soil and energy balance through changes in litter chemical properties, albedo, surface roughness and soil temperature.

1.2 Research Objectives

An Eddy Covariance (EC) system was set up near Churchill, MB and was operational from May 31 to September 18, 2007, as part of the Arcticnet Theme 3.2 campaign. The purpose of this study is to investigate the influence of onshore and offshore wind regimes on the rate of photosynthesis through the direct measurement of CO_2 fluxes and energy balance component fluxes. These results provide an estimate of the energy balance and net ecosystem exchange (NEE) of carbon dioxide between the atmosphere and the underlying peatlands. An assessment of the driving forces is made with respect to macro- and micro-meteorological drivers with a climate change perspective.

An additional objective in this research is to utilize the data from sampled plant cover around the EC tower in two ways. Firstly, to understand whether changes in photosynthesis and energy balance proportions between onshore and offshore wind regimes are due to the presence/absence of the advective influence of Hudson Bay or due to differences in the vegetation within the measured footprint. Secondly, to compare ecosystem photosynthesis with known plant cover proportions to individual plant group photosynthesis measured with a gas chamber from an adjacent peat plateau. Subsequently, the aim is to produce an analysis on what the influence of vascular plants is on the carbon dynamics of a non-vascular dominated polygon peat plateau.

The importance of northern wetlands in the global vegetation places them as a key component in the global carbon cycle. This study will contribute to the current knowledge by providing information on how peatland ecosystems function, how meso-scale wind regimes

affect NEE; what the impact of decreasing sea-ice of Hudson Bay is on regional terrestrial systems; what the influence of vascular plants is on the carbon dynamics as opposed to non-vascular plants. This would contribute to the existing limited knowledge of CO_2 and water vapour (H_2O) fluxes of the HBL with implications for understanding the multi-faceted climate system and how wetlands of central Canada might behave in the future with an ice-free Hudson Bay. Better comprehension of the turbulent surface-atmosphere flux and biological processes will also aid future climate scenarios to be produced with better accuracy and data accessibility. With projected increase in temperatures (IPCC, 2012), it is imperative to understand how climate change will influence the energy and carbon dynamics in the Hudson Bay Lowlands.

2.0 THEORETICAL BACKGROUND

2.1 The Greenhouse Effect

Greenhouse gases (GHG's) absorb reflected infrared radiation and radiate it back towards the earth's surface and atmosphere. This greenhouse effect is a naturally occurring phenomenon which helps keep the Earth warm enough to sustain the variety of life it hosts. CO_2, H_2O and methane (CH_4) are the most abundant GHG's residing in the atmosphere. However, with increasing anthropogenic activity due to fossil fuel combustion, urbanization and technological advancements, the concentration of GHG's has been increasing (IPCC, 2012), thereby contributing to the warming of the atmosphere. As a result of the exponential increase in the concentration of GHG's, the mean global annual temperature is expected to increase by up to 1.5°C by the end of the century (IPCC, 2012). Northern regions are expected to undergo the most pronounced warming, with expected rise in mean global annual temperatures of up to 5°C by the end of the century (ACIA, 2004).

There are two primary positive feedback processes that influence the physical and biological dynamics in the Arctic and Subarctic. The ice-albedo feedback process results from the melting of snow and ice, increasing the absorption of incoming solar radiation; this warms the atmosphere and further increases the rate of snow and ice melting (Oke, 1987). The second feedback effect is the biological CO_2-peatland feedback, whereby warming temperatures cause increased decomposition in northern peatlands, increasing the amount of CO_2 released into the atmosphere (Armenato and Menges, 1986). This results in an enhanced greenhouse gas effect, causing yet more increases in temperatures which would further warm the peatlands. As a result, northern biological systems are both affected by, and cause, climate warming; therefore,

measurements of land-atmosphere exchange of energy and gases within the Arctic regions require enhanced investigation, coupled with observed physiological processes.

2.1.1 Feedback Processes and Hudson Bay

Due to increasing climate warming, northern sea ice extent is decreasing, which leads to warmer temperatures in regions around Hudson Bay, which is currently frozen for most of the year (Etkin, 1991; Smith, 1998; Parkinson *et al.,* 1999; Gough *et al.*, 2004). As a consequence, a northward movement of the continuous permafrost and tree lines is expected, affecting the current photosynthetic regime (Tans *et al.*, 1990). There is a concern that northern ecosystems will experience a net loss of CO_2 to the atmosphere in response to high latitude warming (Armenato and Menges, 1986; Else *et al.,* 2008). This biological feedback process may further amplify the greenhouse effect, as these systems release more CO_2 into the atmosphere (Desjardins *et al.*, 1994). The issues presented above can be better explained through the ice-albedo and CO_2-peatland feedback effects. It was first discovered in 1949 that Hudson Bay completely freezes over for most of the year (Hare and Montgomery, 1949a; Hare and Montgomery, 1949b), which refuted previous claims that it remained an open water body. Due to the southward extent of this ice-covered water body, Hudson Bay has been characterized as one of the most anomalously cold places on Earth. The zone of continuous permafrost, the tree line and Arctic front boundary are pulled southward by the Bay, compared to what would normally be observed at higher latitudes (Rouse, 1991). This dominance of ice cover contributes to the 'winterization' of spring through the persistence of high albedo of approximately 80% (Rouse,

1991). The high albedo reduces the amount of energy that could have been used to warm the surface, for evaporation and for subsurface heating (Lafleur *et al.*, 1987; Rouse *et al.*, 1987; Rouse, 1991). However, with increasing temperatures as a result of climate change, the ice albedo will be reduced, thereby leaving more energy available for the aforementioned mechanisms. The energy partitioning that favours evaporation and ground heat flux is associated with the positive feedback process of CO_2-peatland. The CO_2 stored in peatlands is in the form of undecomposed organic matter due to high water table and low air and soil temperatures; upon its decomposition, peatlands will begin to respire more strongly and release more CO_2 into the atmosphere. The ice that is formed over Hudson Bay is essential to the maintenance of the existing northern ecosystems, as they depend on the persistence of high albedo and low energy regimes (Oke, 1987).

2.2 Carbon Dioxide Processes

In order to model how different wind regimes affect net photosynthesis, it is necessary to differentiate between carbon assimilation and respiration. Assimilation is the process by which plants remove CO_2 from the atmosphere in order to gain dry matter; the by-product is carbohydrates for plant food (Eq. 1) (Oke, 1987). Respiration refers to the mechanism through which organic compounds are oxidized through stomatal openings, to create the energy that is necessary to maintain basic plant functions; the by-product is CO_2 that is released into the atmosphere (Eq. 2). Respiration rates are independent of light availability and therefore take place over an entire diurnal cycle. Dark respiration transforms organic carbon within plant tissue

into CO_2 that is released back into the atmosphere or into the soil through roots. Soil respiration occurs through the decomposition of soil organic material that is broken down by bacteria, and is temperature dependent (Bonan, 2008). The photosynthetic uptake by vegetation can be expressed as:

$$CO_2 + H_2O + LIGHT \Rightarrow CH_2O + O_2 \quad (1)$$

where CH_2O is carbohydrates and O_2 is oxygen. The availability of water is an essential part of photosynthesis as plants require moisture to keep their turgor. When wilting begins to take place, stomata close in order to preserve the available moisture. This is an illustration of the balance that plants have to keep between opening stomata to maximize CO_2 intake and minimize water loss. Respiration can be expressed as:

$$CH_2O + O_2 \Rightarrow CO_2 + H_2O + ENERGY \quad (2)$$

In order to express the net rate of CO_2 assimilation, photosynthesis (or gross primary productivity, GPP) and ecosystem respiration (ER) can be written to represent NEE as (Oke, 1987):

$$NEE = GPP - ER \quad (3)$$

During the night, sunlight is not available to drive photosynthesis, which leaves ER unopposed by GPP; the result is a positive NEE (indicating CO_2 release into the atmosphere). With the

rising of the sun, light energy becomes available for carbon fixation into carbohydrates. Through this process of assimilating carbon during the day, plant biomass increases. Carbon is supplied by the atmosphere and the soil, which is uptaken by the stomata and the root systems, respectively. The stomata act as a control system for the uptake and release of carbon and water vapour, and is dependent on a variety of environmental variables and their combined factors. As the stomata open during the day to uptake CO_2, the openings expose the internal moist plant tissues, which release moisture into the atmosphere through transpiration. As a result, transpiration is an inevitable byproduct of GPP, the value of which is most often combined with evaporation to form evapotranspiration (ET) (Oke, 1987).

As a control system of the plant, the stomata open and close in response to environmental factors to create a resistance between the inside of the leaf and the atmosphere, called stomatal resistance (r_{st}). This resistance decreases with increasing availability of light, as stomata open to capture more of it; the resistance takes on a U-shaped trend with increasing leaf temperature, as it drastically increases beyond an optimum temperature at which the leaf functions at a maximum efficiency; it increases with decreasing moisture availability; it slightly increases with increasing CO_2 concentration; and it decreases with increasing soil moisture (Oke, 1987). The environmental controls on r_{st} are reflected in the interplay between GPP and ER; their individual contribution to NEE is difficult to estimate due to their co-occurrence during the day, whereby open stomata and low resistance will result not only in increased GPP, but also in increased ER.

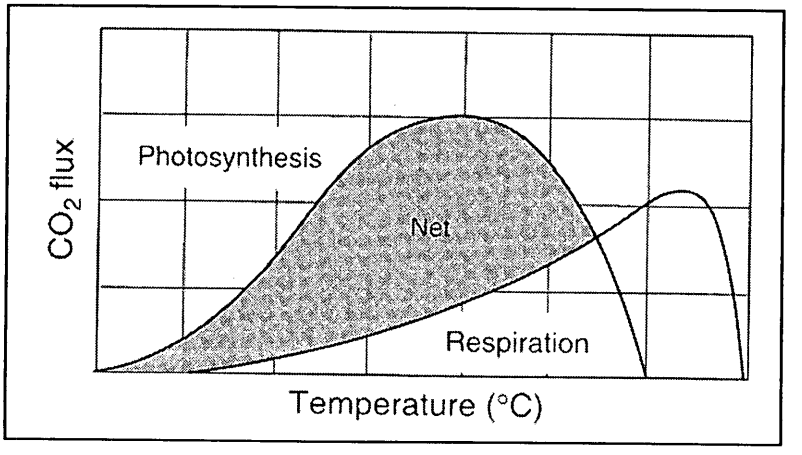

Figure 1. Characteristic rates of change of CO_2 flux with temperature for photosynthesis and respiration (from Bonan, 2008).

Air temperature, which is a controlling factor for leaf temperature, will be used as the independent variable upon which the relationship between GPP and ER will be modeled. From Fig. 1, the generic relationship between the two can be visualized, as both increase with increasing temperature. However, the rate at which each increases plays a crucial role in the determination of NEE (indicated as *Net* in the schematic). With initial rise in air temperature, GPP is expected to increase faster than ER; however, with subsequent rise in temperature, the rate of ER will surpass that of GPP, eventually transforming the ecosystem from a CO_2 sink to a CO_2 source. As temperature continues to rise, GPP diminishes, while ER peaks at a certain temperature before it drastically drops off. Using a well-established method by Lloyd and Taylor (1994), daytime ER can be estimated based on nighttime ER through the adoption of a temperature response model. With a known ER value for nighttime conditions and associated temperature, the relationship can be extrapolated for daytime temperatures to represent the daytime ER. Thus, ER can be written as an exponential regression model:

$$ER = ER_{ref} e^{\left[E_0\left(\frac{1}{T_{ref}-T_0}\right)-\left(\frac{1}{T-T_0}\right)\right]} \quad (4)$$

where ER_{ref} is the respiration rate at the reference temperature, T_{ref}, set to 10°C and T_0 is the regression parameter kept constant at -46.02°C as in the original model. The activation energy parameter, E_0, was determined for an optimal fit of the model to the data.

2.2.1 Peatland Vegetation

The presence of mosses and lichens in peatlands is prevalent and can comprise up to 50% of the land cover, as in our study area, whereas further inland they make up majority of the plant cover. The vascular plants that make up the other 50% tend to be smaller in size and concentrated close to the ground, similar to moss and lichen. Mosses and lichens are significant regulators of the soil thermal regime due to their insulating properties that help maintain the presence of permafrost by restricting of the active layer growth (Woo, 2012).

They are non-vascular plant species that have no stomatal openings and therefore do not transpire. Instead, only standing water is available for evaporation in addition to unrestricted moisture loss from the plants themselves (Woo, 2012). Although they do not have stomata and no stomatal resistance, they do have canopy resistance, which relies on the passive role of the canopy. This resistance controls the movement of water within the canopy to be made available for evaporation. The canopy of lichens is a good storage for water through small capillary openings and tunnels, restricting evaporation rates (Hayward and Clymo, 1983). However, unlike vascular plants, non-vascular plants peak in their GPP before solar noon, indicating that

moisture and/or heat stress results in their dessication (Swystun, 2011). Thus, non-vascular plants are important photosynthesizers in the morning when dew formation from the previous evening provides a short supply of moisture that lasts for few hours after sunrise. If water becomes available again during the day due to precipitation or high relative humidity (80-97% for lichens and 90% for mosses), photosynthesis will resume within minutes (Schreader, 1995). As a consequence, the photosynthetic regime of non-vascular plants may change rapidly during the day, depending on moisture availability.

Since mosses are not intense photosynthesizers, especially after any standing moisture has evaporated, increasing air temperatures tend to stimulate ER more effectively than GPP (Grogan and Chapin, 2000). Although global warming may result in higher GPP from vascular plants, mosses are important in peat formation and organic matter maintenance through its chemical properties that alter the soil chemistry. In addition, the high albedo of lichens reduces the ice-albedo positive feedback effect by reflecting a larger proportion of the incoming solar radiation back into space, in comparison to the dark-coloured vascular vegetation species. Thus, mosses and lichens are able to manipulate the environment to favour organic carbon accumulation, low energy regime, and shallow active layer.

2.3 Surface Radiation Budget

The surface radiation budget governs the energy state of the ecosystem through differing albedo and emissivity properties and the incoming solar radiation. The equation can be written as:

$$Q^* = (K\downarrow - K\uparrow) + (L\downarrow - L\uparrow) \quad (5)$$

where Q^* is the net all-wave radiation, $K\downarrow$ is the incoming shortwave radiation, $K\uparrow$ is the outgoing shortwave radiation, and $L\downarrow$ is the incoming longwave radiation, and $L\uparrow$ is the outgoing longwave radiation (Oke, 1987). $K\downarrow$ is the energy from sunlight and varies with time of day, time of year, atmospheric conditions and latitude. $K\uparrow$ is dependent on the amount of incident solar energy and the reflectivity of a surface or albedo ($\alpha = K\uparrow/K\downarrow$). Lightly coloured surface such as snow and ice have high values of albedo, thereby reflecting a major proportion of incoming solar radiation back into space, reducing the heating of the ground surface and atmosphere. $L\downarrow$ represents the infrared energy emitted by cloud and atmospheric constituents as well as objects such as trees and buildings that are only able to reemit energy in the longwave part of the spectrum. $L\uparrow$ is similar to $L\downarrow$ except for its direction pointed away from the earth's surface and atmosphere.

The surface energy balance governs the driving forces behind the vertical movements of heat, mass and momentum and is central to the study of micrometeorology (Oke, 1987). The energy balance equation can be written as:

$$Q^* = Q_G + Q_E + Q_H \quad (6)$$

where Q^* is the net all-wave radiation, Q_G is the ground heat flux, Q_E is the latent heat flux due to evaporation, and Q_H is the sensible heat flux due to convection, in W/m^2. The partitioning between the turbulent fluxes determines the atmospheric state of the atmosphere and the depth of

the boundary layer. Q^* is a function of the surface albedo, which is large when snow and ice are present, and rapidly decreases with their disappearance (Oke, 1987). Thus, under surface conditions dominated by the presence of high albedo, there is less energy available for the terms on the right hand side of the equation.

2.4 Micrometeorological Theory

2.4.1 Boundary Layers

It is important to understand the controlling factors and differences between the overlaying atmosphere in order to produce more accurate models of the source area of fluxes. The lower part of the troposphere can be broken down to include various types of layers with distinct characteristics. The *planetary boundary layer* (PBL), the height of which varies with the strength of surface-generated mixing and convective heating is generally investigated by micrometeorological studies. The turbulent nature of this layer is an important characteristic, which is generated by the frictional drag created as the overlaying atmosphere moves over the rough and varying surface, and the vertical movement of air parcels in eddying motion which carry with them heat and turbulence (Oke, 1987). It can be subdivided into two main components – the *outer (Ekman) layer* and *the inner (surface) layer* (Garratt, 1992). In the former, air flow is influenced by a balance between the Coriolis force and the pressure gradient, with very little influence from the frictional drag at the surface. In contrast, the inner layer is strongly influenced by the frictional force resulting from surface characteristics, with very little influence from the Coriolis force. This inner surface layer is of importance to micrometeorological measurements,

as one has to distinguish between its two sublayers – *inertial constant flux* and *roughness sublayers* (Fig. 2). Although the surface layer comprises the lowest 10% of the PBL, it is quite dynamic. The interfacial roughness sublayer (also canopy layer) is directly influenced by the surface properties directly underneath, such as shape, density and flexibility of the elements (Oke, 1987). Flow within this layer is highly irregular and has a thickness of roughly $3h$, where h is the height of the canopy. Within the inertial sublayer (also constant flux layer, turbulent surface layer), fluxes are constant with height and measurements representative of a larger fetch can be obtained. The properties for each layer discussed above are for homogenous surfaces with minimal variability of surface roughness and properties of the elements for a large fetch area. However, most surfaces of interest are heterogeneous in nature, and the production of *internal boundary layers* (IBL) needs to be considered with respect to measurement height and source area of the fluxes being studied (Garratt, 1992).

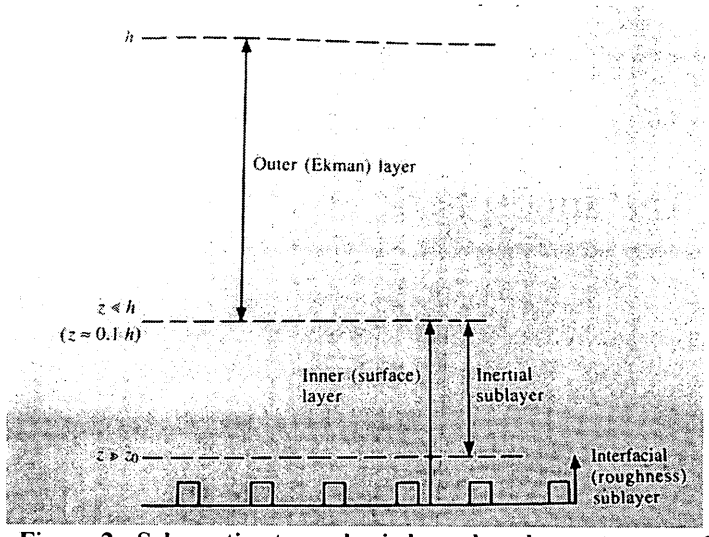

Figure 2: Schematic atmospheric boundary layer structure for aerodynamically rough flow in neutral conditions. (From Garratt, 1992)

In the natural environment, the surface is made of up patches of various elements that have unique internal properties. Each patch is characterized by its own thermal, radiative,

moisture and aerodynamic properties, resulting in differing energy and water balances. Due to these internal properties, each surface depending on its fetch will produce varying overlaying micro- and macro- climates, producing spatial discontinuities over the larger landscape (Oke, 1987). The influence surface heterogeneity on air flow is illustrated in Figure 3. The line of discontinuity between the two surfaces is called the *leading-edge*; as wind blows from left to right, the local climate of the surface on the left will cross the leading-edge and begin to be influenced by the new surface on the right side. This is due to the tendency of turbulence characteristics in the surface layer to be apt to blend with conditions of the underlying surface. Note that each surface has unique temperature, water vapour and roughness characteristics; thus, as the wind crosses the leading-edge, the overlaying air will begin to adjust to the new surface properties. This adjustment begins at the surface with the *fully adjusted boundary layer* (FABL) and diffuses upward into the *transition zone*. These two layers combine to produce the IBL, the properties of which have been influenced by the new surface and it grows with distance downwind. The FABL is in equilibrium with the new surface; the transition zone contains properties that are a mixture of both surfaces; and above the IBL, the properties are of the surface upwind. Thus, the portion of the surface that the instrument 'sees' will depend on where within these layers should the EC tower be located (Schmid and Oke, 1990) in relation to the desired scale of observation.

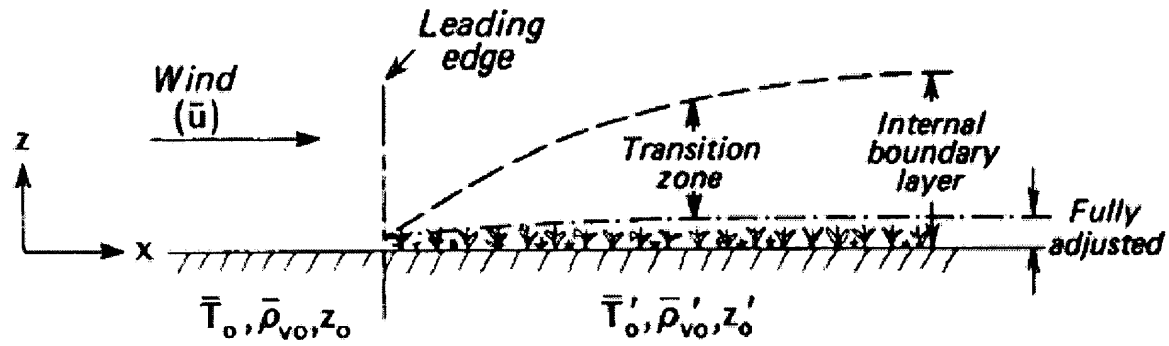

Figure 3: The development of an internal boundary layer as air flows over changing surfaces. (From Oke, 1987)

2.4.2 Scale, homogeneity, heterogeneity

The data obtained from a measurement site within each of the zones explained above will yield different results. This is because of the strong dependence of the source area on scale. Generally, a surface can be classified as homogenous if one views it from distant, small-scale perspective, resulting in the blending of smaller heterogeneous features in it. However, if the scale is increased to a large-scale, less of the surface area will be viewed, increasing the visibility of smaller heterogeneous elements that it contains. Thus, the influencing elements on the data obtained will differ depending on the scale measurement. To illustrate this using Figures 2 and 3, consider a case when measurements are taken within the roughness sublayer of the FABL for heterogeneous surfaces (for homogenous surfaces, this will parallel with the roughness layer within the surface layer from Figure 2). Within this roughness sublayer, the measurements obtained will reflect the properties of individual roughness elements; the fluxes and properties of these elements would not have blended together to a uniform mixture of their properties. Rather, the result will be stochastic and non-linear at this point, making the data interpretation difficult

due to its varying sources at this micro-scale. The surface will be sensed as heterogeneous and highly variable with respect to the horizontal location of the sensor.

Moving the sensor higher up into the FABL or *equilibrium layer* (Schmid and Oke, 1990), the measurements will show different results. At this point of measurement, the resultant data will reflect properties of the surface directly below the instrumentation; this will show an atmosphere that is fully in equilibrium with the surface immediately underneath. This means that the sensor 'sees' a homogenous patch of land that represents a uniform blend of the varying properties of the individual roughness elements beneath. Since the scale has changed, the resultant data will represent a different set of data. The FABL will continue to grow in depth with distance downwind, until a new patch is encountered with new surface properties. Thus, several FABL will develop overlaying one another, where each interface is developed over varying local regimes; this will result in different growth rates for each successive FABL, making computation of the flux source area more difficult. However, with the placement of the instrument within FABL at the site of interest, measurements can be obtained that are representative of the surface fetch, without going beyond the horizontal scale of interest.

If the instrument is brought even further up into the transition zone, the horizontal scale will increase accordingly, and the measurements will reflect the properties of surfaces some distance upwind as a blend with properties of the surface below. Thus measurements will once again become heterogeneous, as they do not represent any particular surface or particular elements; the decreased scale from larger to smaller results in the inclusion of more patches and elements, but it is not able to resolve them individually. If the intended scale of the study is as far-reaching as this, then the fetch requirements of an individual patch are no longer critical.

Above the transition zone at the top of the IBL, measurements taken at this height will represent a small-scale view of a homogenous large-scale source from a patch upwind of the patch directly below. However, at this height, the IBL developed as a result of each patch are decreasing in thickness due to the successive developments of more IBL's below. This means that precise placement of the sensor is difficult, especially due to the varying height of all boundary layers due to changing atmospheric stability. It can therefore be assumed that the IBL's are separated only up to a certain height. The height above the successive IBL's is termed the *blending height* (Garratt, 1992), in which mixing may be sufficient in order to produce horizontal homogeneity that is representative of a large spatial average. This means that the flux above this height is area-averaged and the properties near the surface are smoothed. The blending height will change position relative to atmospheric stability, which in turn will affect the footprint of the data, or what the instrument sees. This is summarized by Schmid (1997) for an EC system mounted at 30m above ground:

> *Thus, with small source areas (i.e. strongly unstable conditions) the blending height is high, and the surface layer is inhomogeneous up to more than 30m. With less buoyancy production, the 'field of view' of the instrument is increased and the measured values are representative of a larger area: depending on its definition, the blending height has then descended to below 30m and the measurements at 30m may be accepted as regional values (pg.196).*

This emphasizes the importance of stability consideration in relation to what is actually being measured. Difficulty arises when one aims to measure at one scale or the other – either the surface flux of a single patch with an appropriate fetch area at a local scale or an aggregated flux of multiple patches on a regional scale. Due to the high variability of flux concentrations over

heterogeneous terrain and their footprints of up to several kilometers, their parameterization and modeling is far from trivial and needs to be adequately addressed. In addition, theories, models and propositions need to be tested and applied to real world scenarios, such as for heterogeneous terrains.

2.4.3 General Site Requirements – Source Areas

The theory behind the EC approach is based on the assumption that measurements are made over extensive homogenous surfaces with stationary conditions and within the constant flux layer. It is expected that within the overlaying air, the surface drag, heat and water vapour fluxes are in equilibrium with their vertical profiles. Although the theoretical framework for micrometeorological measurements depends on this assumption, extensive homogeneity is hardly ever achieved. Most natural and anthropogenic landscapes have varying physical attributes with space, time and scale. Thus, turbulence characteristics over heterogeneous surfaces do not remain in equilibrium with the immediate underlying surface, but are rather influenced by a land surface some distance upstream of the point of measurement. The area from which the flux originates from can be referred to as the source area or flux footprint. The extent of the flux footprint is dependent on measurement height, characteristics of the surrounding terrain and atmospheric stability. Various combinations of these influencing factors will produce a footprint of various scales, as the structure and height of the mixed layer and IBL change in relation to the static measurement height.

The requirements that have to be met when using the EC method are stationarity of the measured data, fully developed turbulent conditions to ensure that the sensor is within the

surface layer, mean vertical wind speed to equal to zero, and no horizontal advection during an averaging period, usually 30 minutes (Gockede *et al.*, 2004). However, these requirements are often violated due to the unavoidable heterogeneity of most land surfaces that are encountered for study. The flux *footprint* can be defined as the influential area of the upwind properties that a sensor measures. In other words, the footprint of the turbulent flux being measured defines the spatio-temporal context of that flux. Footprint functions help to assess how representative the measurements are at a given location, through point-to-area representation. A complex function arises in order to determine the area influencing the measured flux, which depends on the height of observation, surface roughness, canopy structure, wind speed and direction, turbulence intensity and atmospheric stability (Horst and Weil, 1992; Schmid, 2002; Vesala *et al.*, 2008).

With a *fetch*, defined as the windward distance from a measuring point to a change in its surface properties (Foken, 2008), that is extensive and homogenous, modeling the flux footprint is not of high priority due to the assumption and reassurance that the measured flux originates from an area within the extensive fetch. However, when heterogeneity is encountered, estimating the flux footprint become quite complex, necessitating extensive numerical modeling. The problem of heterogeneity for obtaining representative fluxes was first brought to attention by Pasquill (1972), who proposed the concept of *effective fetch* in patchy surfaces. His aim was to better understand and model the extent to which a local, point measurement of the turbulent characteristics is representative of the surrounding area of presumed fetch. He proposed a simple two-dimensional example of a sudden transition between two surfaces of different roughness characteristics with the junction (or leading-edge) positioned normal to the wind direction. Table 1 lists the crosswind and alongwind dimensions of the flux footprint as a function of sensor height, atmospheric stability and surface roughness, as presented in Pasquill's original paper.

The values presented clearly show the dependency of the flux footprint geometry on the presented parameters. From it, it can be concluded that the footprint increases with measurement height due to the positioning of the sensor beyond interfaces of evolving boundary layer properties and influences. Also, the footprint area increases with decreasing surface roughness, z_0, as mixing capability and turbulent generation decreases with smoother surfaces. In addition, the footprint area increases with increasing stability due to suppression of eddy production and mixing under strongly stable conditions.

Table 1: Influences of stability, instrument height and roughness on the flux footprint. (selected values from Pasquill, 1972)

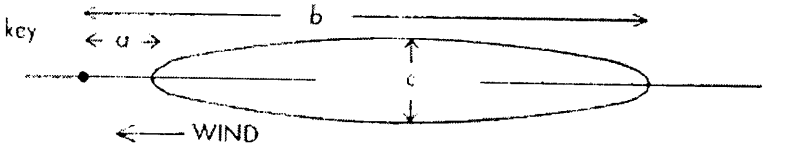

Height	Stability	Dimensions in km					
		Generally smooth z_o = 3 cm			Generally rough z_o = 1 m		
		a	*b*	*c*	*a*	*b*	*c*
50 m	neutral	0·6	2·8	0·4	0·3	1·5	0·2
	stable	5	40	6	2·9	28	3·4
	unstable	0·5	1·5	0·2	0·3	0·9	0·1
100 m	neutral	1·4	7	1	0·7	4·4	0·6
	stable	15	(270)	21	10	(150)	14
	unstable	0·8	3·2	0·5	0·5	2·1	0·3

The peak of the flux footprint occurs with minimal surface area for strongly convective conditions due to the expected high turbulent intensity. This facilitates the timely vertical transport of atmospheric constituents, minimizing the horizontal distance they need travel before being carried in the vertical direction by turbulent eddies. In contrast to this, stable atmospheric

conditions do not have a strongly defined flux concentration peak, as it tails off more gradually in the upwind direction. Its area is several times larger than that under convective conditions, which means that the flux measured at the sensor location will represent a more spatially-averaged set of values.

2.5 Eddy Covariance Method

The theory and method behind eddy covariance is not new, but rather the result of fundamental research over the last century in the fields of fluid dynamics and microclimatology. Sir Osborne Reynolds, after whom the Reynolds Number is named, is recognized as the person who formulated the essential theory behind the EC method. He was able to build on the pre-existing experimental theory by Calude Luis Navier and later expanded by Sir Gabriel Stokes, who worked on the derivation of formulae on the steady motion of incompressible fluids and on fluid mechanics. The resultant equations dealt with the case of fluids exposed to stresses and subjected to various rates of distortion; it was shown that these stresses are linearly related to the experienced rates of distortion (Reynolds, 1895). Although the theoretical assumptions were closely related to experimental results for fluids moving at low velocities through small-diameter tubes, the theory disintegrated when the experiment involved fluids moving at high velocities through large-diameter tubes. Stokes was able to show, with the help of previous equations by Navier, that this discrepancy was caused by the presence of eddies, which distorted the laminar flow seen in the former experimental design. This resulted in the expression called the

Dissipation Function, named by Lord Rayleigh (Reynolds, 1895). Reynolds was able to compile the work done prior to his investigation and bring it to the forefront of the readers of *The Philosophical Transactions of the Royal Society*. He derived a number, now known as the Reynolds Number, which differentiated between the maintenance of sinuous motion and that of eddying motion. Essentially, it is the ratio of internal forces that are characteristic of the horizontal motion of the fluid, to the viscous forces that are generated by inter-molecular interaction (Monteith & Unsworth, 1990). Based on this, the onset of the turbulent boundary layer can be identified, for which the Reynolds decomposition formulae can be applied; it breaks down the turbulent flow properties by decomposing them into mean and instantaneous wind speeds (or deviations from the mean wind speed). The EC method measures these turbulent fluctuations to determine the net vertical movement of a material that moves between the surface and the atmosphere over some averaging period. However, as part of the conservation of energy law, for CO_2, "the conservation of mass states that the sum of the local time rate of change of the CO_2 mixing ratio, c , and advection is balanced by the sum of the flux divergence of CO_2 in the vertical, lateral and longitudinal directions and the biological source sink-strength" (Baldocchi, 2003). Due to this assumption, there are limitations and requirements that have to be taken into consideration when applying the EC theory; these can be summarized as (Burba and Anderson, 2010):

a) Measurements at a point can represent an upwind area
b) Measurements are done inside the boundary layer of interest
c) Fetch/footprint is adequate – fluxes are measured only at the area of interest
d) Flux if fully turbulent – most of the net vertical transfer is done by eddies
e) Terrain is horizontal and uniform; average fluctuation is zero; air density fluctuations, flow convergence and divergence are negligible

In order to determine the atmospheric stability to ensure that measurements are taken within the turbulent boundary layer (or constant flux layer), Lewis Richardson extended Reynolds' theory to tackle this problem (Richardson, 1920). The Richardson Number can be expressed as the ratio of potential to kinetic energy, or buoyant to mechanical turbulence. Thus, it characterizes the atmosphere as stable, unstable or neutral (Oke, 1987). This is an important expression of stability for the EC technique, as the measurement could be erroneous under strongly stable conditions due to the suppression of vertical eddy transport. Under such conditions, the air is too stable to allow for eddies to freely travel and exist inside, whereas unstable conditions facilitate eddy formation and vertical transport (Richardson, 1920). Later, the Monin-Obukhov Length scale, which describes the height above which buoyant mixing is non-existent (Monin and Obukhov, 1954), becomes an important concept; it is defined as the quantitative descriptor of the turbulent structure of the stratified boundary layer (Arya, 2001). This length is proportional to the thickness of the dynamical sublayer, or mixed layer, which is ideal for EC measurements (Foken, 2006).

The increasing concern surrounding global warming has prompted a large number of scientific studies to direct their energy and resources towards the estimation of carbon budgets and carbon fluxes. The eddy covariance technique has proved useful for such research, as it is able to directly measure carbon and water vapour fluxes from a large contributing fetch area over a long period of time. In addition, the application of the eddy covariance technique has expanded into the measurement of heterogeneous and complex surfaces, as opposed to its intended use of short-term measurements over a flat and homogenous natural terrain.

The EC method relies upon the rapid measurement of three-dimensional wind speeds in correlation with the vertical flux of a given gas, most commonly CO_2, H_2O and CH_4. The density

of gas (mmol/m^3) is measured by a gas analyzer by accounting for the number of molecules transferred by a volume of air through eddies in the vertical plane in correlation with vertical wind speed (m/s). Thus, if the humidity, temperature and concentration of each moving air parcel can be correlated with the corresponding vertical wind speed, the flux can be obtained. The formulae that defines the core of the EC method can be expressed as

$$F = \bar{\rho}_a \overline{w's'} \tag{7}$$

where F is the flux of a substance given as a density, $\bar{\rho}_a$ is the air density (mmol$_{gas}$/m^3), $\overline{w'}$ is the vertical wind speed fluctuation component (m/s), and $\overline{s'}$ is the mixing ratio $\frac{g_{gas}}{g_{dry\ air}}$; note that the overbar denotes an average, and the accent denotes a fluctuation from the average (Burba and Anderson, 2010). This form of the equation can be extended to calculate the Q_H, the Q_E, the CO_2 fluxes and other trace gases. Most commonly, measurements of these gases in correlation with fluctuations of vertical wind speed are recorded at a frequency of 10 or 20 Hz; however, in order to make the large amount of output data more manageable, fluxes are recorded as 30-minute time averages.

3.0 METHODS

3.1 Field site description

The study was conducted at an elevated peat plateau, 20 km ESE of Churchill, Manitoba (58° 43' 46.240"N, 093° 49' 57.839"W) and approximately 5 km south of the Hudson Bay shoreline (Fig. 4). It is underlain by continuous permafrost, characterized as a northern wetland due to the presence of water table near the ground surface. The average active layer is between 25-45 cm deep, with a peat depth of continuous permafrost 3-4 m thick (Riley, 2011). Peat plateaus have relatively flat tops that favour the persistence of lichens and are segregated by ice wedges between individual peat mounds or polygons (Woo, 2012). They are similar to fens in vegetation cover except for the overwhelming presence of lichens on the raised parts. The location is just north of the treeline, which diminishes northward and coastward. Within 5-50 km of the shoreline there are sparse trees that represent a vague tree line, whereas surrounding the study site, there are mostly tamarack, white spruce and larch. Shrubs such as birch and willow are also common at the study site. The surrounding area includes an agglomeration of lichens, mosses and vascular plants growing in a well-drained upland environment called a peat plateau, of which the bog moss Sphagnum is one of the more abundant non-vascular species for peatland environments (Hayward and Clymo 1982). The vegetation of the peat plateau consists mainly of *Ericacrea* such as *Ledum* decumbens, *Rubus* chamaemorus, *Empetrum* nigrum, different mosses (e.g. *Dicranum* sp.) and lichens (e.g. *Cladina* sp.).

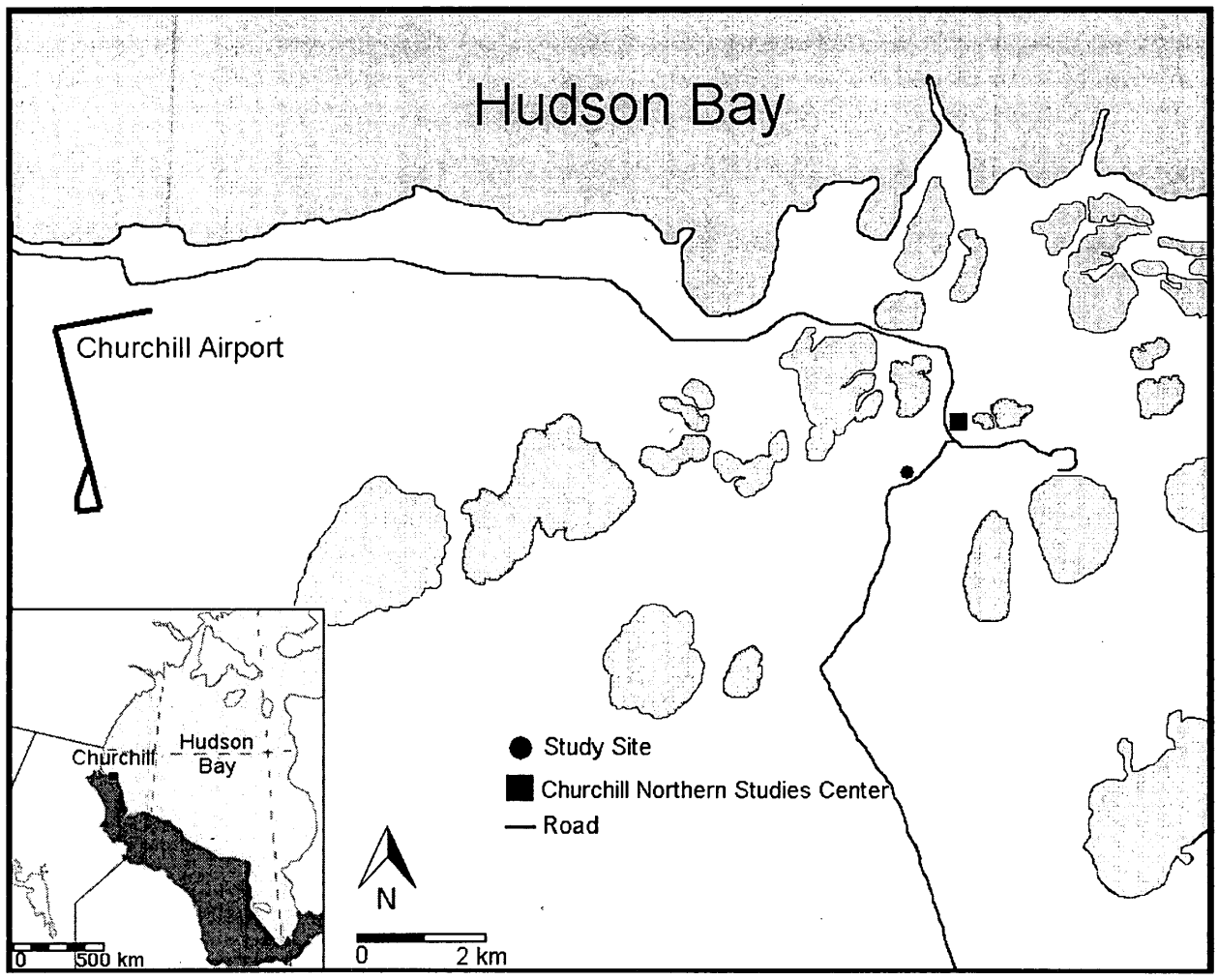

Figure 4. Map of study location, near Churchill, Manitoba and within the Hudson Bay Lowlands.

Vegetation sampling took place during the peak biomass season in the HBL in mid-July during the 2012 field season for an area of 32 km^2. It was conducted to determine the extent to which changes in the vegetation cover may be responsible for changes in the CO_2 flux as wind direction shifted, as well as to quantify how the plant cover photosynthesizes. The vegetation classes of interest are lichens, mosses, vascular plants (dominated by heath species), cloudberry (*Rubus chamaemorus*, an herb) and bare land. Although the cloudberry is a vascular plant, its dominance during the peak biomass season renders its placement in the overstory category, as it

reaches its peak biomass much later than other vascular plants. The sampled vegetation cover is shown Table 2, with measured percent cover for both understory and overstory plant cover groups. The radial distribution of both understory and overstory plant cover groups is shown in Figure 5. It represents the directional distribution of each plant cover with respect to onshore and offshore wind direction.

Table 2. Sampled plant cover for understory and overstory vegetation cover, expressed as percent cover.

Plant Cover	Percent Cover
Understory	
Vascular	47.8
Lichen	25.4
Moss	23.2
Pond	1.0
Rock	2.7
Overstory	
Cloudberry	13.6
Birch	2.1
Willow	4.0
Evergreen	1.9

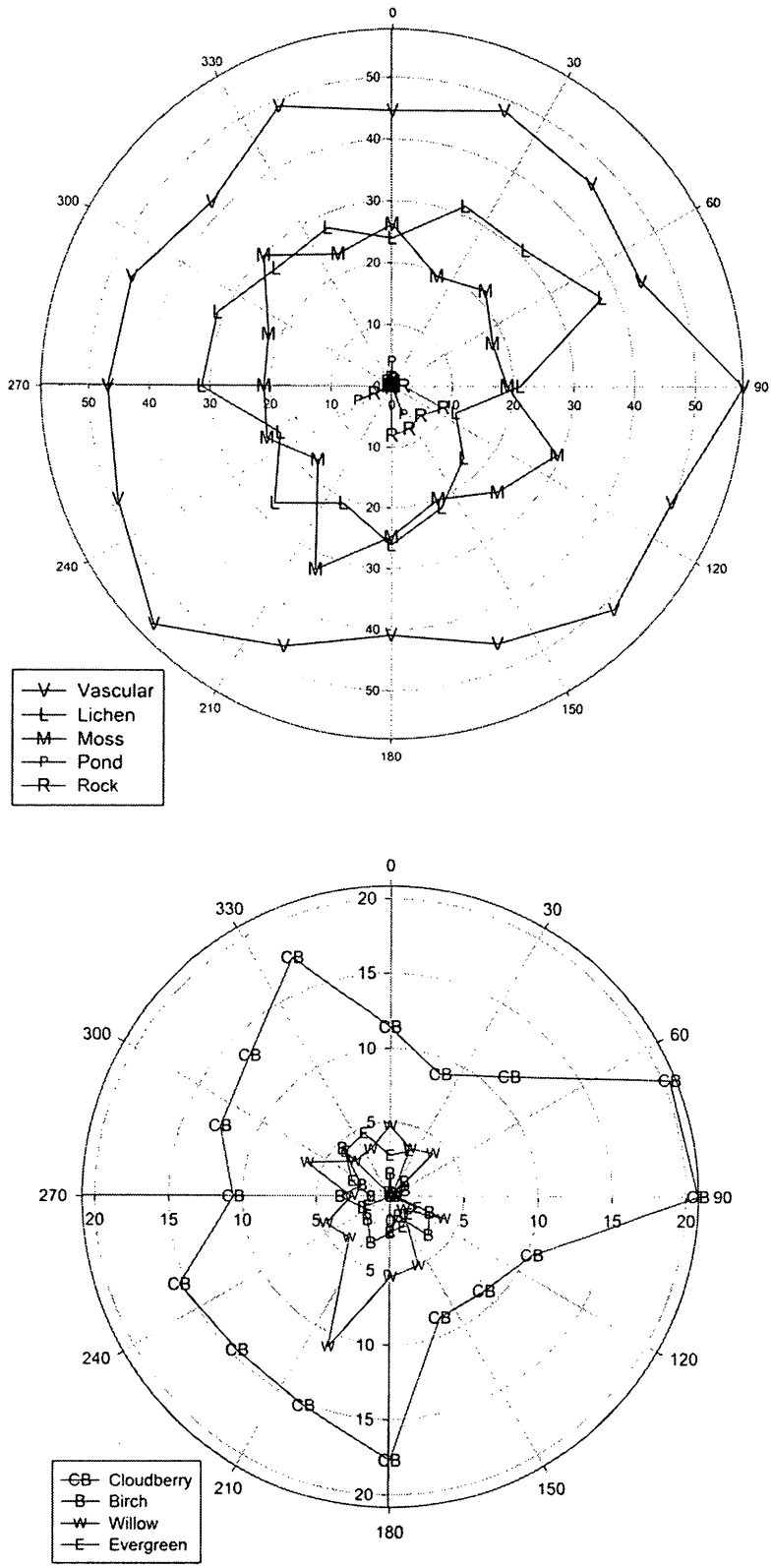

Figure 5. Directional distribution expressed as percent cover of (a) understory and (b) overstory plant cover groups, centered around the eddy covariance measurement tower.

3.2 Data Collection and Instruments

The eddy covariance technique was used to collect carbon dioxide and energy flux measurements in Churchill, Manitoba during 2007 (DOY 151-261). The displacement height was set to 0 m since the tundra peat plateau vegetation is concentrated near the ground. The surface roughness length is 0.02 m, while the overall average vegetation height is 0.04 m. The fast-response instruments were placed 1.49 m above the ground surface with a 160° offset to the east (Figure 6). The sonic anemometer was placed 14 cm north of the infrared gas analyzer (LI-7500), which is taken into account when computing the covariances. The CO_2 and H_2O concentrations are measured in molar density (mmol/m^3) by the instrument, which then have to be converted to a mixing ratio (Section 3.4.5). The ambient pressure is measured in kPa by LI-7500.

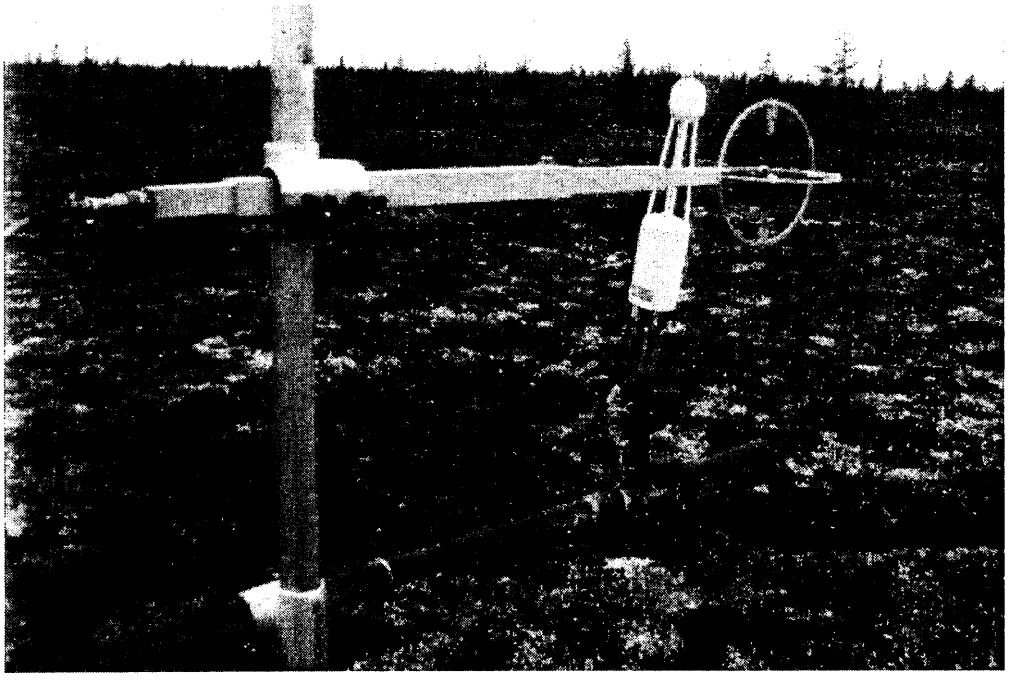

Figure 6. LI-7500 and ATI fast response instruments mounted on the 1.49 m tower.

3.2.1 Fast Response Instruments

The instrumentation included a V-style probe (V-Probe Ultrasonic, Applied Technologies, Inc., Longmont, CO) to measure wind speed in three orthogonal directions. It is able to capture small and large fluctuations in turbulent eddies as they pass through the pars of the ultrasonic transducers that make up the sonic head. The three pairs of transducers transmit and receive signals per pair in an x,y,z plane, or u,v,w, or alongwind, crosswind and vertically, respectively. By measuring the speed of sound in correlation with moving eddies, the sonic is able to measure velocity and sonic temperature. The sonic temperature does not take water vapour density into account, which has been corrected prior to data analysis. A median filter of 200 s, is used to produce a sampling rate of 20 Hz. The path length of each orthogonal axis is 10 cm, which is small enough to capture small-sized eddies that are common over peatland ecosystems. The anemometer was mounted 1.49 m above the ground surface on an arm extending 0.82 m due west at 265°. Due to the sea-breeze effect, the predominant wind directions at Churchill are either onshore or offshore, so pointing the arm due west minimizes any obstructions during both onshore and offshore wind regimes.

A separate arm extending in the same direction held the open-path infrared gas analyzed (IRGA), LI-7500 (LI-COR Biosciences, Lincoln, NE) to measure the scalar entities of CO_2 and H_2O. The LI-7500 is a fast-response and high-precision instrument that measures absolute molar densities of CO_2 and H_2O ($mmol/m^3$) in the eddies as they vertically pass through the optical path length of the instrument (12 cm). An infrared source within the instrument head is programmed to discharge a beam at high frequency, to be received by a detector at the other end

of the open air path length, which measures the absorption of the gas in question at a specific wavelength.

3.2.2 Slow Response Instruments

Slow response instrumentation was set up to complete the dataset necessary for analyzing the eddy covariance data. A net pyrradiometer (Middleton CN1) was placed on an adjacent tower at the same height, which measured the net radiation of the location Q* (W/m^2). It takes the incoming and outgoing all-wave radiation in order to compute the net value. A pyranometer (Epley PSP) was used to measure incoming solar radiation ($K\downarrow$ or R_g) (W/m^2). A soil heat flux plate (Middleton CN3) was buried at 2 cm below the ground surface to measure the substrate heat flux, Q_G (W/m^2). In addition, ten copper-constantan thermocouple wires were buried at depths 0.05, 0.10, 0.15, 0.20, 0.25, 0.30, 0.35, 0.45, 0.50 m to record vertical soil temperature profiles.

3.3 Operational Setup and Routine

The fast response instruments were connected to a Campbell Scientific CR3000 datalogger. During the first week of data collection, a 2GB Micro SD card was placed in the datalogger and data were transferred to a computer every three days. Following this type of data collection, a telemetry operation was set up between the study site and the nearby Churchill Northern Study Center. The latter method was constructed in order to accommodate the constant

inflow of large amounts of high frequency data that were produced. Two radio frequency modems were connected to two antennas at each end of the information transmission. Although a CR Basic program was written to produce time-averaged and corrected fluxes, the raw data (20 Hz) were processed using EddyPro 4.1.0 software (LI-COR Biosciences, Lincoln, NE) for this project. The slow-response instruments were connected to a Campbell Scientific CR7 data logger, sampled at every 5 seconds and logged at 30-minute intervals as per an internal CR Basic program. The power supply necessary to keep both systems running was generated using solar panels connected to two 12V car batteries.

3.4 Data Processing

The data were downloaded on an irregular basis, resulting in files with varying time stamps. Thus, the original TOA file formats were converted into TOB1 file formats using a LoggerNet extension in order to upload the files into LoggerNet. Then, using the Card Convert option, the files were separated into files of 30-minute time stamps, for a total of 2298 30-minute files. Having consistent time stamps, the TOB1 files were then uploaded into LI-COR's EddyPro 4.1.0 processing software. The analysis and corrections applied are shown in Table 3 and are explained below.

Table 3. Corrections applied to the high frequency data using EddyPro processing software.

Corrections and Analyses	Processing Method
Axis rotation for tilt correction	Planar fit, Wilczak *et al.*, 2001
Turbulent fluctuation detrend method	Block average
Time lags compensation	Covariance maximization with default
Compensation of density fluctuation	Webb *et al.*, 1980, (WPL)
Quality check flagging system	Foken, 2003 (1-9 system)
Footprint estimation	Schuepp *et al.*, 1990
Spectral correction – low frequency(high pass filtering)	Moncrieff *et al.*, 2004
Spectral correction – high frequency (low pass filtering)	Moncrieff *et al.*, 1997
Statistical Analysis (does not alter data)	Vickers & Mahrt, 1997

3.4.1 Metadata

The metadata parameters were directly entered into the software program. The flux averaging interval was set for 30 minutes, which is the more commonly used time. In addition, it serves as a balance between the capture of an improved spectra, by being long enough to capture large eddies and short enough to take small eddies into account. In addition, an ogive curve was plotted, which has the natural frequency on the x-axis and the cumulative measured flux on the y (power spectral density), and it has to level off. It was tested on a number of 30-minute periods and leveled off within the 30-minute averaging time, indicating that the majority of the fluxes were captured within 30 minutes.

3.4.2 Axis rotation for tilt correction

The high frequency data have been corrected for the sonic anemometer tilt with respect to the mean wind based on Wilczak *et al.* (2001). The sloping terrain, whether gentle or not, and the tilt of the sonic after placement will result in a non-zero mean vertical wind component, causing deviations from the EC theoretical requirements. It is highly improbable that the position of the sonic anemometer is exactly in line with local mean wind streamlines, and for this reason this rotation scheme is intended to virtually tilt the sonic and align it to the ground surface. Since micrometeorological theories and equations depend on the mass conservation equation for surface-air exchange studies, the data collection needs to satisfy this condition as well, and the vital component to getting to that stage is to align the sonic with the landscape being sampled (Lee *et al.,* 2004). When it was first proposed by Tanner and Thrutell (1969), only the vertical streamlines were considered worthy of correction, under the assumption that the field site has a completely flat terrain. The removal of these tilt errors is necessary in order to avoid cross-contamination among eddy flux vector components (Lee *et al.,* 2004). A double rotation (DR) aligns the x-axis (u) with respect to mean streamlines, but it also allows for y and z (v and w) to vary with respect to x, which produces an infinite amount of rotations that are possible (Wilczak *et al.,* 2001) (yaw and pitch angles – cross stream and vertical wind components over 30 minutes – the assumption is that they are equal to 0 over this 30-minute period). Then, McMillen (1988) proposed a triple rotation (TR), by also aligning the y and x axes to be rotated around the x axis until the cross-stream stress becomes zero (yaw, pitch and row angles). However, the TR method has been found to be prone to error (Kaimal and Finnigan, 1994; Wilczak *et al.,* 2001). For a planar fit (PF) correction, the mean streamline is computed over a long period, and the whole season was selected for the current study. Therefore, since many data runs are used to compute

the streamlines for the calculation, it is less susceptible to error, whereas the DR and TR methods use individual 30-minute files. In the PF method, the vertical wind component is allowed to vary around the zero mark without being forced to equal zero for individual 30-minute averaging periods. However, it averages out to zero over a longer period, which is chosen as the entire measurement period for the current project (Wilczak *et al.,* 2001). The DR and PF methods were tested against each other, and the PF method produced more reliable data than the DR by producing less bad flagged data.

3.4.3 Turbulent fluctuation Detrend Method

A detrending technique is applied in order to remove turbulent fluctuations from the dataset that are observed within an averaging period. At an ideal site, the flow field would be stationary over an averaging period, which means that there would not be an accumulation of a gas within the measurement volume (Law and Verma, 2004). Thus, we need to distinguish between active turbulent transport that can be categorized as a gas eddy flux, from the outside noise such as slower atmospheric motions and instrumental drift. The two detrending methods, block average and linear detrending, are considered to be more robust and more widely used (Law and Verma, 2004) than other methods such as running mean. When tested, the block average and linear detrending produced almost identical results in the total fluxes, which was reassuring. However, block average was chosen because it is the only one that follows the Reynold's decomposition, which is embedded in eddy covariance theory. It simply computes the average for a given period and removes the fluctuations by extrapolating the average for the whole period.

3.4.4 Compensation for Time Lags

To compensate for the time lags between the sonic and LI-7500, a correction needs to be applied to optimize the covariance between the fluxes. The covariance maximization with default was selected, which automatically finds and optimizes the covariance between the two instruments. In addition, this is a good option for changing wind regimes, which is the case for the study location.

3.4.5 Compensation for Density Fluctuation

In order to compensate for air density fluctuations, the Webb, Pearman, Leuning (WPL) method was applied. One of the more significant corrections for eddy covariance measurements was parameterized by Webb *et al.* (1980), more commonly known as the WPL correction for density effects. It investigates the effect on a constituent's density due to air expansion caused by heat and water vapour fluxes. The essence of this correction is to compensate for the effects of changing temperature and water vapour on the measured constituent, whether it is CO_2, H_2O or others. The mixing ratio, $'$, is required for the calculation of the constituent flux; however, gas analyzers measure the gas's density which is influenced by fluxes in temperature and water vapour. Thus, as a volume of air expands, a flux would be measured simply due to this air expansion as its top boundary reaches the equipment; also, once the parcel of air has expanded its CO_2 density will seem lower than for a parcel of smaller size at the same temperature. This WPL correction has been in strict use since it was first introduced and the method is applied to all flux measurements (Burba and Anderson, 2010).

3.4.6 Quality Check Flagging System

Although there exist other flagging methods, like Mauder and Foken (2004) (0-1-2 system) and Gockede *et al.* (2004) (1-5 system), the one chosen for the present study was Foken (2004) (1-9 system). In this system, classes 1-3 have high accuracy and can be used for theoretical research, classes up to 6 can be used for long-term research, classes 7-8 should be used with caution, and class 9 should be discarded. The flag placed on each 30-minute average is a representation of how well the application of all corrections has affected the data. Such quality tests are presented in order to validate the eddy covariance micrometeorological theory, such as steady-state conditions, homogenous land covers and developed turbulence. A steady-state test is performed by testing for stationarity of fluxes over different averaging periods (Foken and Wichura, 1996). In addition, the development of turbulence is considered when outputting a flag, where measured and modeled integral turbulence characteristics are compared.

3.4.7 Footprint Estimation

Although not an option in EddyPro, the Schuepp *et al.* (1990) formulation was manually integrated. It is an analytical solution of the flux footprint curve that takes into account different atmospheric conditions. The Schuepp model (10-18% uncertainty (Finn *et al.*, 1996), but at lower range for short towers as in this study) uses a height-integrated wind velocity, roughness characteristics and atmospheric stability in order to calculate the relative flux density measured at the tower.

3.4.8 Spectral Correction – Low Frequency (High Pass Filtering)

Turbulence transports gases over a large range of frequencies, which should ideally be captured. However, as a result of a finite averaging time, in this case 30 minutes, a correction to account for flux spectral losses needs to be applied (Finnigan *et al.,* 2003), to account for trends in the data such as instrumental drift and atmospheric changes (Moncrieff *et al.,* 2004). The error can be as high as 2.7% (Moncrieff *et al.,* 2004). Low frequency fluxes may need more than 30 minutes to be measured by the system. Ideally, the instruments should measure the entire spectrum of the flux, but also exclude intermittent large scale background variations (Moncrieff *et al.,* 2004), but low frequency eddies are difficult to distinguish from external noise (Sakai and Fitzjarrald, 2001). An ogive test can be performed by using the cumulative integral of the cospectrum of the turbulent flux over their natural frequencies (Desjardins *et al.,* 1989; Foken *et al.,* 1995). If the flux reaches its maximum value and the cumulative function levels off, the averaging period is sufficient and there is no additional flux beyond this period. The selected detrending method (block average) is used to perform the high pass filtering procedure, by subtracting the trends from the mean cospectra (Aubinet *et al.,* 2000). The flux attenuation (missing low frequency flux) is estimated by applying the high pass transfer function (block average) to the modeled flux cospectrum from the ogive curve

3.4.9 Spectral Correction – High Frequency (Low Pass Filtering)

The chosen method for high frequency spectral correction is based on Moncrieff *et al.* (1997), which describes flux attenuation due to instrument setup. The conventions after Moore

(1986) are followed for theoretical cospectra and transfer functions, and extended for the use of high frequency sensors. The physical separation (path length) between the anemometer and the gas analyzer results in a distortion of the cospectral shape of the frequency response characteristics. As a result, the resolution in time between the two high-frequency instruments needs to be corrected. All of these instrumentation issues increase the effective response time to capture high frequency fluxes, resulting in some loss of measured flux. The correction to compensate for this loss is done with the aid of transfer functions for wind velocity, flux, sensor separation, measuring path length and time constant (Foken, 2008). The loss of high frequency flux can be estimated by applying a low-pass transfer function to the estimated flux cospectrum, similarly to the low pass filtering.

3.5 Data Analysis

3.5.1 u_**Filtering*

Prior to processing this dataset, a u_* threshold for friction velocity was applied after Reichstein *et al.* (2005) in order to remove periods when non-turbulent conditions dominated. A 95% threshold was determined, whereby data were split into 6 temperature classes of the same size, and each temperature class was further split into 20 u* classes of increasing u_*. The u_* threshold was then defined as theu_* value beyond which the mean of u* was exceeded within 95%. The threshold was determined to be 0.082 m/s, so all data below this threshold were discarded and marked as missing in order to be subsequently gap-filled. Overall, 30% of all data

were considered missing due to instrument failure, weather conditions and flagged values, and when the data were screened for u_*, this increased to 34%.

3.5.2 Gap-Filling

The nighttime and missing data were gap-filled for calculating seasonal totals. The dataset was uploaded to an online gap-filling tool formulated by Max Planck Institute researchers, led by Markus Reichstein (http://www.bgc-jena.mpg.de/~MDIwork/eddyproc/). The method is based on Falge *et al.* (2001) with new formulations after Reichstein *et al.* (2005). Falge *et al.* (2001) reviewed two methods – mean diurnal variation (MDV), which replaces missing values with the mean for the same time of day derived from adjacent days, usually applying a 14-day window. However, this takes no account of day-to-day meteorological variations, so the look-up table is applied when meteorological data are accessible. Through this method, flux values can be looked up based on weather conditions similar to those observed for the missing periods, where the environmental variables are photosynthetically active radiation (PAR) or R_g, and vapour pressure deficit (VPD). Reichstein *et al.* (2005) applied a hybrid method by considering both the covariation of fluxes with available meteorological variables, as well as the temporal auto-correlation of the fluxes when meteorological variables are missing. Three different options are available for gap-filling, the best case scenario being that fluxes are missing but all associated meteorological data are available (R_g, T_{air}, VPD). In this case, the missing value is replaced by the average of those fluxes under similar weather conditions within a 7-day window; if none are found, the window increases as necessary. Similar meteorological conditions are defined when R_g, T_{air} and VPD do not deviate by more than 50 W/m^2, 2.5 °C and

5 hPa, respectively (Reichstein *et al.,* 2005). The second method is applied when only R_g is available, resulting in the definition of similar meteorological conditions dependent only on R_g within ±50 W/m2. Lastly, when all meteorological conditions are missing, MDV is applied.

3.5.3 Flux Partitioning

The EC method measures the total flux exchange between the ecosystem and the atmosphere, NEE, which is comprised of two contrasting components of photosynthesis and respiration by the formula, *NEE=ER-GPP*. The daytime ecosystem respiration is modeled by extrapolating nighttime respiration as a function of temperature (Lloyd and Taylor, 1994) (See Chapter 1.2.2). Air temperature was chosen for the independent variable as opposed to soil temperature, as the former is more spatially uniform throughout the sample footprint. Similarly to the gap-filling procedures, the non-turbulent conditions were removed and only the original, non-gap-filled data were used to derive the nighttime respiration model. This is because the turbulence is often suppressed at night, so only well-mixed conditions need to be used to derive the model. Once the nighttime model was constructed, it was extrapolated to daytime with known air temperature, resulting in ER values with the same temporal resolution as temperature (30-minute). Subsequently, GPP was calculated as the difference of NEE and ER.

3.5.4 Energy Balance Closure

In order to assess how the EC system performed, an energy balance closure was performed. This involves the ratio calculation between and inferred fluxes (Q_E+Q_H) and measured fluxes

(Q^*+Q_G). On average, the system underestimated the turbulent fluxes, which is expected with the use of the EC method. There was a distinction between onshore and offshore wind regimes, as the closure for onshore regimes was 87% and the closure for offshore regimes was 64%. The reason for this large difference and poor performance under offshore regimes is that they tend to occur at night or close to sunrise and sunset. This is a result of the sea-breeze effect associated with the presence of Hudson Bay.

4.0 INFLUENCE OF HUDSON BAY ON THE CARBON DYNAMICS OF HUDSON BAY LOWLANDS

4.1 Abstract

Northern peatlands and wetlands contain 30% of the world's soil organic carbon (C) within persistent waterlogged soil conditions that hinder the rate of decomposition and respiration. The stored C could potentially be released into the atmosphere due to rising temperatures and possible changes in precipitation regimes. Eddy covariance (EC) measurements have been made on an elevated peat plateau within the Hudson Bay Lowlands (HBL) near Churchill, MB (58° 43' 46"N, 93° 49' 57"W) during the growing season of 2007. The EC data were also used to derive an energy balance. The data were segregated based on onshore and offshore wind regimes to assess the advective influence of the generally cold and moist Hudson Bay air mass on the ecosystem in comparison to generally warm and dry continental air masses. With the use of a respiration model it was estimated that the HBL sequestered 26.96 $gC/m^2/year$ or 0.11% of the total anthropogenic global emissions. Daily average net ecosystem exchange (NEE) ranged from -0.23 $\mu mol/m^2/s$ in September to -5.55 $\mu mol/m^2/s$ in July. NEE was 27% stronger for onshore wind regimes when comparing the means of all half-hourly measurements. When normalized to PAR, GPP/PAR was found to be 26% stronger for offshore regimes, while ER/PAR was 71% stronger, suggesting a decreased role of GPP in the carbon budget when winds originate from offshore. A 4.15°C difference in seasonal air temperature was observed between the onshore and offshore regimes, with higher temperatures favouring the latter. Q_H/Q^* was almost twice as high for onshore than for offshore; Q_E/Q^* and Q_G/Q^* were both stronger for offshore regimes. Onshore and offshore NEE converged with increasing temperatures, attributed

to converging light level curves. With observed historical increases in offshore regimes, the ecosystem will behave as a weaker sink for CO_2 if the present patterns persist.

4.2 Introduction

The carbon (C) balance of northern ecosystems plays an important role in observed and projected climate warming. Although the photosynthetic rates for peatlands are relatively low, the total amount of C stored in them is approximately $450x10^9$ tgC, or about 30% of the global terrestrial C (Gorham, 1991; Smith *et al.*, 2004), as they represent strong C sinks in rich and slowly decomposing soils (Corradi *et al.*, 2005). The Hudson Bay Lowlands (HBL), off the west coast of Hudson Bay, are the second largest continuous peatlands in the world, spanning 250,000 km^2 and comprising 25% of Canada's wetlands (Riley, 2011). In the northern portion of the HBL in the Province of Manitoba, peat thickness reaches 4 m deep, with an overall average depth of about 1 m (Dredge and Mott, 2003). The strength of the C sink is a result of inhibited decomposition in anoxic soil conditions (Burton *et al.*, 1996; Cai *et al.*, 2010), as it has been accumulating at a long term average rate of 21 gC/m^2/year (Clymo *et al.*, 1998). However, projected climate warming will likely affect northern ecosystems stronger than any other parts of the globe, with measurable consequences on the growing season length, as well as on the hydrological and carbon cycles (Cess *et al.*, 1991, Rizzo and Wiken, 1992; Chapman and Walsh, 1993; Myneni *et al.*, 1997, Serreze *et al.*, 2000).

The amplification of the warming in the north is a result of positive feedback processes, most notably the surface albedo-surface temperature feedback, whereby increased air temperatures will result in the melting of snow and ice, which will further decrease the albedo,

and enhance warming through greater absorption of solar radiation at the surface (Cess *et al.*, 1991; Chapin *et al.*, 2005; Hinzman *et al.*, 2005). Another important positive feedback effect is from a prolonged thawing of carbon-rich permafrost soils, which could release stored organic carbon through microbial respiration in the form of carbon dioxide (CO_2) and methane (CH_4), depending on the water table depth. The carbon released under increasing temperatures further increases the greenhouse effect by contributing to the atmospheric CO_2 concentration (Armenato & Menges, 1986; Oechel *et al.*, 1993; Zimov *et al.*, 2006).

Although estimates are made for climate change prediction models through the interplay of feedback mechanisms, there still remain large uncertainties as to how particular ecosystems will respond to a warming climate (Callaghan *et al.*, 2004; Luo, 2007; Heimann & Reichstein, 2008), particularly in the north. Thus, it is important to quantify with additional field measurements the exchange of carbon dioxide between northern ecosystems and the atmosphere that will increase our understanding of their functioning under the predicted warming scenarios. Characterizing the drivers of the CO_2 exchange in Subarctic peatlands will further reveal the sensitivity of these active carbon sinks. In addition, warming temperatures have the potential to stimulate evaporation rates (Chapin *et al.*, 2005) and dry out substantial areas of wetlands (Chivers *et al.*, 2009). Peatlands are exceptionally vulnerable to drying out, as they have extremely large water contents when wet, and an equal amount of air content when dry (Rouse, 2000), which suggests that a sink-source threshold is easy to cross. The sensitivity of these ecosystems is still uncertain, as some studies report that they are sources (Griffis *et al.*, 2000; Rouse *et al.*, 2002), while others report them as sinks (Tans *et al.*, 1990; Griffis *et al.*, 2000; Aurela *et al.*, 2002; Roulet *et al.*, 2007; Cai et al., 2010). What is certain is that productive, peat-accumulating wetlands have the potential to become carbon sources under increasing air

temperatures, which will induce greater respiration (Armaneto & Menges, 1986; Oeochel & Billings 1992; Zimov *et al.*, 1999; Callaghan *et al.*, 2000; Aurela *et al.*, 2002; Dutta *et al.*, 2006; Cai *et al.*, 2010).

There have been a number of studies that have measured carbon fluxes in northern wetlands (Hamilton *et al.*, 1994; Burton *et al.*, 1996; Waddington & Roulet 1996, Griffis *et al.*, 2000; Roulet *et al.*, 2007), but the influence of Hudson Bay on these fluxes has not been investigated. Hudson Bay is a massive inland sea (3.9×10^9 km^2) which historically was completely free of ice only in September (Danielson, 1971). It is responsible for extending southward the range of Arctic flora and fauna, the continental treeline and permafrost into central Canada. The current rate of disappearance of sea-ice is 11% per decade since 1968 (Henry, 2011), resulting in the extension of the ice-free season which will impact its closely linked terrestrial environment. An energy balance study by Rouse & Bello (1985) concluded that there is a strong correlation between wind regimes and the energy balance of three different ecosystems, indicative of a strong advective influence of Hudson Bay, also confirmed by others (Lafleur & Rouse 1988; Rouse *et al.,* 1997). The current study serves as an extension to these findings to fill an important gap in our understanding of the advective influence of Hudson Bay on terrestrial carbon dynamics. It is expected that ER (ecosystem respiration) will increase with warmer temperatures, associated with offshore regimes, but the response of GPP (Gross Primary Productivity) to different wind regimes requires further investigation. Offshore wind regimes are associated with warmer and drier air, while onshore wind regimes are associated with cooler and wetter air.

This study addresses the gap in understanding the advective influence of Hudson Bay on the carbon dynamics of the HBL at an elevated peat plateau near Churchill, Manitoba, Canada.

The primary objectives are to (1) understand the environmental variables that influence the variability in Net Ecosystem Exchange (NEE), GPP and ER of a Subarctic peat plateau during the growing season in 2007; (2) quantify the advective influence of Hudson Bay on the CO_2 dynamics of the coastal peatlands through onshore and offshore wind analysis; (3) ensure that site heterogeneity bias is considered in flux computations for onshore and offshore directions.

4.3 Methods

4.3.1 *Study site description*

Measurements considered for this study were collected between May 31, 2007 and September 18, 2007 as part of the Arcticnet Theme 3.2 campaign. The study was conducted at an elevated peat plateau, 20 km east of Churchill, Manitoba (58° 43' 46"N, 093° 49' 57"E) and approximately 5 km south of the Hudson Bay coastline (Fig. 7) which runs east-west locally. The location is 17.5 m above sea level, while the ground gently slopes down towards the shore. Based on the elevation, it can be estimated that the mineral soils at the site emerged from Hudson Bay approximately 1600 years ago, based on a 0.01 m/year isostatic rebound rate (Stella *et al.*, 2007). The climate is subarctic with cold winters and large summer-winter temperature gradients. Mean annual temperature is -6.9 °C, and mean total precipitation is 431.6 mm. The lowest daily average temperatures occur in January (-26.7 °C), and the highest daily average is in July (12 °C) (Environment Canada, 2013). The peat layer is 1.5 m thick, while maximum active layer depths are 45 cm. The site is located approximately 80 km north of the continental treeline, with scattered trees such as *Larix laricina* (larch and tamarack) *and Picea glauca* (white spruce)

are present in low numbers locally with shrubs such as *Salix spp.* (willow) and *Betula glandulosa* (birch) common at larger distances away from the tower. The peat plateau comprises high center ice-wedge polygons dominated by mosses (*Dicranium elongatum, Tomenthyp numnitens, Aulocomnium spp.*) and lichens (*Cladina spp.*) as well as *Ericacae* notably *Rhododendron decumbens* (dwarf labrador tea), *Empetrum nigrum* (crowberry), *Vacinium vitis-ideae (low ground cranberry) and the herb Rubus chamaemorus* (cloudberry).

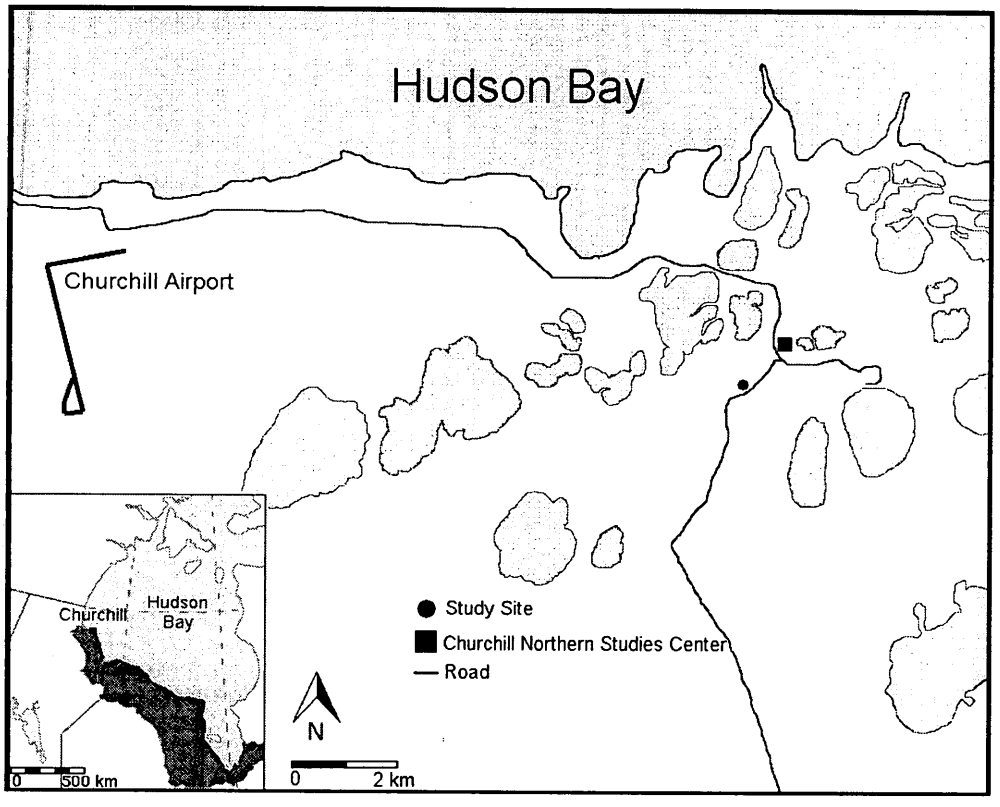

Figure 7. Map of tower location and surrounding water bodies. Small ponds have been omitted. Inset: Location of Churchill Manitoba near the northern limit of the Hudson Bay Lowlands (black).

In order to assess whether differences in the the plant cover between the onshore and offshore wind directions would have an influence on NEE measured at the tower, a detailed quadrat sampling was conducted. This was done for understory groups - vascular, lichen, moss, pond, rock- and overstory groups - cloudberry, birch, willow, evergreen (Table 4); cloudberry

was classified as overstory due to its late leafout in comparison to other vascular plants. The difference in how influental a plant cover group is for onshore and offshore regimes was devised using a weighted footprint analysis after Schuepp *et al.,* (1990). The results were statistically tested (Table 5) to ensure that the site asymmetry did not influence the differences in measured fluxes. Although plant cover proportions for north and south fetches were statistically different, they amounted to less than 4.5% percent in all cases, well within the closure accuracy of the flux system.

Table 4. Percent plant cover surrounding the EC tower within 100 m radius. Sampling methods are based on 50 cm quadrat sampling at 2 m intervals in 16 compass directions.

Plant Cover	Percent Cover
Understory	
Vascular	47.8
Lichen	25.4
Moss	23.2
Pond	1.0
Rock	2.7
Overstory	
Cloudberry	13.6
Birch	2.1
Willow	4.0
Evergreen	1.9

Table 5. Relative influence for four dominant plant covers (vascular, lichen, moss, cloudberry) computed for onshore and offshore wind directions. T-tests were performed, and a difference in magnitude is shown. Relative influence was computed using a weighted footprint model after Schuepp *et al.*, (1990). (* $p<0.05$; ** $p<0.01$, *** $p<0.001$).

		Relative Influence		Difference Magnitude
	Statistical Significance	Onshore	Offshore	
% Understory Vascular	*	33.12	32.51	1.02
% Understory Lichen	*	22.90	21.94	1.04
% Understory Moss	***	17.85	13.54	1.32
% Overstory Cloudberry	***	12.73	11.70	1.09

4.3.2 Instrumentation

The micrometeorological method of eddy covariance (EC) was applied to measure the turbulent fluxes of carbon dioxide, latent and sensible heat in the surface layer. It directly measures the vertical fluxes of scalar constituents in correlation with the vertical wind velocity. The system consists of two fast-response instruments; three-dimensional wind components were measured by an ultrasonic anemometer, model ATI-V style, (Applied Technologies, Inc.) logging the 20Hz median of u,v,w wind components sampled at 200 Hz; the mean concentrations of CO_2 and H_2O were logged at 20 Hz using an non-dispersive infrared gas analyzer (NDIR) sampling at 300Hz, model LI7500, (LI-COR Inc., Lincoln, NE, USA). Both instruments were mounted adjacent to each other separated by 12 cm, at a height of 1.49 m above the peat surface.

Data were logged to a datalogger (Campbell Scientific Inc., CR3000) using serial and SDM communications.

Slow-response ancillary data were collected to describe the meteorological conditions of the site every 30 minutes. A net pyrradiometer (Middleton CN1) was placed on an adjacent tower at the same height as the fast-response instruments, which measured the net radiation surrounding the tower as Q* (W/m^2). A pyranometer (Eppley PSP) measured incoming solar radiation as R_g (W/m^2); three soil heat flux plates (Middleton CN3) were placed at 2 cm below the surface as Q_G (W/m^2). The slow-response instruments were connected to a Campbell Scientific CR23x data logger. PPFD was acquired by applying a linear model to R_g (W/m^2) data. The linear model was developed from data collected at a nearby EC station.

4.3.3 Data Processing

The high frequency flux data were processed with the help of an open-source EC software, EddyPro 4.1.0 (LI-COR Biogeosciences, Lincoln, NE, USA). The eddy fluxes were calculated as the covariance between turbulent fluctuations in the vertical wind component and the scalar densities of CO_2 and H_2O using a time lag compensation for covariance optimization. The data were averaged over 30 minutes, derived from Reynolds block averaging for trend removal. The sonic anemometer was adjusted for tilt using the planar fit method (Wilczak *et al.*, 2001) by taking into account wind fields observed throughout the data collection period. A high-pass filtering for low frequency data loss was performed using a block average detrend method after Moncrieff *et al.*, (2004). A low-pass high frequency filter for data loss in the high frequency

range was performed after Moncrieff *et al.*, (1997), which accounts for lateral and longitudinal sensor separation, sensor time response, scalar and vector path averaging (Foken, 2008). The fluxes were corrected for the effect of temperature and humidity fluctuations in trace gas concentrations that were not part of the investigated flux, using the WPL correction (Webb *et al.*, 1980). Periods when less than 90% of the high frequency flux was unavailable were marked as missing values and addressed during the post-processing. The resultant 30-minute CO_2 fluxes represent NEE, or the balance between the total flux that entered the ecosystem (negative NEE) and the total flux that left the ecosystem (positive NEE).

4.3.4 Post Processing

The flux data were flagged using the 1-9 system after Foken (2003), which incorporates a steady-state, integral turbulence test, and horizontal advection tests. As advised, classes 7-9 have been removed from the dataset and marked as missing data, accounting for 6.9 % of the total data. Data loss due to adverse weather and instrument malfunctioning accounted for 16 % of the total data. Data loss due to data failing statistical analysis tests, performed after Vickers & Mahrt (1997), and after manual screening accounted for 7.3 %. Nighttime flux was removed using a u_* filter, resulting in a 4.9 % data loss for that reason. For the removal of periods under non-turbulent conditions, the u_* filter was used after Reichstein *et al.*, (2005). The method involves the binning of temperature values to produce 6 temperature classes, which are further subdivided into 20 u_* classes. The u_* threshold value was determined to be 0.082 m/s. The total data loss added up to 35.1%, which was gap-filled. A random error of ±0.12 μmol/m^2/s was estimated following Moncrieff *et al.*, (1996).

The gap-filling was done after Falge *et al.*, (2001) and modified by Reichstein *et al.*, (2005). Single 30-minute gaps were filled by linear interpolation (Falge *et al.*, 2001); larger gaps were filled using mean diurnal variation with a 14-day window that looks for the flux under similar atmospheric conditions (R_g, air temperature (°C, T), vapour pressure deficit (kPa, VPD)) (Reichstein *et al.*, 2005), which was the most consistent method based on 15 different methods analyzed by Moffat *et al.*, (2007). The gaps in the energy fluxes were filled in the same manner.

Since the EC method is only able to measure NEE, it is necessary to partition that into the two component fluxes that make up the total exchange – ER and GPP. The most common method is to employ nighttime respiration data as a function of air temperature and extrapolate that relationship to the daytime. The respiration has been modeled using an Arrhenius equation modified by Lloyd & Taylor (1994) as an exponential regression model:

$$ER = ER_{ref} e^{\left[E_0\left(\frac{1}{T_{ref}-T_0}\right)-\left(\frac{1}{T-T_0}\right)\right]} \quad (4)$$

where R_{ref} is the respiration rate at the reference temperature, T_{ref}, set to 10°C and T_0 is the regression parameter kept constant at -46.02°C as in the original model. The activation energy parameter, E_0, was determined to achieve the most optimal model fit.

4.3.5 Data Treatment

In order to better understand and quantify the effects of Hudson Bay on the HBL, the flux data were differentiated between onshore and offshore wind regimes. The study site is situated on a nearly perpendicular tangent with respect to the Hudson Bay shoreline, which runs east to

west. For this reason, winds originating from north of the east-west tangent were considered to be onshore winds; winds originating from south of the east-west tangent were considered to be offshore winds.

In order to assess how well the EC system performed, the energy balance closure was considered, calculated as the ratio of $(Q_H + Q_E)/(Q_G + Q^*)$. On average, the system underestimated the turbulent fluxes, but there was a difference between onshore and offshore regimes. During onshore regimes, the closure was 87%, while under offshore regimes it was 64%. The difference may be due to larger amount of nighttime hours occurring during offshore regimes, more stable atmosphere and large-scale synoptic-conditions that favour onshore regimes. The fluxes presented below have been compensated for the lack of energy balance closure.

4.4 Results

4.4.1 *Environmental Conditions*

During the measurement year of 2007, the mean daily air temperature was -9.9°C, slightly cooler than the climate normal of -6.9°C (Table 6). July experienced the highest mean temperature of 15.4°C, while September had the lowest mean temperature of 5.4°C. All historical mean temperatures are within 1 standard deviation of the observed mean monthly temperatures. The 2007 measurement year was drier than normal, with 337.5 mm of precipitation, compared to a 30-year average of 431.5 mm. The observed precipitation values

were 48.2, 30.22, 44.4 and 87.5 mm for June, July August and September, respectively. The historical averages are 44.3, 56, 68.3 and 63.47 mm for the same months, respectively. Thus, July and August were slightly drier and warmer than average.

The precipitation (P) and evaporation (E) patterns over the study period are shown in Fig. 8, during which evaporation exceeds precipitation for most of the season. For a two-week period from JD160 to JD 170, precipitation exceeds evaporation, associated with spring showers and lower temperatures that prevented strong evaporation rates. The daily evaporation rates decrease over the season and are especially low into September when the curve almost reaches a plateau, during which temperature is not an efficient driver. The total evaporation during the measurement period is 217.5 mm, while the total rainfall amounts to 193.44 mm, resulting in an evaporative efficiency (E/P) of 1.12, indicating a net loss of ecosystem water resources.

Table 6. Monthly precipitation (mm) and temperature (°C) for the study year of 2007 and historical average (HA) values. Bracketed terms show one standard deviation.

	June		July		August		September (until 18th)	
	2007	HA	2007	HA	2007	HA	2007	HA
Precipitation (mm)	48.2	44.3	30.22	56	44.4	68.3	70.6	63.4
T (°C)	5.9 (3.98)	6.6	15.4 (4.72)	12	12 (2.62)	11.7	5.4 (3.16)	5.6

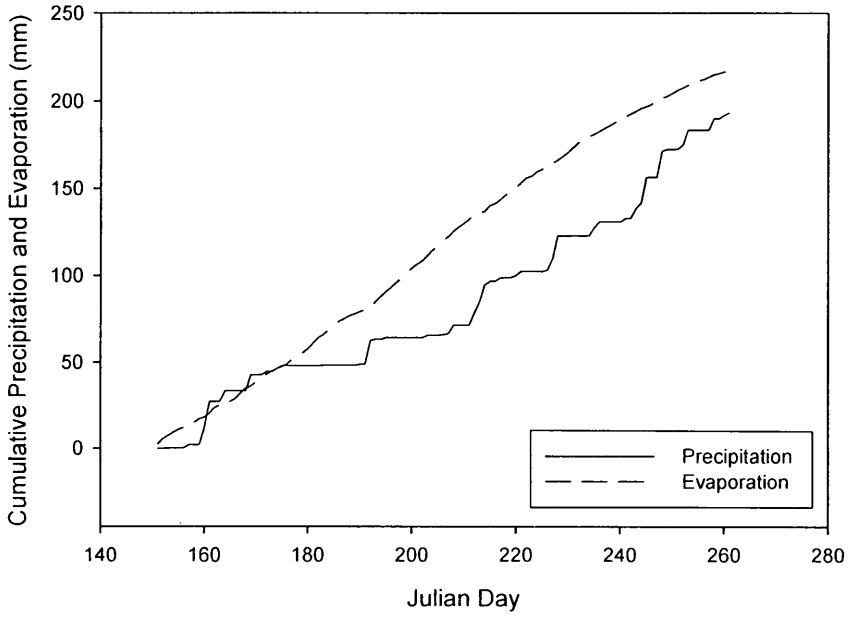

Figure 8. Cumulative precipitation and evaporation rates (mm) over the study period.

4.4.2 Temperature Regimes

The differences in meteorological conditions between the two wind regimes are most pronounced when looking at the temperature (Fig. 9). It is important to note the apparent difference in amplitude between on- and offshore regimes, where offshore regimes rise significantly during the day, while onshore temperatures do not show large deviations between day and night values. Overall, the diurnal pattern for the temperature change over the four months is the same for both wind regimes, but the magnitudes are different. In June, the onshore diurnal temperatures do not rise beyond 6°C, while the offshore temperatures hover around 10°C during the daytime hours. Both regimes experience a drastic increase in summer temperatures into July, where daytime highs average 16°C for onshore and 23°C for offshore; this is the month

that experiences the largest gap between onshore and offshore temperatures. Into August, both regimes cool, but offshore temperatures continue to be greater than onshore. September temperature patterns mimic those for June signifying the onset of rapid senescence. From these temperature curves, it is evident that the peak seasonal temperatures are captured within the measurement period, during which a majority of photosynthesis and respiration take place.

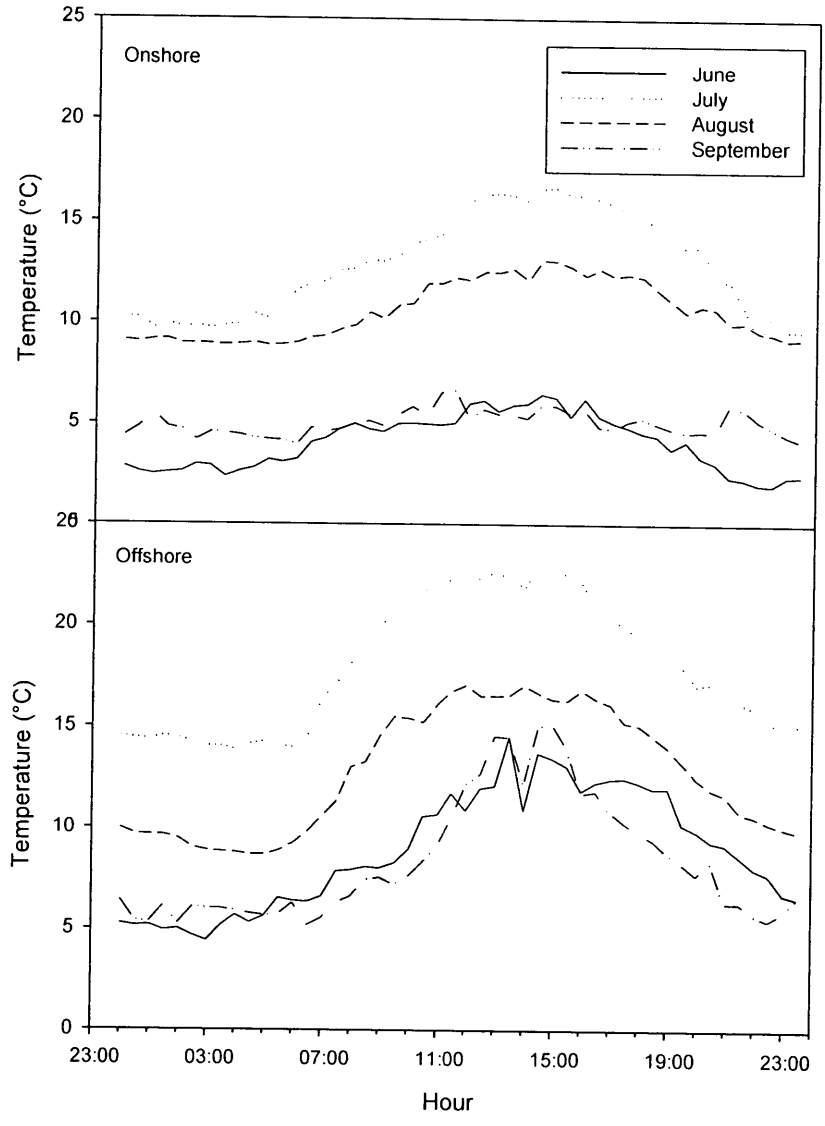

Figure 9. Mean monthly diurnal temperature curves for onshore and offshore wind regimes.

4.4.3 *Energy Balance*

The difference in the energy balance partitioning between onshore and offshore wind regimes throughout the season is shown in Fig. 10. The net radiation, Q* (W/m^2) is larger when winds are blowing offshore during the two coldest months, June and September, which are also the months when the temperature difference between onshore and offshore is most pronounced. The ground heat flux, Q_G (W/m^2), follows the same pattern as Q*, by being larger for offshore during June and September, but nearly equal or reversed during July and August. The sensible heat flux, Q_H (W/m^2), is generally higher for onshore than offshore wind regimes, except for September. There is a progressive decrease in Q_H over the four months, rather than a peak during July, at which time Q* and T experience their highest values. The latent heat flux, Q_E (W/m^2), is generally smaller for onshore regimes, except for the month of August.

Although patterns emerge when looking at mean diurnal values for the energy balance components, they do not represent the relative strength of each flux component with respect to the available energy. Table 7 shows the flux ratios of monthly means of Q_H/Q^* Q_E/Q^* and Q_G/Q^*. The ratios are derived from an average of all 30-minute measurement periods occurring in the onshore or the offshore directions for the given month, from June-September (until the September 18th). Q_E/Q^* does not show any significant differences between onshore and offshore for any month of the season, despite the pattern shown in Fig. 10 where offshore generally has larger values. Although not statistically significant, more energy goes into Q_E for the offshore values on a seasonal basis. The sensible heat flux ratio, Q_H/Q^*, shows the most consistent and strong significant difference in means between onshore and offshore regimes, favouring the former. Lastly, Q_G/Q^*tends to be stronger for the offshore wind regimes, and is significantly

different for July and August. As a seasonal average, Q_G/Q^* is statically different between onshore and offshore regimes, favouring the latter.

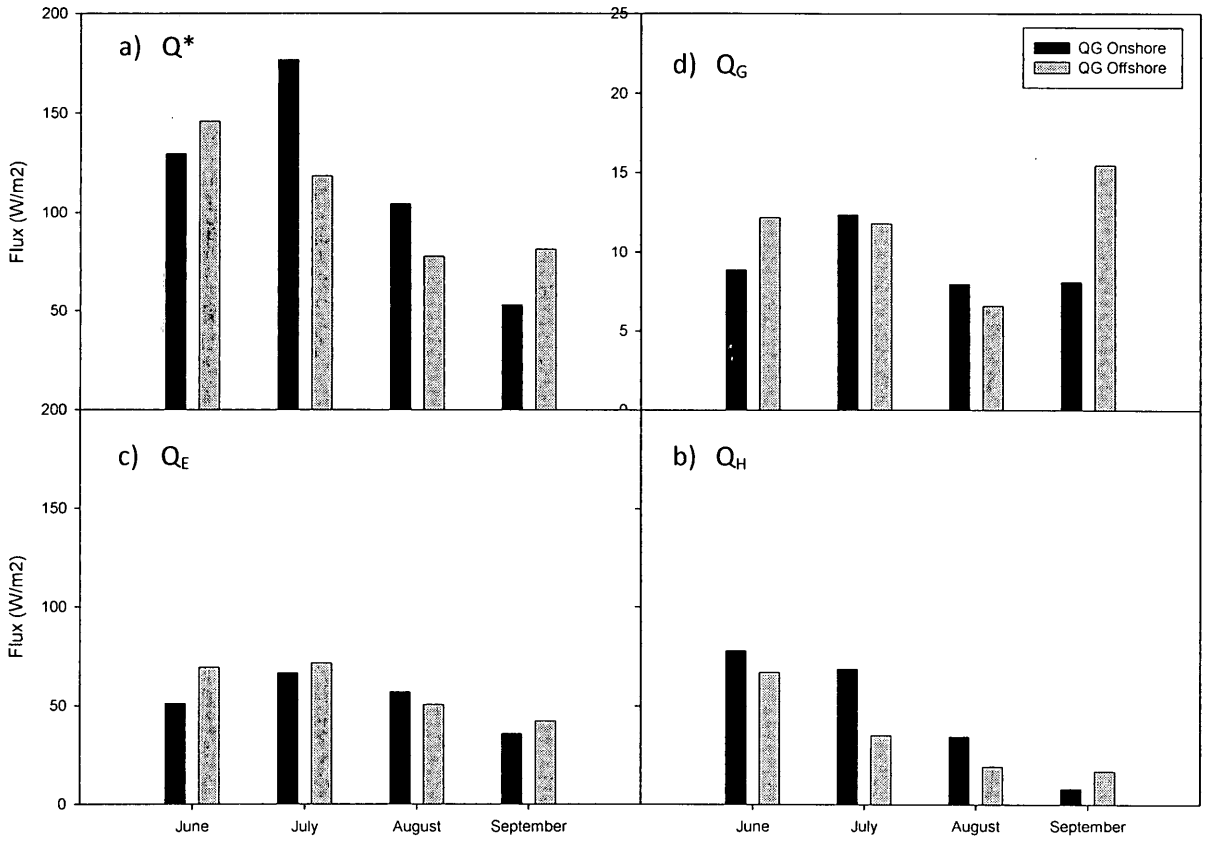

Figure 10. Mean monthly energy balance for onshore and offshore wind regimes. September values are calculated until September 18th. Note the different axis scale for Q_G.

Table 7. Energy balance components as proportions of net available energy for onshore (ON) and offshore (OFF) wind regimes for the four study months. SS-statistical significance. * P<0.05; ** P<0.01; *** P<0.001.

	Q_E/Q^*			Q_H/Q^*			Q_G/Q^*		
	ON	OFF	SS	ON	OFF	SS	ON	OFF	SS
June	0.46	0.41	-	0.61	0.44	**	0.05	0.05	-
July	0.49	0.58	-	0.45	0.23	***	0.09	0.17	**
August	0.61	0.63	-	0.28	0.11	**	0.10	0.13	*
September	0.69	0.40	-	0.11	0.38	*	0.12	0.26	-
Season	0.46	0.53	-	0.44	0.26	***	0.08	0.14	**

4.4.4 *Response of GPP, ER and NEE to Climatic Variables*

Daily average NEE during the four month period ranges from -0.23 μmol/m^2/s in the middle of September (JD 261), to -5.55 μmol/m^2/s towards the end of July (JD 207) (Fig. 11). The month of June begins with relatively strong NEE, around -1.5 μmol/m^2/s, and does not get stronger until the end of the month, after which it picks up quickly (after JD 171). Into September, NEE drastically decreases to rates lower than early June. The ecosystem was a consistent net sink for CO_2 throughout the measurement period, but much weaker into September. On a monthly basis, the largest uptake occurs in July (53.08 gC/m^2/month), while the lowest uptake (excluding September since data were available only until the 18^{th}) occurs in August (25.74 gC/m^2/month). Although GPP is larger for August (103.76 gC/m^2/month) than for June (78.70 gC/m^2/month), the total ER is substantially higher in August (78.02 gC/m^2/month) than in June (46.83 gC/m^2/month), mainly due to differing air temperatures and their effect on the active layer depth and soil respiration.

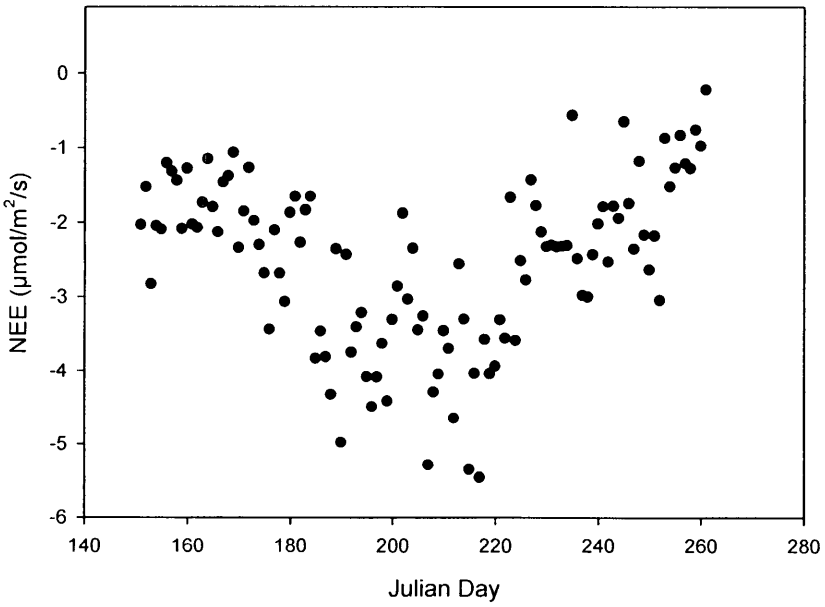

Figure 11. Seasonal daily average NEE.

The distinctiveness of the ecosystem functioning under opposing wind regimes is shown in Table 8, as mean monthly values for all 30-minute measurements within each wind regime, and associated t-test results (Table 8b). NEE is consistently larger for onshore regimes with statistically different results for all months except for September, with the largest difference occurring in July with 37% more uptake during onshore regimes. The ER values are always larger during offshore winds, with magnitudes 20% higher in August to 45% higher in June. The monthly average GPP varies over the summer, as it is higher for offshore regimes in June and September only. Over the whole measurement period, there is not a statistically significant difference in GPP between onshore and offshore regimes. The temperature difference between onshore and offshore is strong for all months, but enhanced for June when offshore T is 4.77°C higher. On average for the season, offshore T is 4.15°C higher than onshore, highlighting the importance of T differences between the regimes.

Since the ER, GPP and NEE values are monthly averages, they do not account for differences in the time of day between the onshore and offshore regimes, given the fact that onshore regimes occur more often during the day as a result of the sea breeze effect. The carbon fluxes have thus been normalized to photosynthetically active radiation levels (PAR, multiplied by 100 for easier interpretation), which reveals a different pattern (Table 8). The PAR-normalized GPP, GPP/PAR, is always stronger for offshore, up to 32% stronger in July. Similarly, ER is always stronger for offshore for a given light intensity, up to 91% stronger in July. In order to emphasize the interplay between GPP and ER, the ratio of the two, ER/GPP, describes how much of GPP is counteracted by ER. For all months and as a seasonal evaluation, ER/GPP is always stronger for offshore, which means that a larger proportion of NEE is fractioned into ER during offshore regimes than for onshore regimes. The ecosystem remained a net sink, except for September under offshore regimes, where ER is 28% larger than GPP. As a seasonal average, offshore ER/GPP is 67% higher than onshore ER/GPP.

Table 8. (a) Monthly and seasonal flux means and flux normalized to PAR for onshore and offshore wind regimes. (b) Ratios of offshore to onshore (OFF/ON) represent % difference with associated statistical test. SS-statistical significance. * P<0.05; ** P<0.01; *** P<0.001.

(a)	GPP ($\mu mol/m^2/s$)		ER ($\mu mol/m^2/s$)		NEE ($\mu mol/m^2/s$)		T (°C)		GPP/PAR		ER/PAR		ER/GPP	
	ON	OFF	ON	OFF	ON	OFF	ON	OFF	ON	OFF	ON	OFF	ON	OFF
June	3.69	4.17	1.53	2.21	-2.16	-1.91	4.93	9.70	0.73	0.80	0.46	0.57	0.53	0.63
July	7.29	7.02	3.31	4.31	-3.95	-2.49	14.39	19.46	1.28	1.69	0.83	1.58	0.55	0.78
August	6.35	5.83	2.82	3.40	-3.54	-2.47	11.66	14.59	1.20	1.58	0.74	1.33	0.56	0.93
September	3.58	4.17	1.75	2.48	-1.80	-1.55	5.28	9.58	1.15	1.19	0.82	1.15	0.71	1.28
Season	5.43	5.45	2.42	3.19	-3.00	-2.20	9.52	13.67	1.07	1.35	0.68	1.17	0.60	0.99

(b)	GPP ($\mu mol/m^2/s$)		ER ($\mu mol/m^2/s$)		NEE ($\mu mol/m^2/s$)		T (°C)		GPP/PAR		ER/PAR		ER/GPP	
	OFF/ ON Mean	SS	OFF/ ON Mean	SS	OFF/O N Mean	SS	°C higher for OFF	SS	OFF/ ON Mean	SS	OFF/ ON Mean	SS	OFF/ ON Mean	SS
June	1.13	***	1.45	***	0.88	*	4.77	***	1.09	-	1.26	**	1.18	***
July	0.96	-	1.30	***	0.63	***	5.07	***	1.32	***	1.91	***	1.43	***
August	0.92	**	1.20	***	0.70	***	2.93	***	1.31	***	1.80	***	1.65	**
September	1.16	-	1.42	***	0.86	-	4.30	***	1.04	-	1.40	***	1.81	**
Season	1.00	-	1.32	***	0.73	***	4.15	***	1.26	***	1.71	***	1.67	***

The light response curves for onshore and offshore (Fig. 12a) do not show much deviation from each other and are not significantly different (P>0.05). GPP tends to be slightly higher under offshore regimes below 1200 $\mu mol/m^2/s$ levels, but plateaus at high light levels and eventually drops just under the onshore curve. This suggests that light levels alone cannot be used to explain differences in the flux dynamics. However, a pronounced gap is observed for temperatures encountered for a given light level (Fig. 12b), revealing that offshore temperatures are consistently higher than onshore temperatures, except for very bright conditions that generally have much lower frequency.

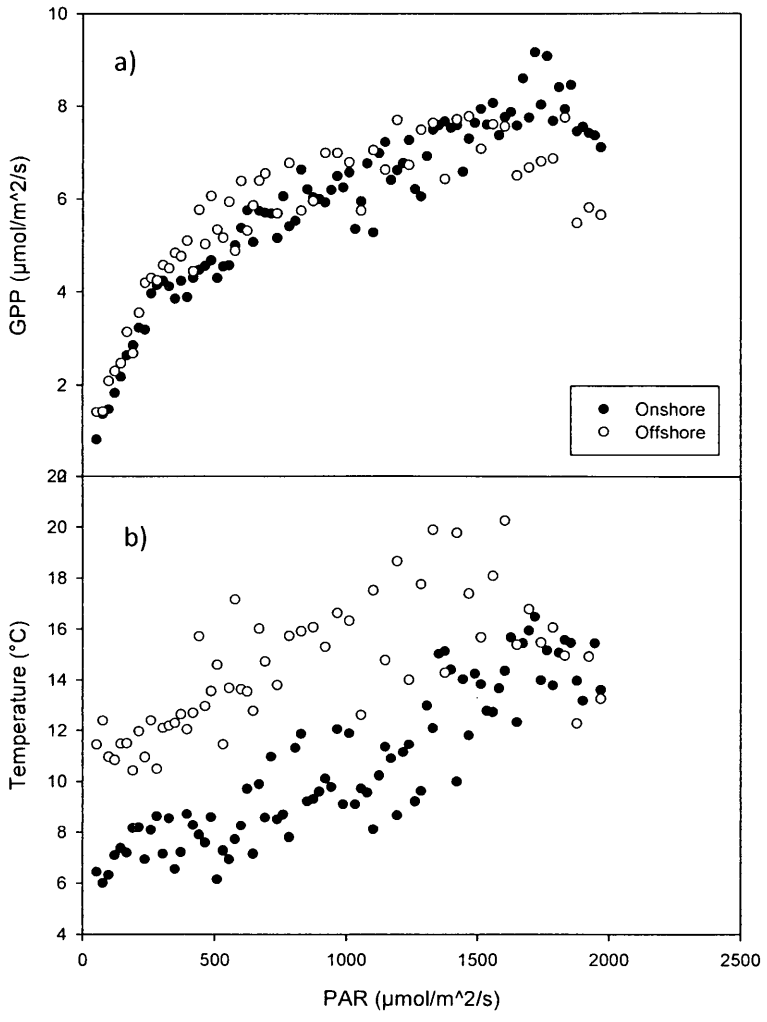

Figure 12. (a) Binned light response curve for GPP for onshore and offshore wind regimes ($p>0.05$). (b) Temperature response over binned light levels for onshore and offshore wind regimes ($p<0.001$).

The temperature influence on the carbon flux is shown graphically for binned air temperatures for onshore and offshore wind regimes (Fig. 13a,b). Exponential curves are fitted and extended to 0°C and to warmer temperatures to provide a rough and very approximate visual estimate of where the curves will intersect. The onshore GPP is consistently higher than the offshore GPP at a given temperature, but quickly drops off after 20°C as shown by the model (Fig. 13a). However, the offshore GPP has a gentler and smaller decrease after 20°C, resulting in

a projected rise up to roughly 30°C. The same curve intersects with the ER curve at 35°C, whereas the onshore curve intersects with ER at 28°C. The resultant NEE (Fig. 13b) shows a large difference between the onshore and offshore for a given temperature, where mid-temperatures (11-20 °C) have the highest difference in favour of onshore winds, coinciding with the highest frequency of occurrence. At higher temperatures, the two models intersect and the offshore regimes become an equally strong sink for CO_2 as are onshore winds.

Given that GPP values are different between onshore and offshore regimes for the same temperature, there are other environmental factors that influence the carbon flux. PAR tends to be larger for the onshore regimes at most temperatures (Fig. 14), producing larger GPP values, as the availability of sunlight results in higher photosynthetic rate for the onshore regimes. At the highest end of the temperature range, the onshore and offshore PAR curves converge, which is reflected in the corresponding convergence of GPP in Fig. 13a. In addition, the onshore VPD becomes higher with increasing temperatures, resulting in a negative effect on GPP, whereas the offshore VPD begins to drop at temperatures beyond 20°C, not restricting GPP (data not shown).

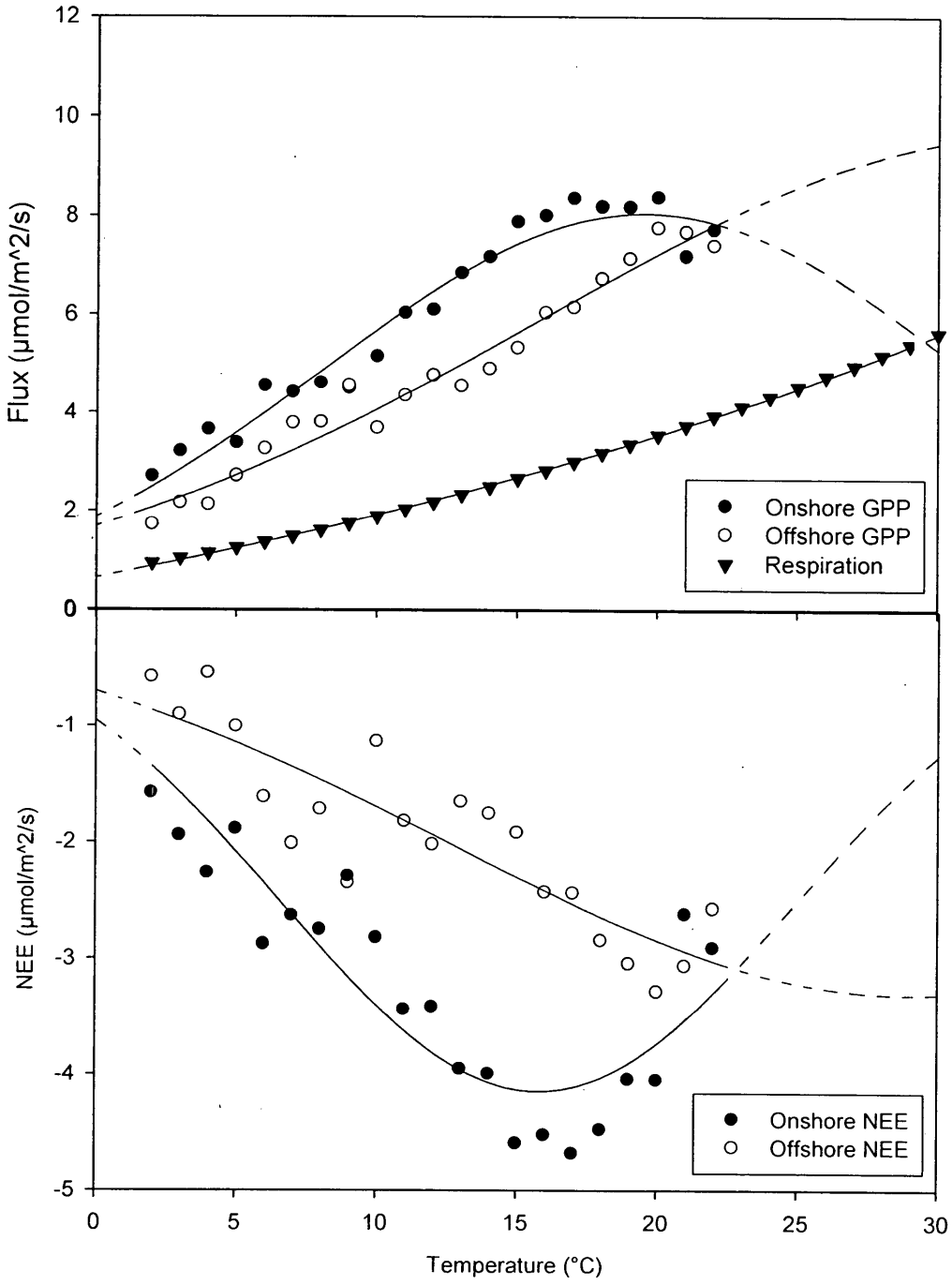

Figure 13. (a) Daytime GPP and R (Lloyd and Taylor (1974) model) curves for binned air temperatures for onshore and offshore regimes. ER estimates are based on the same model for both wind directions due to the same model that was used. (b) Daytime NEE curve for binned air temperatures for onshore and offshore wind regimes. All curved have been extrapolated to 0°C and 35°C.

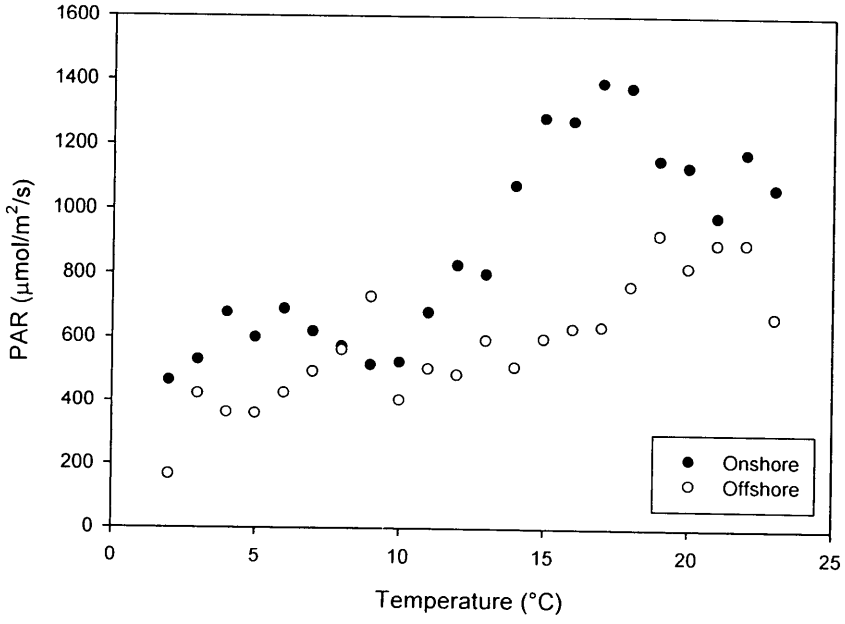

Figure 14. PAR over binned air temperatures for onshore and offshore regimes.

4.4.5 Seasonal Course of Fluxes

Although characteristic diurnal curves present a good picture of how the carbon fluxes vary by month, cumulative flux curves serve better the purpose of distinguishing between onshore and offshore contributions (Fig. 15). The fluxes have been binned for each half-hour during the diurnal cycle and then accumulated until the end of the cycle. Since ER is based on an exponential relationship with T, the differences in ER for onshore and offshore are only a function of T, so the temperature differences can also be deduced from these plots. At the start of the season in June, the cumulative curve for GPP is stronger for offshore beginning at sunrise as photosynthesis begins. However, the differences in ER are larger, where ER is higher for offshore as a consequence of higher temperatures, evident during all fourth months. Due to the

larger offshore ER, the NEE is stronger onshore, with a cumulative value of -54.18 μmol/m^2/s for onshore and -42.4 μmol/m^2/s for offshore. The pattern of GPP in July shows a near-identical cumulative GPP for onshore and offshore winds, translating into a larger difference in total NEE, with offshore fluxes of -53.22 μmol/m^2/s and onshore fluxes of -96.64 μmol/m^2/s. Into August, flux magnitudes begin to decrease and the strength of the sink becomes similar to that in June. September photosynthesis is drastically smaller than for August as plants are senescing. The offshore GPP is stronger, but so is ER with similar magnitudes, resulting in an almost identical NEE for offshore (-12.1 μmol/m^2/s) and onshore (-11.01 μmol/m^2/s).

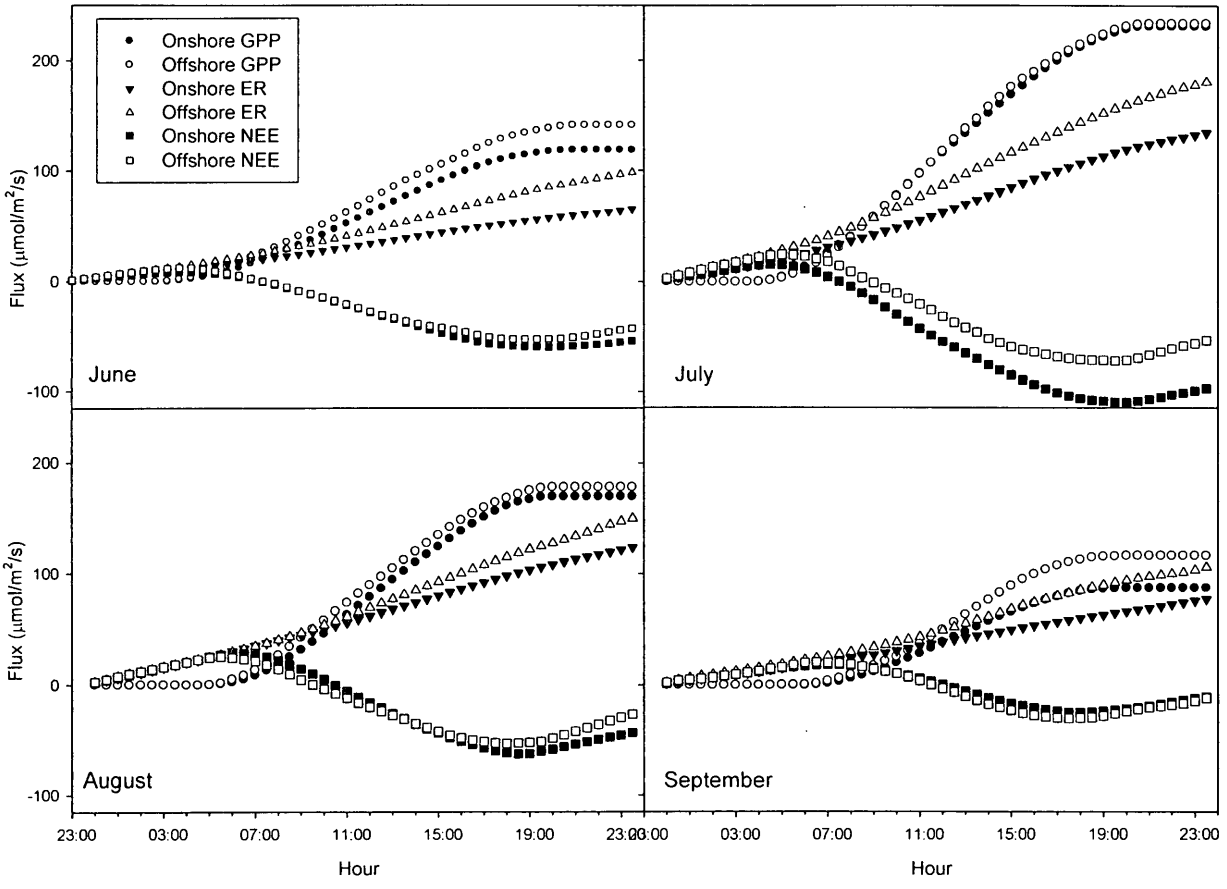

Figure 15. Cumulative diurnal curves for R, GPP and NEE for all months during onshore and offshore wind regimes.

4.5 Discussion

4.5.1 Interplay Between Fluxes

The results of the interplay between GPP and ER under the influence of different environmental conditions revealed important aspects of the HBL as a coastal environment. Hudson Bay's overall influence is reflected in the adjacent landscape of the HBL that extends as far south as northern Ontario. HBL's presence and persistence is due to the mostly frozen water body of Hudson Bay that carries with it tundra-like ecosystems into southern latitudes. Thus, the presence of ice on the Bay is imperative to the persistence of the surrounding HBL through climate modification. Winds originating from the Bay were found to enhance the CO_2 sink of the peatlands in comparison to winds originating from inland, as a result of meteorological influences such as temperature, light availability, energy partitioning and frequency of occurrence.

The progression of seasonal daily average values of NEE (Fig.11) follows a typical pattern as observed for other years in an adjacent location (Lafleur *et al.*, 2012). At the beginning of the season, the flux was relatively strong (-2 $\mu mol/m^2/s$) even shortly after snowmelt (Aurela *et al.*, 2002). Since a thin layer of snow can drastically alter the energy balance of an ecosystem, the complete snowmelt allows for an increased energy balance and a concurrent onset of photosynthesis, largely a result of the presence of mosses and lichens (Oechel & Collins, 1976). Bryophytes are present immediately after snowmelt, making them important photosynthesis contributors earlier in the season before many vascular plants have leafed out. Into September, the NEE drastically drops from its August levels (Fig.11), similar to Lafleur *et al.* (2012),

indicating a quick senescence common to northern environments (Corradi *et al.,* 2005; Lund *et al.,* 2010). At this time, light levels decrease and temperatures are much cooler, therefore unable to sustain strong NEE (Fig.9).

Onshore and offshore differences are evident through a number of physiological parameters. The light-response curves for GPP between onshore and offshore regimes are not significantly different from one another, which means that for the same light levels other environmental forces are influencing the GPP rate. From Fig. 12b, it is evident that the two wind regimes are characterized by significantly different temperatures ($p<0.01$) despite identical light levels. Thus, when GPP is normalized to PAR in order to remove time of day and cloudiness bias, it is stronger for offshore regimes for all four months of the season, associated with the consistently higher temperature regimes, stimulating both ER and GPP.

Figure 13 reveals that GPP increases at a higher rate than ER with increasing temperature for both wind regimes. This occurs for the measured temperature range until the exponential curve of ER reaches the plateau curves for GPP, as presumed from the projected curves. Other studies have found various outcomes depending on different seasonal or ecosystem variations, as some report that ER is more sensitive to increasing temperatures than GPP (Billings *et al.,* 1982; Silvola *et al.,* 1996; McGuire *et al.,* 2000), while others report the opposite (McKane *et al.,* 1997). Chivers *et al.* (2009), instead, found that ER and GPP increase by the same proportion with increasing temperatures, not causing a net effect on the NEE. Their increase in GPP has been linked to an increase in nutrient availability in warmer soils for arctic tundra sites. For the current study, there is a distinction between the cooler onshore regimes and the warmer offshore regimes with increasing temperature. At mid temperatures (11-20°C), the onshore GPP is higher than the offshore GPP; this range of temperature hosts the majority of wind frequency

occurrences and thus has the highest influence on NEE. When both GPP curves are projected into higher temperatures (21-30°C), onshore GPP drops off while offshore GPP remains strong. The interplay between onshore and offshore GPP curves can be attributed to the varying light levels observed for the same binned temperature range (Fig. 14). At mid temperatures, onshore light levels are higher than offshore levels, allowing for enhanced photosynthesis. At the end of the observed range after 20°C, the two light level curves converge, resulting in the convergence of the two GPP curves. This suggests that with increasing temperatures in the Arctic, the ecosystem will uptake more CO_2 under offshore regimes than onshore regimes, with the assumption of continued higher offshore light levels. Considering the small dataset to represent temperatures beyond 20°C, it would be difficult to predict how light levels will change under a warming climate, requiring further research. Nevertheless, the Bay is associated with high pressure systems due to cooler temperatures and restricted moisture availability as a result of ice cover, associated with clear skies. This illustrates its strong influence on the surrounding ecosystems, brought on by its current state of a nearly frozen massive sea.

4.5.2 Energy Balance and Permafrost

The partitioning of the energy balance is expected to have a significant effect on the structure of the soil column and the boundary layer conditions. The way energy is partitioned at the land surface directly influences the micrometeorological conditions of the ecosystem through the interaction between heat and moisture and thus temperature and precipitation. Net radiation does not show a trend between onshore and offshore regimes, but its partitioning into Q_E, Q_H and Q_G does (Fig. 10). Although Q_E/Q^* is not statistically significant when tested for the difference

between onshore and offshore (Table 7), the average of individual half-hourly values show a bias towards the offshore regimes (Fig. 10). Rouse & Bello (1985) discovered a similar pattern for their sea site, near-coast site and inland site, illustrating the strengths of the advective influence of Hudson Bay on the energy balance of the HBL. This enhanced difference is reflected in more evapotranspiration during offshore regimes due to an increased vapour pressure deficit. Q_H experiences a significant difference between onshore and offshore regimes for each month, whereby Q_H/Q^* is significantly stronger for onshore regimes. This occurs when solar radiation heats the ground surface substantially, creating a strong gradient between the warm surface and the cooler onshore air (Rouse, 2000). Q_G is generally larger for offshore regimes as the energy from the sun- and wind-heated surface of the ground penetrates through the cool or frozen permafrost soils. For tundra sites, a large proportion of Q_G is expected to account for 10-20% of Q^*, due to the sparse canopy that allows for deeper penetration of energy into the soil to create a steep gradient between the warm soils and cold permafrost (Lafleur*et al.*, 1997; Eugster*et al.*, 2000; Kellner, 2001) coinciding with the present results.

The potential shift to more frequent offshore winds coupled with larger scale air warming has significant implications for the degradation of the permafrost layer by contributing to a deepening of the overlaying active layer. Its thickness is directly a result of warmer air temperatures and precipitation percolation to deeper layers that increase soil heat content and thermal conductivity (Nelson *et al.*, 1997; Hinzman *et al.,* 1998; Schuur *et al.,* 2008). A deeper active layer will free up a larger portion of the organic soils available for respiration (Callaghan *et al.*, 2004). Permafrost degradation due to global warming is considered to be a significant threat to the frozen peat which currently behaves as a strong CO_2 sink. As the wind regimes switch between onshore and offshore, we are able to see the differences in increased

temperatures and Q_G characteristics of two different ecosystems, and thus providing a glimpse of how global warming may affect the Arctic (Rouse, 2000). In addition to the ecological implications, the degradation of permafrost soils will have negative consequences on transportation and housing structure for northern populations.

4.5.3 What to Expect Under a Warming Climate

In the mid 80's and 90's, northern latitudes were generally considered to be sinks for atmospheric CO_2 (Tans *et al.,* 1990; Ciais *et al.*, 1995; Rayner *et al.,* 1999), but with increasing temperatures this may change. Extensive studies on carbon dynamics have demonstrated that temperature has an observed influence on NEE (Callaghan *et al.,* 2004; Groendahl *et al.*, 2007, Permantier *et al.,* 2011), although others have not found a strong link (Griffis *et al.*, 2000; Aurela *et al.*, 2004). Since warmer temperatures are associated with drier conditions around the Hudson Bay, an increase in respiration is expected to take place as a result of aeration of the soil through increased oxygen diffusion into the soil column (Moore and Knowles, 1989; Nykanen *et al.,* 1995; Silvola *et al.,* 1996). Such results are commonly found (Shurpali *et al.*, 1995; Joiner *et al.,* 1999; Griffis*et al.,* 2000; Bubier *et al.,* 2003; Callaghan *et al.,* 2004; Aurela *et al.*, 2007), whereby ecosystems can transition from a net sink to a net source under decreasing soil moisture conditions and increasing temperature.

Under a warming scenario, we expect that the ecosystem begins to mimic offshore wind regimes, characterized by higher temperatures, higher ground heat flux, higher latent heat flux, reduced light levels and reduced moisture availability. There exist two main scenarios, where carbon sinks strengthen due to increase nutrient availability or where carbon stocks become

sources due to increased respiration. Since higher temperatures are expected to prolong the growing season (Myneni *et al.,* 1997) a shift in vegetation dynamics is to be expected alongside. This is anticipated to increase carbon stocks by accumulating newer and larger quantities of organic matter into the peat (Aurela *et al.,* 2004; Euskirchen *et al.,* 2006; Schuuer *et al.,* 2008). However, Permantier *et al.* (2011) conducted a multi-year analysis of NEE, GPP and ER, and concluded that longer growing season and warmer temperatures do not increase the NEE uptake in their Siberian location, mainly a result of increased ER sensitivity to increased air temperatures in comparison to GPP; similar results were found by others (Dorrepaal *et al.,* 2009; Cai *et al.,* 2010). They found that GPP strengthened during such periods due to increased nutrient availability and favourable growing conditions, but ER increased by either by the same amount or by a larger amount, resulting in either no change or a decrease in the NEE when compared to cold and short seasons. Similarly, HBL offshore wind regimes show an increase in GPP but a stronger increase in ER, making such regimes weaker sinks.

Due to warming temperatures, the sea ice has been significantly decreasing (Barber *et al.*, 2012), which is likely the driver for shifting winds. Positive temperature anomalies are correlated with negative sea-ice trends, most pronounced on the western and south-western part of the Bay, with a decrease of 23.3% to 26.9% per decade (Hocheim and Barber, 2010). Evidence of changing wind regimes is presented by Hocchiem *et al.* (2011), who found that anti-cyclonic atmospheric rotation occurs under high sea level pressure and low land surface pressure, resulting in onshore regimes. This pattern has been observed prior to 1989, whereas the post 1989 period is characterized by cyclonic atmospheric circulation which results from low sea level pressure and high land surface pressure, resulting in offshore winds. The summer of 2007 frequency ratio of onshore to offshore regimes was 1.56:1 with an observed shift in wind

direction since 1953 off the coast of Hudson Bay, whereby offshore regimes are increasing in frequency during the summer months, especially in June (Fig. 16). A 60-year average shows that onshore winds frequency has decreased by 8.6% and a mirror increase in offshore winds frequency. Although not statistically significant (P=0.06), this gradual decrease in the frequency of onshore regimes has likely had a negative influence on the carbon dynamics of the HBL and is expected to follow the same trend in the future. Under a warming climate, it is expected that the frequency of onshore regime increase due to enhanced surface heating and therefore enhances sea-breeze effect; however, as explained above, synoptic scale atmospheric patterns may at play, thereby decreasing the frequency of onshore winds. The decrease in onshore wind frequency will result in a weakened advective influence of Hudson Bay on the HBL, thereby increasing air and soil temperatures and decreasing the strength of the carbon sink. This will occur as a result of increasing ER under the increased frequency of offshore regimes, decreased sunlight availability due to increased offshore wind regimes and warming air temperatures due to global warming. The conclusions reached are reinforced by those found by Rouse & Bello (1985) who identified a modest shift from onshore to offshore wind regimes as a result of advanced melting in the early growing season. A coupled increase in air temperature was also predicted for even a 10-day earlier snowmelt, emphasizing the direct influence Hudson Bay has on the ecosystem dynamics of the HBL. In addition, they calculate that an increase in the length of the growing season by 30 days would place the current study location up to 4°C further south of its current latitudinal line, and within the discontinuous permafrost zone. This illustrates the extent of influence that Hudson Bay has on carbon dynamics, energy balance, temperature, flora and fauna, and built infrastructure. The inability to isolate any one of these factors reinforces the negative impact global warming will have on northern ecosystems.

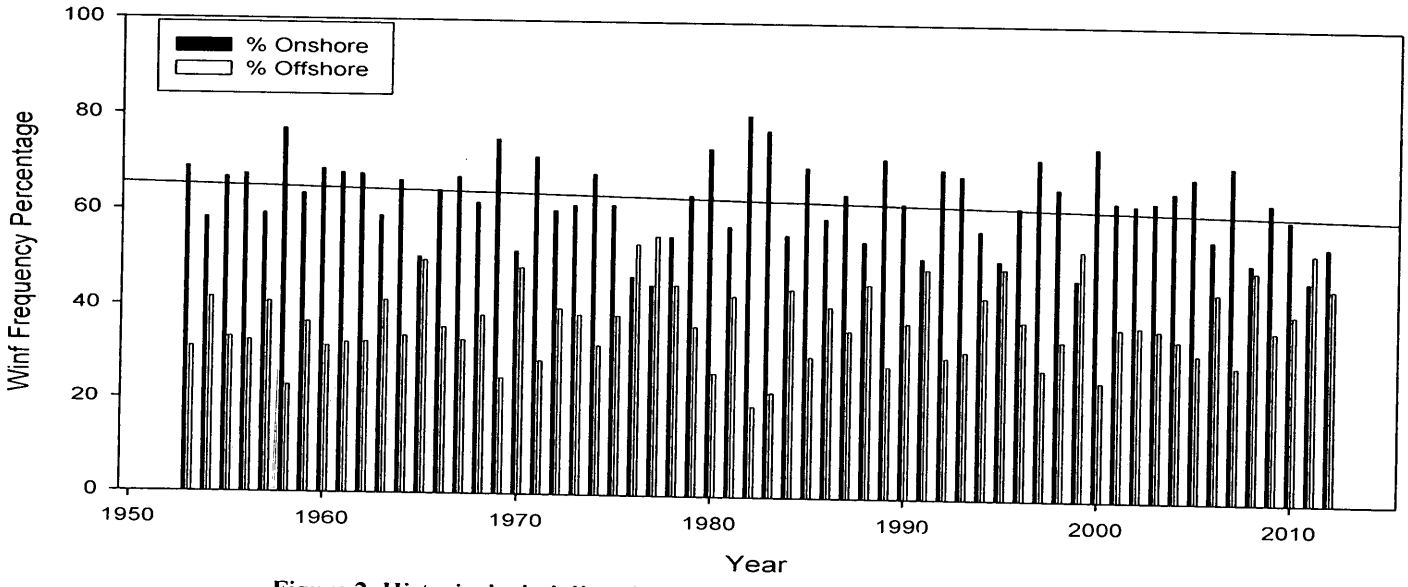

Figure 2. Historical wind direction shift between onshore and offshore regimes.

4.6 Conclusion

The difference in the CO_2 flux from upland tundra during onshore and offshore wind regimes was measured using the EC method in the Hudson Bay Lowlands near Churchill, MB. It was confirmed that the Hudson Bay has an advective influence on the carbon dynamics and energy balance of the HBL as others have concluded (Rouse & Bello, 1985; Lafleur & Rouse 1988; Rouse *et al.,* 1997). The CO_2 flux between the two wind regimes differed significantly, reinforcing the importance of Hudson Bay as mostly frozen water body dominated by onshore wind regimes. Although offshore winds regimes were associated with enhanced GPP when normalized by PAR compared to onshore regimes, ER/PAR was significantly stronger resulting in a weaker NEE sink. For the same air temperatures, onshore GPP is significantly stronger than offshore GPP until the two curves converge at 20°C. Past this temperatures, onshore and

offshore light levels also converge, thereby exerting control over GPP. The observed shift from onshore to offshore regimes in conjunction with melting sea ice will weaken the carbon sink of the HBL, in consequence reducing its capacity to sequester the increasing global emissions.

During the 2007 growing season, the peat plateau experienced a substantial net gain of carbon, 115.87 gC/m^2. If the respiration before and after the growing season is accounted for by using the measured air temperatures from the Churchill airport (Environment Canada, 2013), the sequestered amount becomes 26.96 gC/m^2/year, which is relatively close to the value of 23 gC/m^2/year obtained by Gorham (1991) for northern peatlands. It is noteworthy that this coastal peat plateau comprises close to 50% vascular plant cover which is not necessarily representative of ice-wedge polygon systems in general. Nevertheless, if this value is extended to the entire surface area of the HBL of 250 000 km^2, the uptake becomes 6.74 MtC/y, which is approximately 62% of the estimated (Greenpeace, 2007) Alberta oil sands CO_2 emissions of 40 million tons (10.9 Mt C/y). Although providing better understanding of how HBL's sink mitigates greenhouse gas emissions, it is important to note the large uncertainty expected when one extrapolates the carbon flux of a small area over vast and heterogeneous ecosystems of the HBL. Considering that this is a tundra ecosystem in a cooler environment, this percentage is significant to help offset global carbon emissions, yielding more reason to better understand the carbon dynamics of these strong sinks.

5.0 INFLUENCE OF PLANT COMPOSITION AND PHENOLOGY ON THE PHOTOSYNTHESIS OF UPLAND ECOSYSTEMS OF THE HUDSON BAY LOWLANDS

5.1 Abstract

Carbon dioxide fluxes were measured utilizing two different methods near Churchill, MB, approximately 5 km south of the Hudson Bay shoreline. A 2007 field campaign included the measurement of carbon dioxide (CO_2) flux using an eddy covariance system (EC) during the growing season months on an elevated peat plateau ecosystem comprising ice-wedge polygons. A 2009 field campaign included chamber CO_2 measurements (LI8100, LI-COR Bioscience, Lincoln, NE) on plots manipulated for plant cover on a polygon tops. A 2012 field season consisted of detailed plant cover sampling on the elevated peat plateau that hosts the EC system. From the CO_2 measurements, light response curves were constructed to assess how photosynthesis changes with the photosynthetic photon flux density (PPFD) over different plant covers and relate these results to phonological cycles of particular vascular species. It was found that plots without the presence of vascular vegetation had very low photosynthetic rates in comparison to the control plot (30% vascular, 70% lichen). In addition, the herb cloudberry significantly influenced the photosynthetic rate, which was higher than plots containing other vascular plants. Its influence was measured with the EC system with the help of weekly light response curves.. Results indicate that GPP in upland tundra ecosystems is very sensitive to the composition and timing of the vascular plant cover and therefore characterization of the carbon dynamics at present and its potential change in the future requires a thorough understanding of variability in plant community composition.

5.2 Introduction

Northern peatlands span over $3.5x10^6$ km^2 (Gorham, 1991) throughout North America and Eurasia, forming important ecozones that hold high significance in global carbon cycling, despite their lack of large and dense vegetation cover. These regions are characterized by continuous and/or discontinuous permafrost throughout the year that keeps the peat within them from decomposing. Such ecozones are known to measurably reduce the impact of greenhouse gases by sequestering large amounts of atmospheric carbon dioxide within thick peat deposits (Tans *et al.*, 1990; Ciais *et al.*, 2000; Griffis *et al.*, 2000; Aurela *et al.*, 2002; Corradi *et al.*, 2005; Roulet *et al.*, 2007; Cai *et al.,* 2010). The observed climate warming (IPCC, 2012) is most pronounced in the north mainly due to the ice-albedo feedback process. This feedback occurs under decreasing snow and ice conditions that drastically reduce the albedo of the landscape and absorbs increasing amount of solar radiation. It is expected that by the end of the 21st century northern land surface temperatures could warm by up to 8°C, according to some models (IPCC 2007). The increasing temperatures are responsible for the rapid disappearance of previously frozen organic C within permafrost soils, thus profoundly changing the hydrological regimes of these peatlands (Chapin *et al.*, 2000; Chivers *et al.,* 2009). The feedback processes are to a certain extent mediated by changing plant cover and large scale ecosystem movement (Callaghan *et al.,* 2004), which have a large influence on the evapotranspiration rates of the ecosystem and therefore hydrology (Lafleur & Roulet, 1992). Small-scale vegetation dynamics can change rapidly over a single year as a result of stress generated by extreme weather events that are becoming more frequent (Backhorst *et al.*, 2012). The current ecosystems are hosts of multitude of plant species that act coherently in order to maintain the current state of the ecosystem,

forming bogs, fens, swamps, and peat plateaus. These habitats that cover the tundra are generally higher in their albedo, which is likely to decrease with increasing density and height of vegetation under a warmer climate. This will be carried over during winter, as not all vegetation will be submerged beneath the high albedo snowpack.

Despite the relative agreement of temperature forecasts amongst models, precipitation forecasts posses much more uncertainty as to whether specific regions will be wetter or drier in the future (Groisman *et al.,* 1991; McGuire *et al.,* 2000), constraining predictions about the future state of northern ecosystems. Although northern regions may become wetter due to increased moisture holding capacity of the atmosphere, the moisture availability on the ground is highly dependent on future evaporation rates. The Hudson Bay Lowlands are generally comprised of wetlands, as they have a relatively high water table, which is partially sustained by low evaporation rates and frozen peat that inhibits percolation. However, wetlands are expected to become drier with increasing temperatures due to increased energy for the evaporation of available water (Callaghan *et al.*, 2004). The optimal temperature range for northern plant species tends to be smaller than for more southern latitudes, which adds to the vulnerability of these ecosystems, as a threshold would be easy to cross during extreme weather events (Gaines & Denny, 1993). Under a warming climate, extreme weather events are expected to increase in frequency and duration (ACIA 2005), restructuring the current synchrony that favours the accumulation of atmospheric carbon within vast peatlands. Backhorst *et al.,* (2012) reported on an extreme winter warming event that profoundly changed the ecosystem functioning during the subsequent growing season, as the normalized difference vegetation index (NDVI) decreased substantially for the following two growing seasons after the death of small shrub plant species. This indicates that plant survival is inextricably connected with established climate and plant

sensitivity to abnormal events can last long after the event takes place. Given that northern regions are expected to undergo the highest anomalies of warming (IPCC, 2007), their summers will get hotter and winters will get milder (Callaghan *et al.*, 2010). This is correlated with earlier break-up dates in the Hudson Bay region (Gagnon & Gough, 2005), reducing the advective influence of the frozen Hudson Bay on the adjacent Hudson Bay Lowlands. This will result in a longer growing season, which can transform an ecosystem from a net sink to a net source over the span of 30 years (Callaghan *et al.,* 2004). The same study also reports on the observed change in physiological, community and ecosystem level modification, associated with increasing temperatures, decreasing moisture availability and a longer growing season.

The known ecological significance of the peatlands of the Hudson Bay Lowlands has been documented in numerous studies, from polar bear habitat (Derocher *et al.*, 2004; Sterling & Dorecher, 2012), to a host to unique bird species (Aubry *et al.,* 2013), to scattered pond formation as a result of unique hydrological cycle (Woo, 2012), to carbon sequestration ability (Tans *et al.*, 1990; Griffis *et al.*, 2000; Roulet *et al.*, 2007; Cai *et al.,* 2010), and to a host of vital transportation routes. The observed changing climate is expected to have a profound influence on the aforementioned functions, with some already occurring (Hocchiem *et al.,* 2011; Serreze *et al.*, 2000). The purpose of this study is to explore how different plant functional groups contribute to the carbon dynamics of the HBL peatlands and to assess the implications of plant phenology and potential future shifts in the composition of the plant community on the carbon budget. This was achieved through the use of three lines of evidence. First, we compare continuous flux measurements over the growing season to the phenology of specific vascular plant species, Second we compare assimilation light curves from habitats sharply contrasting in species composition. Third we compare assimilation light curves for habitats undergoing the

manipulative removal of specific functional plant groups. The dataset consists of chamber and eddy covariance measurements of growing season CO_2 exchange on an upland peat plateau containing ice-wedge polygons near Churchill Manitoba, Canada.

5.3 Methods

5.3.1 Study Site Description

The study locations are located approximately 20 km east of Churchill, MB, approximately 5 km south of the Hudson Bay coastline and within the Hudson Bay Lowlands (Fig. 17). The Hudson Bay Lowlands are mainly composed of mineral wetlands or organic peatlands, generally north of the treeline and adjacent to the western and southern coasts of Hudson Bay (Riley, 2011). Over thousands of years, the mineral soils within the coastal areas of Hudson Bay emerged due to isostatic rebound, where peat has accumulated and persisted to create the current carbon sink. The present day peat plateau, where the measurement sites are located, is approximately 20 ha. in area and emerged from Hudson Bay approximately 1600 years ago, based on an isostatic rebound rate of 0.01 m/year (Stella *et al.,* 2007), During this time peat has infilled depressions to a depth of 2 m such that the present day topography is very flat. The terrain is composed of a mosaic of habitats with a range of hydrological and soil characteristics, comprised of ponds, bogs, fens, copse of white spruce and larch, exposed gravel moraines and high-centre ice-wedge polygons. The vegetation comprising these ecosystems is mainly moss, lichen, and vascular species belonging to the heaths and shrubs, as the hydrology is relatively drier than other tundra ecosystems supporting sedges. Such habitats are mainly

oligotrophic as they are generally nutrient deprived and obtain their nutrients from the soil substrate and precipitation through minerotrophy (Riley, 2011). These types of polygon dominated systems comprise 22% of the land cover within the expanse of the entire Hudson Bay Lowlands (Riley, 2011) though they form the dominant landscape component north of the treeline in the Manitoba portion of the Hudson Bay Lowland (Bello & Smith, 1990).

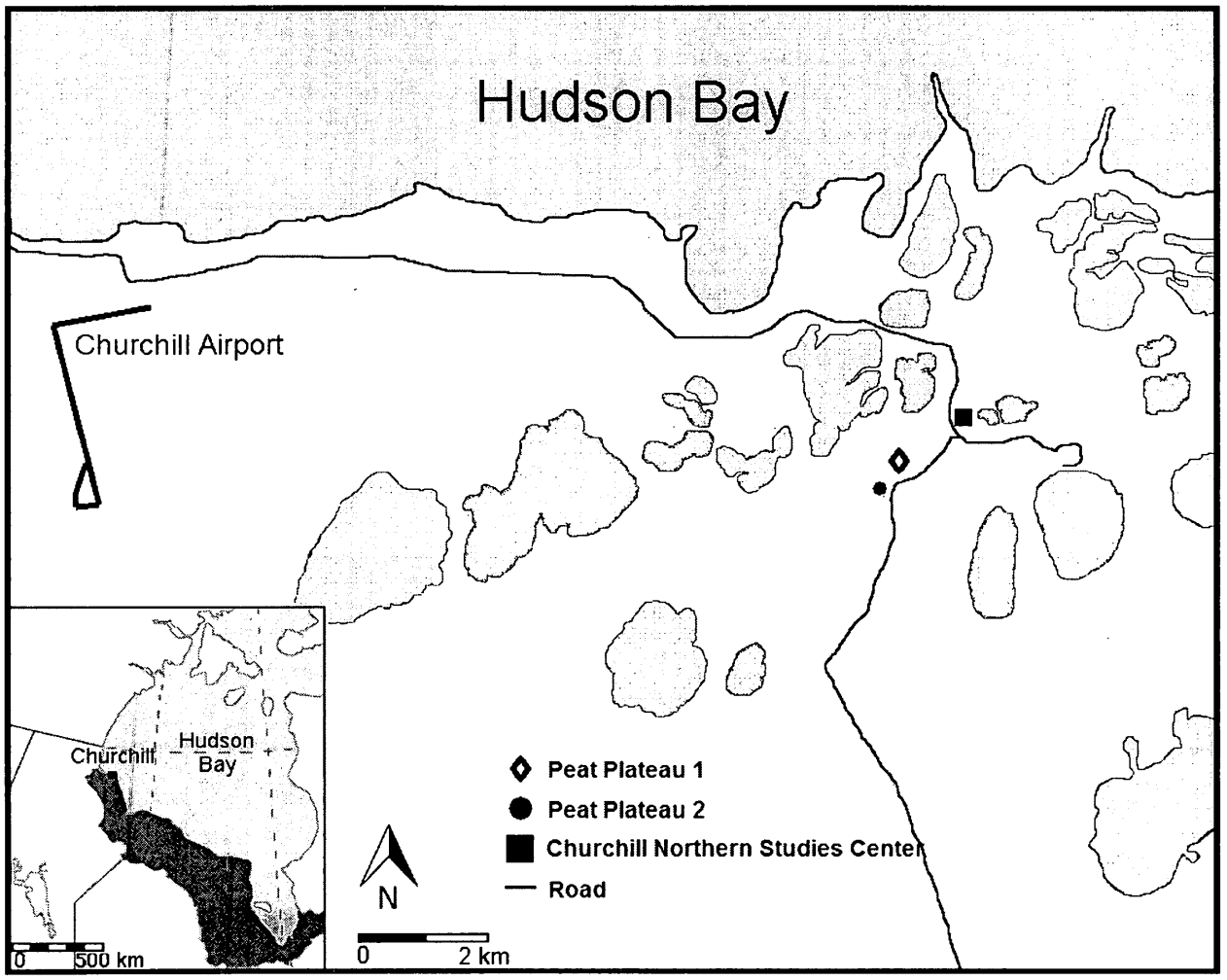

Figure 17. Location of the two study sites (Peat Plateau 1 and Peat Plateau 2) near Churchill, MB and within the Hudson Bay Lowlands.

5.3.2 Plant Cover Sampling

Plant cover was sampled in two layers at the north-east portion of the peat plateau during the 2012 field campaign, (Peat Plateau 1, PP1, Figure 17). The understory comprised all vascular plants, mosses and lichens growing next to the peat surface. The overstory comprised shrub birch, willow and conifers. The understory vascular group was dominated by *Ericaceae*; *Rhododendron decumbens* (dwarf labrador tea), *Empetrum nigrum* (crowberry), *Vaccinium vitis-ideae (low ground cranberry)* which are all evergreen and change their leaf area very little seasonally and the herb *Rubus chamaemorus* (cloudberry). Cloudberry was given particular consideration due to its late and rapid leaf-out and its tendency to grow over pre-existing understory groups and was thus included in the overstory. Moss species were primarily *Dicranum elongatum, Tomenthypnum nitens and Aulocomnium spp.*, while the lichen species mainly consisted of *Cladina rangiferina, C. mitis, C. stellaris*, Alectoria ochroleuca, and Flavoc*etraria nivalis*, Dispersed at a larger distance away from the meteorological tower were *Larix laricina* (larch/tamarack) *and Picea glauca* (white spruce) present in low numbers locally with shrubs such as *Salix spp.* (willow) and *Betula glandulosa* (birch). A 60x60 cm frame was constructed with 36 sampling points for both over- and understory enumeration. Cover was recorded at 2 m intervals extending along 100 m transects at 16 equally spaced compass directions from the base of the meteorological tower supporting the eddy covariance system. Model estimates after Schuepp *et al.,* (1990) indicate that at least 50% of the H_2O and CO_2 flux measured at the tower originated within a 100m radius 91% of the time.

In addition, experiments were conducted on Labrador tea and crowberry to determine their leaf area index (LAI) which is the ratio of leaf area to plant area. A quadrat was placed over an individual plant cluster of the same root and a photograph was taken from above, minimizing

angular distortion. These images were processed using image software (Photoshop) and scaled appropriately, allowing for area calculation as was described earlier for the collars in PP2. A sample size of 70 leaves were removed and scanned onto a computer to process in Photoshop for area calculations. All leaves were then removed from the plant and weighted to determine a relation between the specific leaf area of the samples (area/weight) and the weight of all leaves. This was repeated for 24 plants of Labrador tea, allowing for 10% error, and 23 plants for crowberry, allowing for 10% error.

5.3.3 Gross Primary Productivity

Light response curves were constructed for the elevated peat plateau (PP1) using the eddy covariance (EC) method. The meteorological tower supported an EC system 1.49 m above the ground that collected CO_2 and H_2O flux data using an open path infrared gas analyzer (LI7500, LI-COR Bioscience, Lincoln, NE) and a fast-response sonic anemometer measuring the three dimensional wind components (V-style ATI probe, Applied Technologies Inc.). Signals were logged at 20Hz using a Campbell CR3000 datalogger. Incoming solar radiation was measured with a pyranometer (Eppley PSP), which was used to create a linear model for photosynthetically active radiation (PPFD) data from a nearby study site. Net radiation was measured with a Middleton (CN1) pyrradiometer continuously aspirated with desiccated air and the soil heat flux was measured with three Middleton (CN3) soil heat flux plates wired in series and buried 1 cm below the peat surface. The EC data was processed with EddyPro 4.1.0 (LI-COR Bioscience, Lincoln, NE) used to apply the necessary corrections to obtain valid flux data. The net ecosystem exchange (NEE) flux was partitioned into gross primary productivity (GPP) and ecosystem

respiration (ER) components after the Lloyd & Taylor (1994) method. This involves modeling of nocturnal ER response to temperature, and extending that model to sunlight hours to obtain daytime ER. The GPP is calculated as the resultant difference between NEE and ER.

Chamber flux measurements occurred in the south-west portion of the peat plateau (PP2, Figure 17) during the 2009 field season. Five (2.5 x 2.5 m) plots within 20 m of each other were selected in each of three habitats: polygon tops, riparian and bogs habitats; for the purpose of this study, only the polygon tops habitat will be considered. The proportional plant cover of the three plant functional groups; vascular, moss and lichen were recorded before treatments within 100, 25 x 25 cm grid cells within each plot. Species level plant cover was recorded using a 30 x 30 cm quadrat with 36 sample points at nine locations within each plot for two canopy levels. Six sampling locations were randomly selected and three sampling locations corresponded to the flux collars. One polygon top was undisturbed forming the control site. In the year prior to flux measurements; one plot had all aboveground biomass removed exposing bare peat, a second plot had only all lichen biomass removed, a third had only all moss biomass removed, and a fourth had only all vascular biomass removed. Three permanent 35 x 35 cm collars were imbedded at three grid cell locations in the central portion of each plot. The selection of collar locations was determined such that the average coverage of vascular plants, moss and lichens within the collars prior to treatment was the same for all polygon tops The flux collars were located centrally to eliminate edge effects. Carbon dioxide exchange was measured over the 2009 summer season with an infrared gas analyzer (LI8100 IRGA, LICOR, Lincoln Nebraska) with the LI8100 survey chamber attached to a 10 cm opening on a clear acrylic 35 x 35 cm chamber 15 cm tall (Figure 18). Point measurements of displacement at 121 equally spaced locations were used to determine collar offsets. Recirculation fans (12V DC) were located within the clear chamber and the survey

chamber to enhance the mixing of air during each 120 second sampling interval. The survey chamber rested on the northern corner of the acrylic chamber to avoid shadows cast by the survey chamber on the growing surface. Ancillary measurements of temperature at the soil surface and 6 cm depth, soil moisture in the top 6 cm (DeltaT Theta probe) and PPFD (LICOR Quantum sensor) were made adjacent to each collar. Measurements were taken in sets of four at each collar; 1) clear chamber (τ = 90%); 2) 33% shading cloth, 3) 66% shading cloth, 4) dark shroud. The first three readings provide NEE at three different light levels, the fourth provides respiration and the difference between respiration and NEE provides GPP at three light levels. A set of readings could be typically completed in 15 minutes per collar. Fluxes reported are based on the best fit exponential model to the final 90 seconds of data, at ambient CO_2 concentrations using the software (FileViewer 3.2) provided by the manufacturer. Fluxes from the fifteen collars at the five ice-wedge polygon plots were collected approximately every second day, weather permitting.

Digital photographs of plant cover within each collar on the day of sampling were taken over the measurement period extending from the last week in June until the last week of August, 2009. These digital photographs were imported into a software program (Photoshop), where the area of cloudberry cover was calculated. This was done by scaling the image to its known collar size and calculating the pixels making up the surface area of cloudberry. Subsequently, the surface cover for each photograph was scaled to the maximum cloudberry plant cover to produce a phenology curve from initial budding to senescence.

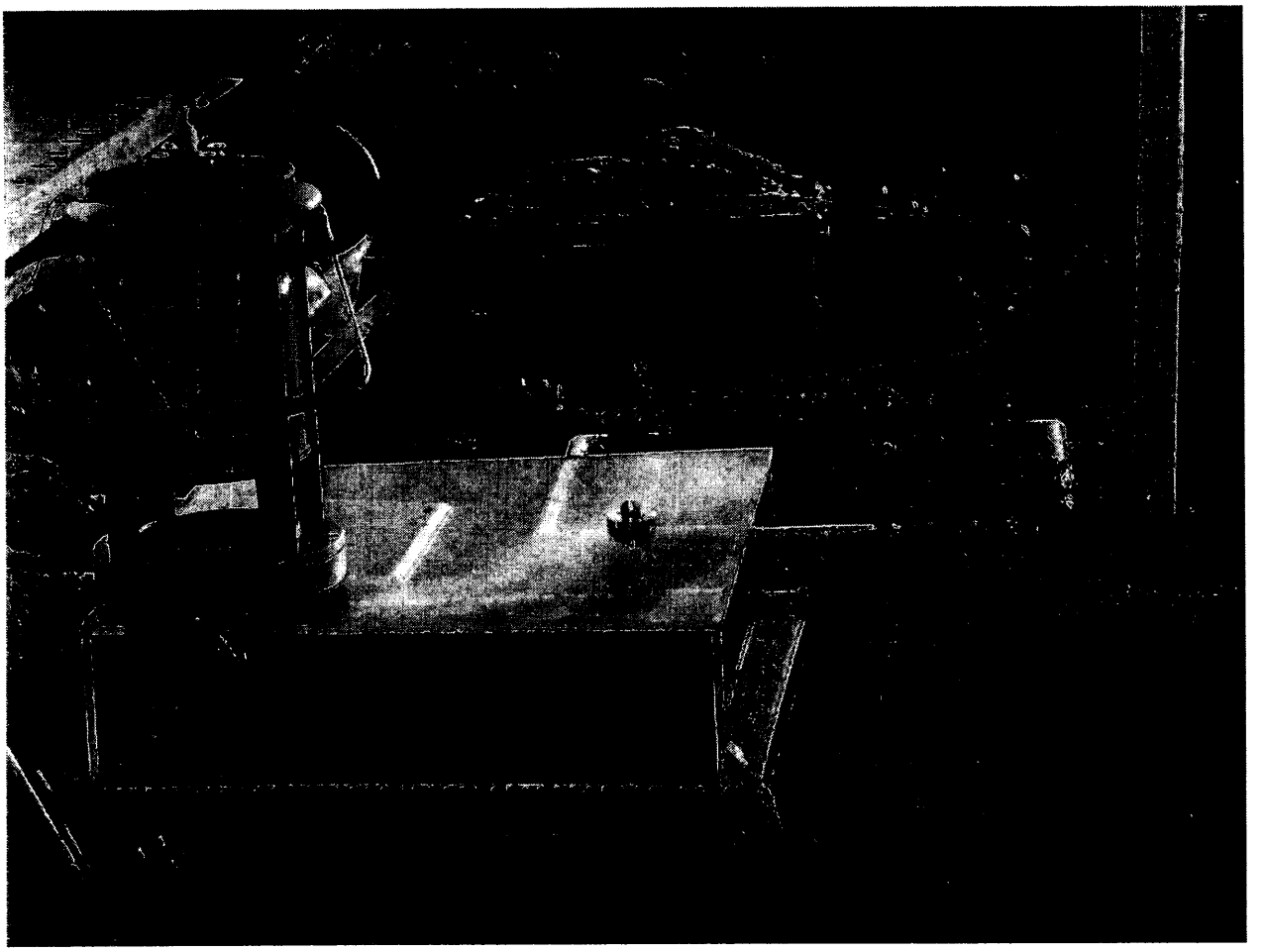

Figure 18. Net Ecosystem Exchange measurements made in 2009 over PP2 using LI8100 chamber. This is an example of a clear chamber that allows all available sunlight to reach the vegetation inside.

5.4 Results

5.4.1 Growing Season Temperature Change

The observed change in air temperatures in Churchill, MB is shown in Fig. 19. It represents the mean growing season temperature increase (June-September) measured by

Environment Canada at the Churchill airport. Although there are periods of stability in the temperature regime (1970's and early 1980's), the general trend points at increasing temperatures at a rate of 0.3°C/decade. The increase over time is statistically significant ($P<0.005$), indicating the strength of the observed warming and its potential impact on the stability of the Hudson Bay Lowlands. On a monthly basis (data not shown), June and September experience the highest rate of temperature increase at 0.32°C/decade and 0.38°C/decade, respectively. July and August have undergone temperature increases at 0.28°C/decade and 0.26°C/decade, respectively.

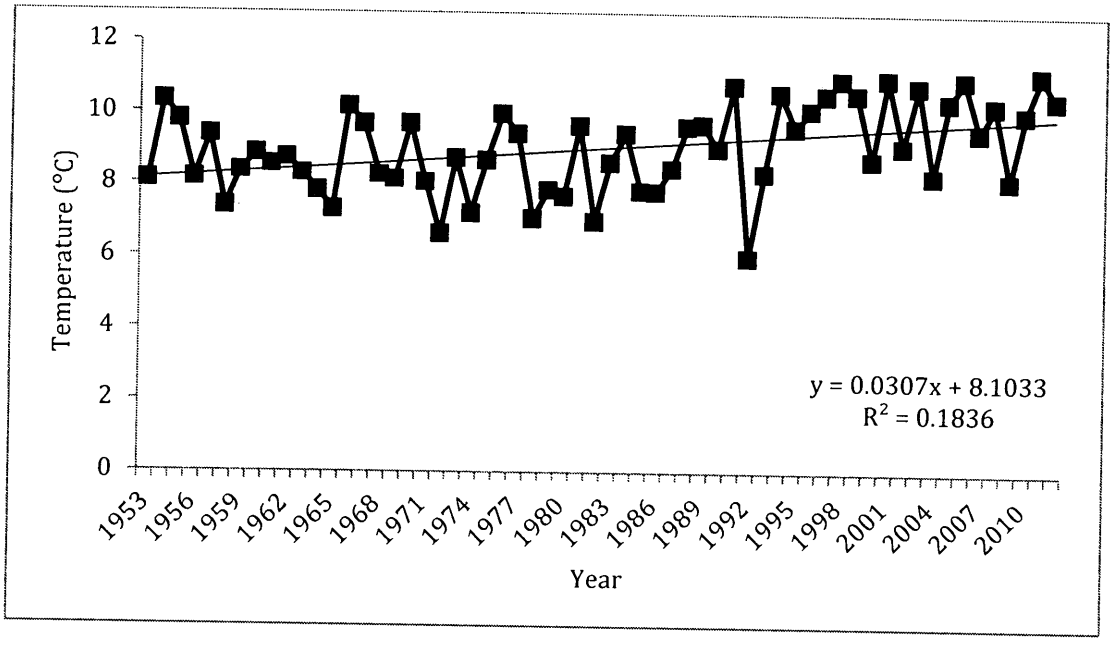

Figure 19. Annual temperature change in Churchill, MB, 1953-2012. Seasons include June-September.

5.4.2 Plant Cover and Light Response Curves (PP1)

The peat plateau hosting the EC system and meteorological tower was sampled for its vegetation cover during the 2012 field season during peak biomass (Table 9). The dominant plant cover was vascular, which comprises nearly half of the peat plateau, at 47.8%. The lichens and mosses comprise approximately the same amount as each other and half of the vascular presence, at roughly 25.4% and 23.2%, respectively. Although pond and rock groups were sampled, they make up insignificant amounts of the sampled ecosystem. The largest influence from the overstory group is from the herb cloudberry, which presented 13.6% cover. The rest of the overstory group – birch, willow and conifer, comprise a combined total of 8%.

Table 9. Plant cover proportions for an elevated peat plateau with understory and overstory sampling groups using quadrat sampling. Data was collected in 2007 which experienced average weather conditions with respect to temperature and precipitation.

Plant Cover	Percent Cover
Understory	
Vascular	47.8
Lichen	25.4
Moss	23.2
Pond	1.0
Rock	2.7
Overstory	
Cloudberry	13.6
Birch	2.1
Willow	4.0
Conifer	1.9

The photosynthetic rate at PP1 over a range in light levels for the entire data collection period is shown in Fig. 20. The figure is constructed by averaging GPP over binned light levels,

in this case every 25 μmol/m^2/s. This light response curve represents the combined photosynthetic capacity from a fully functional and undisturbed ecosystem that contains the plant groups described in Table 9. The assimilation rapidly increases with initial rise in light levels until about 300 μmol/m^2/s of PAR. Beyond that point, the increase becomes more gradual until it levels off at very high light levels of under 2000 μmol/m^2/s. At this point GPP remains within the range of 7-9 μmol/m^2/s.

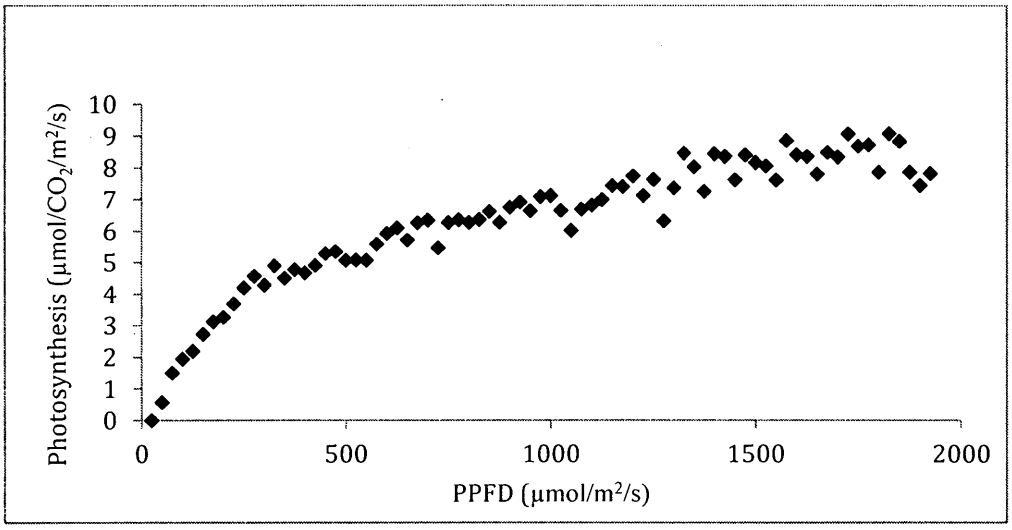

Figure 20. Light response curve for the PP1 study site for the entire 2007 growing season.

The light response curves for PP1 on a weekly basis throughout the 2007 field season are shown in Fig. 21. The associated mean GPP on a weekly basis is shown in Table 10. Figure 21a shows weeks 1-5 associated with pre-growth and initial growth of vegetation. The growing degree days (GDD) range from 1 to 100 for this five week period. GDD is a quantification of the accumulated heat (T>5°C) in an ecosystem which helps in assessing the phenological cycle of plants. Since plants are highly dependent on ambient temperature, the cumulative temperature in the form of GDD helps establish important phenological milestones for particular plant species

with the aid of observational data. Weeks 1-3 are nearly overly each other and only reach a maximum of 6 μmol/m^2/s.; at this point the vascular plant canopy is still expanding. Weeks 4 and 5 show proportionately stronger GPP, which reaches nearly 10 μmol/m^2/s. The mean GPP in Week 5 is 35% stronger than that for Week 1, indicating the strength of the end of the initial growth period (Table 10).

Figure 21b shows weeks 6-10, associated with the strongest seasonal photosynthetic rates and corresponding range of GDD from 108 to 411, which is much larger than the range for Figure 21a as a result of higher temperatures during that period. The light response curves for all five weeks are very similar to each other without any distinctive deviations. The rise in photosynthesis with increasing light levels is sharper than in Figure 20a and the GPP values reached at high light levels are 12 μmol/m^2/s. The reduction of peak photosynthesis can be observed at Week 10 (Table 10), which shows a 15% decrease from Week 9, although still within the range of data observed for this period of time.

Lastly, Figure 21c shows weeks 11-16, which is the period of senescence. The GDD range for this period is from 419 to 611, but GDD stop accumulating after week 14. Weeks 11 and 12 resemble the pattern observed in Figure 21b, although they only reach as high as 10 μmol/m^2/s. The following weeks have markedly lower GPP values that drop down to as low at 4 μmol/m^2/s for Week 16. The mean GPP during Week 16 is nearly 70% smaller than that for Week 9, which is the maximum for the season (Table 10). In addition, the peak light levels during this period of time decrease as a result of larger zenith angles.

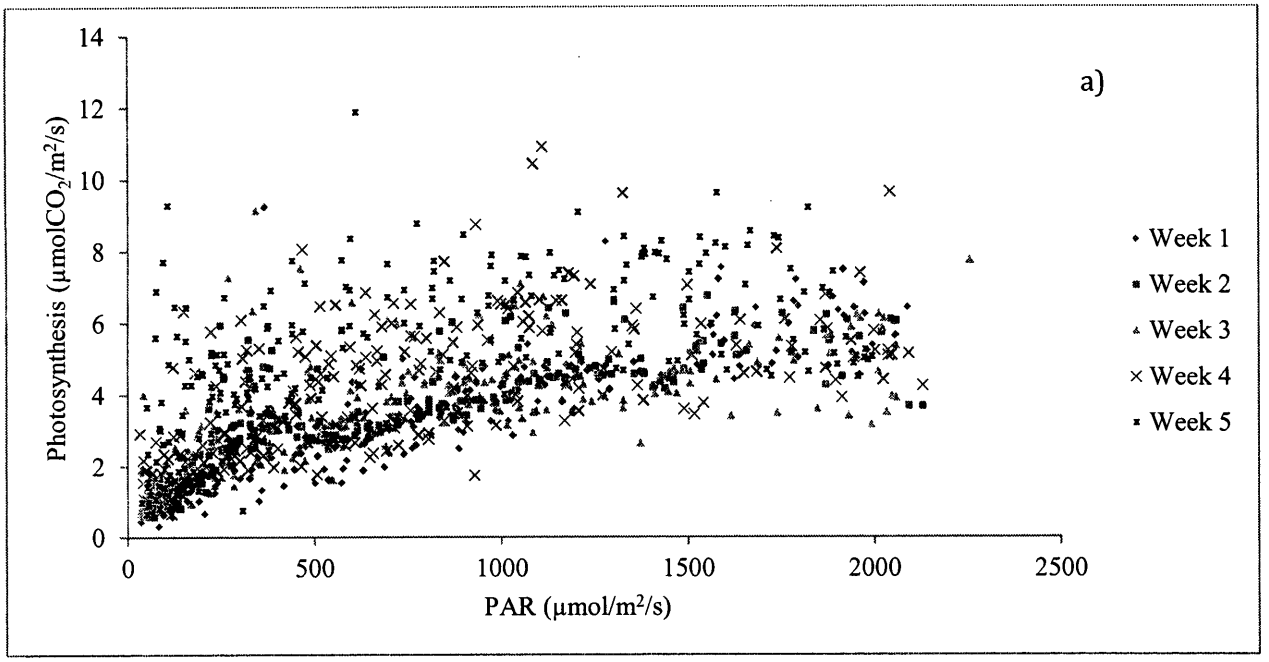
a)
Photosynthesis (µmolCO2/m2/s)
PAR (µmol/m2/s)
0
2
4
6
8
10
12
14
0
500
1000
1500
2000
2500
Week 1
Week 2
Week 3
Week 4
Week 5

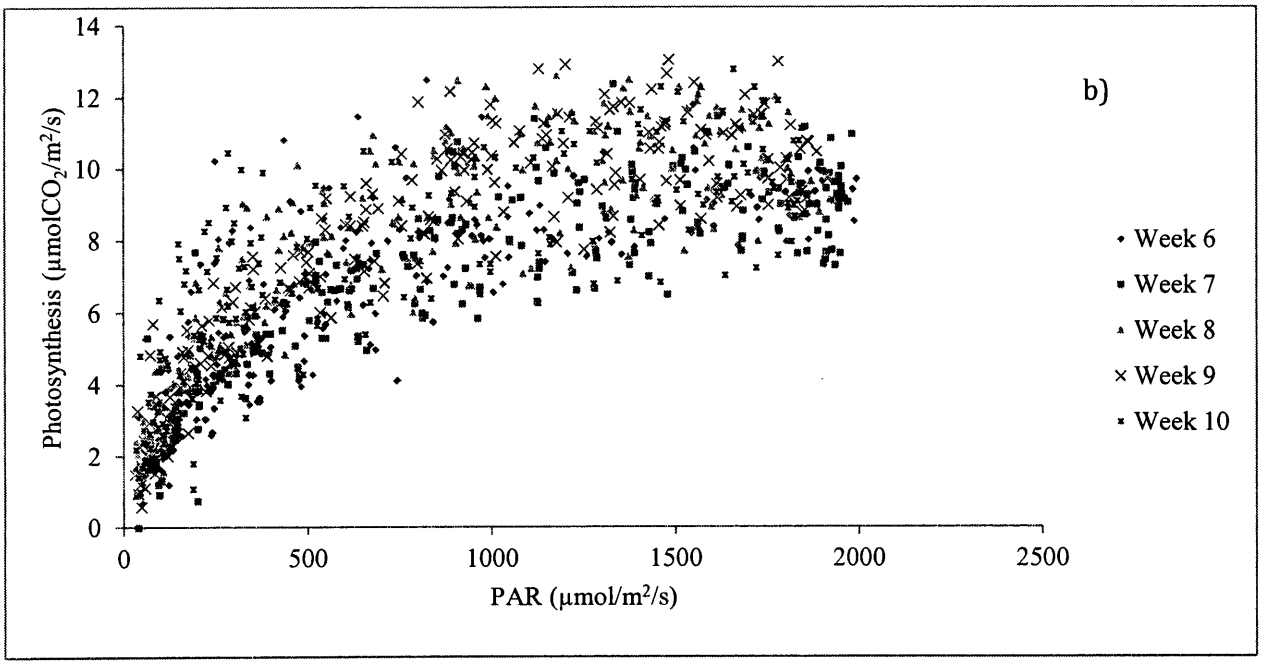
b)
Photosynthesis (µmolCO2/m2/s)
PAR (µmol/m2/s)
0
2
4
6
8
10
12
14
0
500
1000
1500
2000
2500
Week 6
Week 7
Week 8
Week 9
Week 10

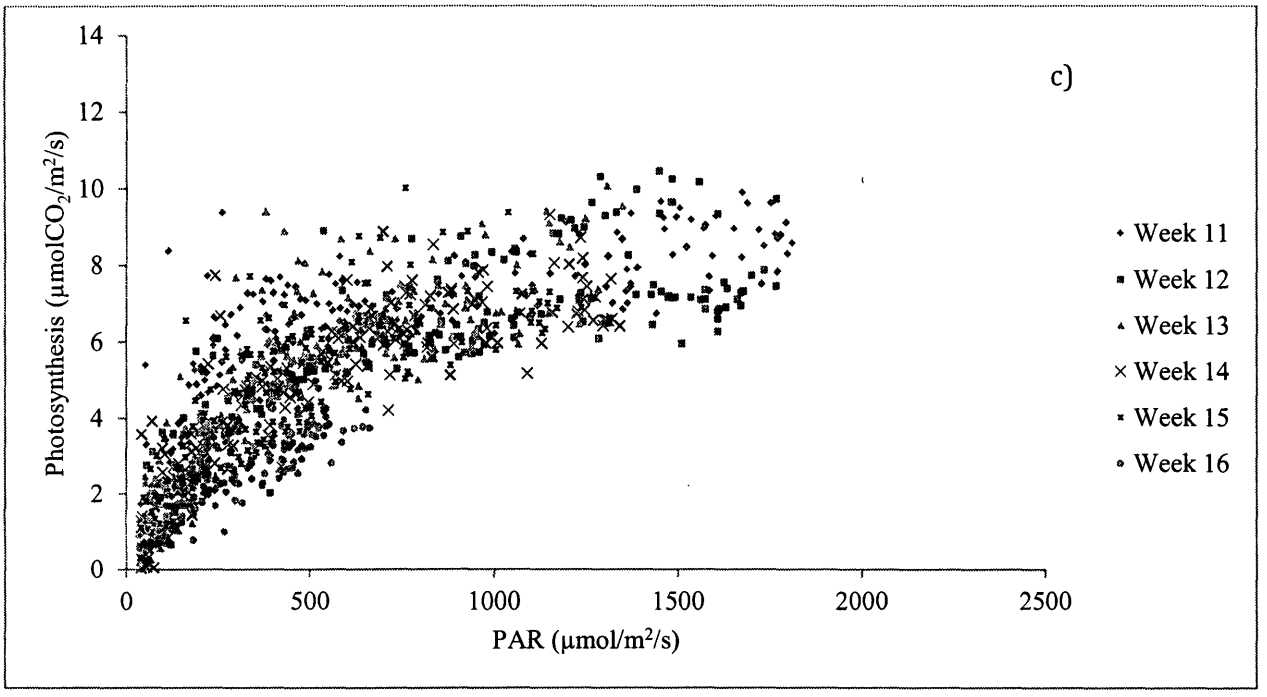

Figure 21. Light response curves measured in 2007 from PP1 displayed on a weekly basis. a) Weeks 1-5 and period of initial growth; b) weeks 6-10 and period of strong photosynthesis; c) Weeks 11-16 and period of senescence.

Table 10. Mean GPP over the 16-week study period.

Week	1	2	3	4	5	6	7	8	9	10	11	12	13	14	15	16
Mean GPP ($\mu mol/m^2/s$)	3.48	3.58	3.47	4.17	5.33	6.07	7.18	7.98	8.05	6.88	6.35	5.99	5.34	4.95	4.42	2.65

Figure 22 shows the phenological growth of cloudberry, where lines of % growth are shown to mark milestone periods. The observational data of cloudberry phenology digitized from sequential photographs from the flux collars is overlain by a modeled curve with R^2=0.99. The buds of the cloudberry begin to leaf out at approximately 100 GDD, coinciding with the end of Week 5 (Figure 21a). Shortly thereafter, the curve sharply increases as the plants photosynthesize more effectively in order to gain more biomass. At approximately 350 GDD, the slope of the line begins to decrease; this is the point which is defined as the GDD when peak

biomass occurs. Although the curve continues to increase to represent an increase in leaf area, the cloudberry leaf is lobe-shaped which has a small surface area when it is fully functional. However, as the plant begins to senesce, the lobe opens up due to loss of turgor and the leaf area increases accordingly. 350 GDD corresponds to Week 9, which is the last week to experience an increase in maximum photosynthesis. Unpublished data gathered on dwarf birch shrubs on the plateau shows the GDD milestones for *Betula glandulosa*, which happens to be very similar to that of willow, of 13 GDD for leaf emergence, which occurs during Week 2 of the 2012 EC dataset. Full leaf-out occurred at 80 GDD, which falls within Week 5. This is the same week that cloudberry begins to emerge. Thus, the carbon footprints of the shrubs and the heath species can be differentiated as a result of different phenological cycles.

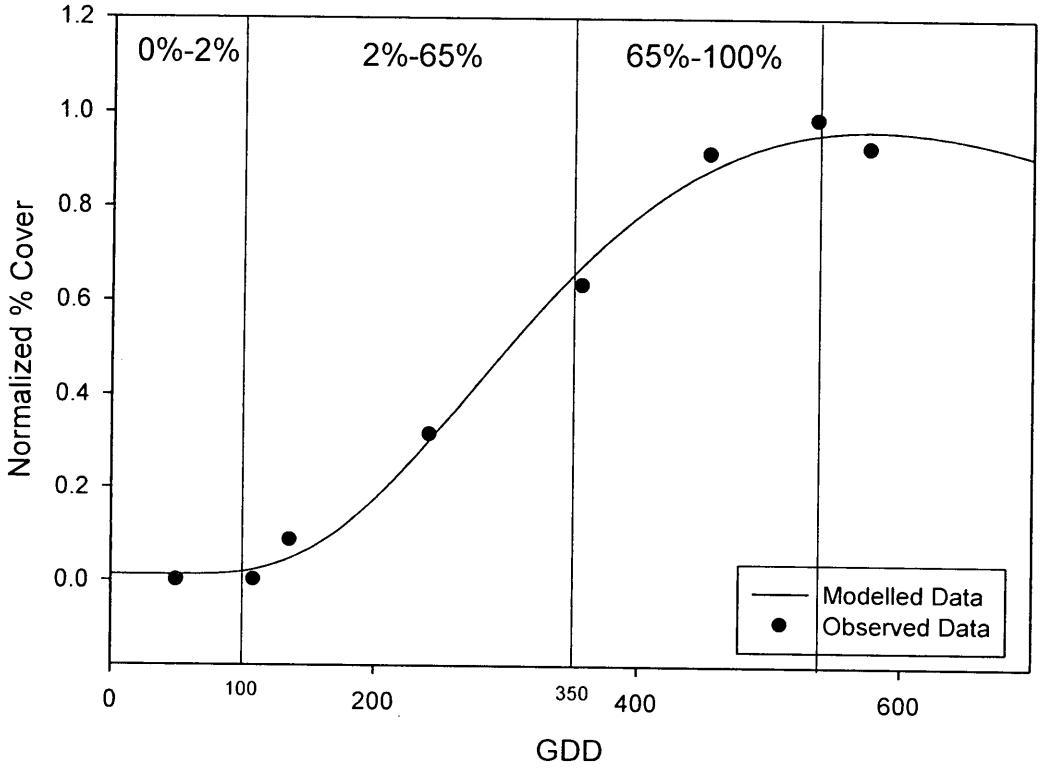

Figure 22. Phenological cycle of cloudberry with respect to growing degree days and leaf area. The model was fitted with a dynamic fitting peak log-normal equation (SigmaPlot 11.0) to maximize the best fit (R^2=0.99),

$$y = y_0 + a * EXP(-0.5\left(\frac{ln\left(\frac{x}{x_0}\right)}{b}\right)^2)x$$

5.4.3 Manipulated Plot Light Response Curves (PP2)

The 2009 field campaign involved CO_2 chamber measurements on manipulated plant cover plots. The light response curve for the control plot is shown in Fig. 23, where all plants have been left in their undisturbed state. The plant composition is non-vascular and vascular species, in contrast to the plant composition for Fig. 20, which also contains shrubs and trees. Table 11 summarizes the plant proportions for all plots, whereby the control plot is comprised of lichens (average 65.7%) and vasculars (average 34.3%). It can be observed that the photosynthetic rate does not increase as quickly as seen in PP1 (Fig. 20) for the low light levels.

At 300 μmol/m^2/s of PAR, GPP is approximately 1 μmol/m^2/s, whereas for the same light level in Fig. 20 it is 4.2 μmol/m^2/s. The observed light levels do not reach beyond 1500 μmol/m^2/s and at such levels, maximum GPP remains relatively low at 4 μmol/m^2/s.

Table 11. Plant cover proportions for manipulated plots on PP2. Values of over 100% represent multi-storey plant structure.

Control	**Moss**	**Lichen**	**Vascular**	**Bare**	**Total**	**Collar**
	0	73.5	26.5	0	100	A
	0	61.8	38.2	0	100	B
	0	61.8	38.2	0	100	C
No Lichens	**Moss**	**Lichen**	**Vascular**	**Bare**	**Total**	**Collar**
	29.4	8.8	0	61.8	100	A
	41.2	5.9	11.8	41.2	100	B
	29.4	8.8	61.8	0	100	C
No Moss	**Moss**	**Lichen**	**Vascular**	**Bare**	**Total**	**Collar**
	0	38.2	41.2	20.6	100	A
	0	35.3	47.1	17.6	100	B
	0	82.4	5.9	11.8	100	C
No Vasculars	**Moss**	**Lichen**	**Vascular**	**Bare**	**Total**	**Collar**
	11.8	79.4	2.9	8.8	102.9	A
	14.7	73.5	2.9	11.8	102.9	B
	14.7	97.1	0	0	111.8	C

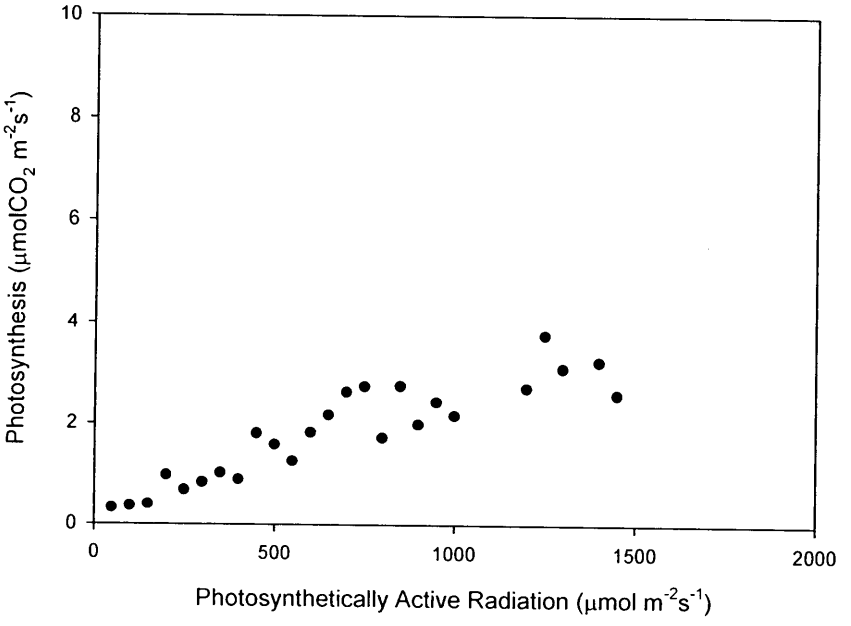

Figure 23. Light response curves from the control polygon at PP2 from 2009. This curve represents an average from three sampled collars that were chosen to have very similar plant proportions.

The manipulated plots are shown in Fig. 24 a-d, while Table 12 shows proportionate differences in mean GPP amongst all manipulated plots as well as mean GPP for each manipulated plot (shaded cells). Fig 24a shows the plots where all vascular vegetation has been removed, including cloudberry. The drastic difference from the control plot can be observed as the photosynthetic rate has significantly diminished to very low values at all light levels, as its GPP is only 15% of that for the control plot (Table 12). There is a very slight increase in GPP from completely dark chamber to when light levels have increased to their maximum. At the highest value, GPP does not increase beyond 1.5 μmol/m^2/s. Fig. 24b shows a light response curve for a plot where all moss has been removed but all other vegetation groups are present. The curve looks very similar to the control curve, whereby GPP gradually increases with PPFD and levels off with a maximum GPP at approximately 4 μmol/m^2/s. Collar C is the only series that lags behind in photosynthetic capacity, due to having significantly less vascular presence in

comparison to lichens (Table 10). However, the mean GPP of Fig 8b is 17% larger than that for the control plot (table 4), which can be attributed to a larger presence of vascular plants (Table 11). The plot with all lichens removed is shown in Fig 24c, which has very different patterns between the sampled collars. Collar C has the higher cloudberry plant cover, which is clearly seen in the significantly higher photosynthetic rate in comparison to the other two collars. Although the presence of other vascular plants is not very strong for Collar C, its photosynthetic capacity is higher than that for the control plot (Fig. 23). Lastly, the plot where all vegetation has been removed is shown in Fig 24d. From that, it is visible that there is insignificant photosynthesis (0.01 $\mu mol/m^2/s$, Table 12) and the data points hover around zero GPP at all light levels. In addition, Fig. 24d is very similar in photosynthetic capacity as Fig 24a, which contains no vascular plants. The strong influence of small vascular species can be attributed to their unexpectedly high leaf area index (LAI). The resultant LAI for Labrador tea and crowberry is 0.68 m^2/m^2 and 2.2 m^2/m^2, respectively. The crowberry leaves are densely packed on a single stem, explaining the significantly higher LAI and therefore strong GPP.

Table 12. Proportional difference of mean GPP (all three sampled collars averaged) for all manipulated plots. Non-shaded valued represent column headings divided by row headings.

Mean GPP	Control	No Lichens	No Moss	No Vasculars	No Vegetation
Control	1.68	0.85	1.17	0.15	0.01
No Lichens	1.18	1.43	1.38	0.18	0.01
No Moss	0.86	0.73	1.97	0.13	0.01
No Vasculars	6.64	5.64	7.76	0.25	0.05
No Vegetation	124.83	106.09	145.92	18.80	0.01

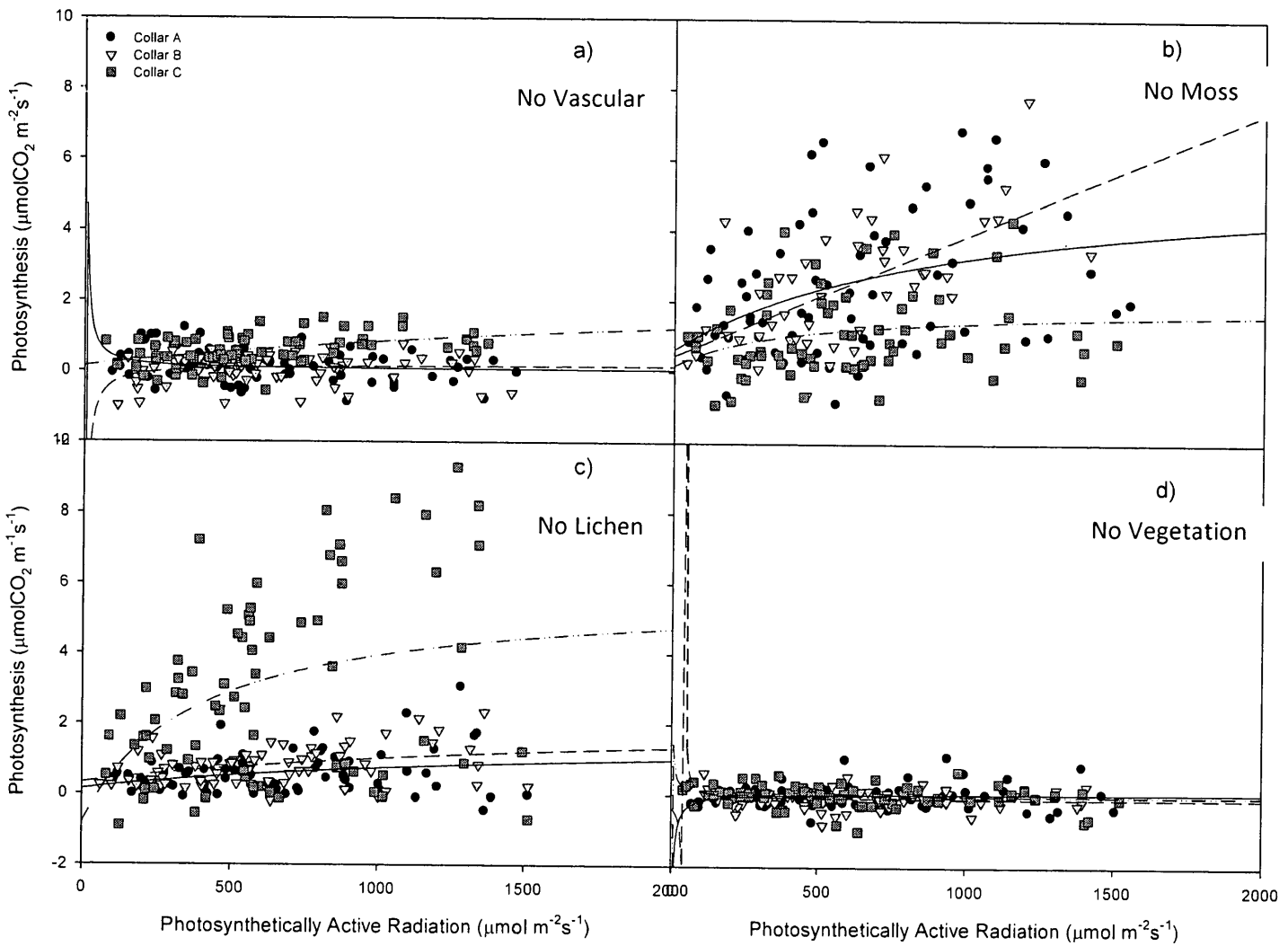

Fig. 24. Light response curves for manipulated plots from PP2.Rectagular hyperbola curve has been fitted on each collar scatter plot. a) all above ground vascular vegetation has been removed; b) all moss has been removed; c) all lichen has been removed; d) all above ground vegetation has been removed (vegetation cover is more than 100% due to lichen plants overlaying moss plants.

5.5 Discussion

5.5.1 Assimilation between Two Fully Functional Habitats

The difference in measured GPP between PP1 and PP2 is mostly a result of the scale of the two measurements and by extension, the composition of the sampled vegetation. PP1, measured with the EC system, is able to capture the influence of a large variety of plant species that includes shrubs and trees within the measured flux. The measured flux originates from sources that are within a 100 m radius, while the radius extends beyond 100 m under stable atmospheric conditions when mixing is suppressed. Conversely, measurements made on PP2 have been scaled down to individual plant groups as targets within the constraints of a 35x35 cm plot. The difference in the two locations and their respective vegetation cover is reflected in the measured photosynthetic rates. The measured flux at PP1 (Fig. 20) was found to be measurably stronger than that for PP2 (Fig. 23). Two reasons can be proposed to explain this difference with respect to vegetation cover. Firstly, the vascular presence in PP1 is nearly 50%, whereas the proportion of vascular plants in PP2 is 34%. Vasculars are better photosynthesizers than non-vascular species, which is reflected in a subdued carbon flux observed in PP2. Secondly, the vegetation cover measured in PP1 contains shrubs and trees, which have the capacity to stimulate photosynthesis to levels unrealistic for a non-vascular and small vascular shrub cover as in PP2. The 8% cover categorized as overstory in PP1 not only adds to the assimilation of carbon dioxide, but it also provides a secondary layer of vegetation that does not exist for PP2. The plant composition of PP2 is more reflective of inland HBL, which is higher in elevation and therefore drier; this favours the growth of non-vascular plants and small vascular shrubs over larger shrubs and trees. Thus, PP1 is suggested to be more representative of plant composition under a

warming climate if vascular plants, shrubs and trees become more dominant with the northward advancement of the Boreal forest.

Although GPP drops with decreasing vascular plant abundance, studies have shown that a decrease in bryophyte cover and a subsequent increase in vascular species resulted in a decline in the ecosystem's photosynthetic capacity (Moore, 1989; McNeil & Waddington 2003; Chivers *et al.,* 2009). Such trends were observed at low water table levels, which are associated with increased bryophyte mortality (Chivers *et al.,* 2009) which includes ER to assess the NEE, while the current study does not. In addition, early season peak for vascular plants due to quick accumulation of GDD resulted in less photosynthesis during the season (Chivers *et al.,* 2009). This is directly related to the observed temperature increase (Fig. 18) which has resulted in an earlier shift of spring occurrence (Gagnon & Gough, 2005). Permantier *et al.,* (2012) found that earlier spring conditions, a longer growing season and increasing temperatures do not result in increased carbon uptake, but rather a decrease or no change, suggesting that northern ecosystems behave as stronger sinks under cool conditions with short growing seasons and little respiration.

The results presented for PP1 suggest that woody shrubs and trees will enhance the carbon sink in northern peatlands through their increased leaf area and large stature. Some predict that dry conditions associated with warming temperatures will increase the abundance of woody species such as shrubs and trees, which will increase GPP (Chivers *et al.,* 2009). However, soil respiration will likely increase with dry soils due to increased aeration that does not limit microbial activity. Even under a scenario of increasing abundance of trees and shrubs, it is uncertain whether the rate of northward tree migration would be able to keep up with the rate of temperature increases (Callaghan *et al.,* 2004), which will stimulate respiration immediately. Also, paleoclimate modeling of the contributing forces to the warming experienced 6000 years

ago, found that the northward advancement of the treeline contributed 50% of the total warming (Foley *et al.,* 1994). The decreased albedo and increased snow bank formation is likely behind this enhanced positive feedback effect, which has the capacity to offset to some degree the increase in GPP brought on by increased woody species cover.

5.5.2 Weekly Assimilation of PP1 with Changing Phenological Cycles

The changing photosynthetic rate over the entire growing season in 2007 was captured (Fig. 21), as the weekly light response curves get larger and then decrease following the peak in Week 9. The increase in GPP can be attributed to increasing seasonal temperature regimes that result in the accumulation of GDD. Subsequently, accumulated GDD stimulate the phenological cycles of plant species. The phenology of cloudberry is reflected in the light response curves, reinforcing the strength of cloudberry influence. In addition, the phenological change in dwarf birch reaches peak biomass during Week 5, the same week which experiences rapid increase in GPP in comparison to earlier rates. Studies have found that cloudberry can reach GPP of up to 13 $\mu mol/m^2/s$ (Gauci *et al.,* 2009). Such values were reached from the EC measurements in PP1 (Fig. 21b), corresponding to the flux footprint of not only cloudberry but from a fully functional ecosystem. This indicates the potentially strong influence of cloudberry on the ecosystem, notably if it was more abundant than present. The maximum values are observed when cloudberry reaches full plant cover in its phenological cycle (Fig. 22), reinforcing its strong impact on the carbon flux. In addition, cloudberry prefers to grow over non-vasculars, maximizing the photosynthesis of the ecosystem by allowing other highly-photosynthesizing vascular plants to absorb sunlight.

As a result of increasing air temperatures, increase in the length of the growing season has been documented, which has resulted in observed increase in photosynthesis (Keeling *et al.,* 1996; Keyser *et al.,* 2000). This has occurred mainly in May and June, which are also the months most affected by decreasing sea ice in the Hudson Bay, as well as spring temperature anomalies (Randerson *et al.,* 1999; Gagnon & Gough, 2005). In this case, the weekly light response curves would shift towards earlier peak of photosynthetic rate due to a quicker accumulation of GDD. However, once the physiologically required GDD have been reached, it is unlikely that the plants, such as cloudberry, would continue to expand in area and biomass (Chivers *et al.,* 2009). A similar conclusion can be made with respect to dwarf birch or other vascular species which may simply shift their phenological cycle towards earlier leaf-out, rather than expand their phenological cycles over a longer period of time with a longer growing season. The increased GPP from the aforementioned studies, however, does not necessarily mean that the ecosystem has become a stronger net sink. The rate of respiration with increasing temperatures is often higher than for photosynthesis (Billings *et al.,* 1982; Silvola *et al.,* 1996; Zimov *et al.,* 1999; McGuire *et al.,* 2000). In particular, Permaniter *et al.,* (2011) found that increasing growing season length due to increased air temperatures resulted in enhanced photosynthesis, but respiration increased by either the same amount or by a larger amount. This resulted in the ecosystem being a net source or remained the same. In addition, increasing temperatures and decreasing moisture has been found to cause a shift in the ecosystem in Alaska from a net sink to a net source, mostly a result of increasing respiration in warm and dry soils (Oechel *et al.*, 1993; Callaghan *et al.*, 2004). Other studies have found that dry seasons resulted in a decrease in NEE (Vourlitis & Oechel, 1999; Griffis *et al.,* 2000; Kwon *et al.,* 2006). The manner in which climate

change will affect plant composition will not be uniform, as it will affect each microtopographic feature according to its present composition and hydrological regime.

5.5.3 Assimilation of Manipulated Plots

The strong carbon sequestering abilities by vascular plants is clearly illustrated by the difference in light response curves for manipulated plots (Fig. 24). Fig. 24a provides a glimpse of the GPP of an ecosystem that is only comprised of moss and lichen, which becomes almost negligible compared to other plots. The vascular species sampled have relatively high leaf area index (LAI), despite their apparent small size (Chen *et al.,* 2009). The leaves on crowberry, for example, are very tightly packed, producing an average LAI of 2.2 m^2/m^2. This unexpectedly large leaf area that is able to photosynthesize helps reinforce the strength of the photosynthetic rate observed in Fig. 24 for vascular plants. The vasculars removed from the manipulated plots include the shrub cloudberry which has been shown to be a strong photosynthesizer in comparison to other vascular species.

Although non-vascular species are not strong photosynthesizers, they are able to contribute to the carbon sink through other avenues. During snowmelt, mosses and lichens are the first plants to photosynthesize, as they do not leaf out every spring, but rather sustain slow growth throughout their lifetime without losing any biomass on an annual basis as vascular plants often do (Chivers *et al.,* 2009). This is also made possible by the sudden drop in albedo from snow to standing water during snowmelt (Lafleur, 2008); the high absorption of energy allows for the non-vascular plants to photosynthesize with little respiration to offset the GPP due to persistent cold soils. During winter, the flat and homogenous land cover of mosses and lichens

will allow for snow erosion by high subarctic winds, creating nearly bare ground conditions, but a thin layer enough to keep the energy away from the ecosystem due to high albedo (Lafleur, 2008). The thin layer of snow allows the ground to completely freeze over during winter and lose enough energy to sustain permafrost conditions for a longer period of time into the spring season. The complete freeze over in winter is imperative, as an extreme winter warming event in Scandinavia resulted in reduced carbon sequestration the following two seasons (Backhorst *et al.*, 2012). Thus, an isolated event that occurs for a short period of time has the potential to affect the ecosystem for numerous seasons thereafter.

In addition to stature-related advantaged of non-vascular plants, mosses are able to modify the soil they grow in to favour their own existence. The litter of moss contains phenolics which inhibit microbial peat decomposition (Verhoeven & Liefeld, 1997). The peat-forming moss Sphagnum is the dominant litter contributor for peat, emphasizing its importance to the maintenance of the ecosystem. It is also able to create an advantageous environment by creating acidic soils and low nutrient conditions, which often occur in continually saturated soil conditions (van Breeman, 1995). Since it is resistant to decomposition, respiration rates for such moss and lichen dominated ecosystems is generally low in comparison to the fast-decomposing vascular plants.

5.6 Conclusion

The type of vegetation present in an ecosystem does not only establish its carbon dynamics but is a key determinant of local and regional weather patterns through the partitioning of energy into heat, water vapour and warming the ground (Chapin *et al.,* 2000). The effect that

the energy balance partitioning has on the landscape can be seen in the melting of the permafrost as a result of increasing ground heat flux due to warmer surface and air temperatures. This, in turn, alters the hydrological regimes and drainage properties of vast tundra areas, thereby affecting the vegetation structure and atmospheric patterns (Hobbie *et al.,* 2000; Rouse, 2000). The carbon dynamics of northern wetlands are highly dependent on the above properties, reflected in different vegetation structures.

The photosynthetic flux of PP1, composed of non-vascular and vascular plants, shrubs and trees had significantly higher rates than the non-vascular and vascular dominated PP2. The latter is located on a peat polygon top which is drier than an ice-wedge peat plateau, as in PP1. This indicates a strong hydrological link to current and future carbon sequestration rates, whereby plant composition change could play both a negative and a positive role. The assimilation rates were shown to differ greatly amongst different types of vegetation groups growing on the peat plateau. Vascular species photosynthesized at a more efficient rate for a given light level than non-vascular plants. The shrub cloudberry was found to have stronger GPP than other vascular plants, making it an important contributor to the carbon sink. Its late leaf-out and short phenological cycle may constrain its photosynthesizing time, but during growth and maturity its influence is important which can be observed through the weekly progression of light response curves.

Since the geographical distribution of vegetation is mainly governed by latitudinal temperature gradients as well as moisture availability (Walker, 2000), it is often presumed that vascular vegetation will increase in size and abundance under a warming climate (Briffa *et al.,* 1995; Berg *et al.,* 2009). However, there are physiological and chemical advantages to sustain an ecosystem dominated by mosses and lichens, which photosynthesize early in the season while

other plants are still dormant; they allow for deep freeze of peat soils in winter due to less snow cover; mosses create structural support in soils that slow decomposition rates, thereby preserving peat soils. An increase in woody plants such as shrubs and trees will have a physical disadvantage through the creation of snow banks and decreased albedo. Thus, a balance is still necessary between the presence of vascular and woody species, and non-vascular species, where the latter inhibits decomposition but the former promote high rates of GPP.

6.0 SUMMARY AND CONCLUSIONS

6.1 Goals and Methods

The goal of this research was to quantify the influence of Hudson Bay on the carbon dynamics of the Hudson Bay Lowlands and to assess how the vegetation cover may respond to a changing climate and what the implications of this vegetation cover would be on carbon and water budgets. Carbon dioxide and energy balance measurements were taken during the 2007 Arcticnet Theme 3.2 campaign from May 30 to September 18 at an elevated peat plateau near Churchill, MB. The fast-response eddy covariance were analyzed using LI-COR's EddyPro 4.1.0 processing software. An addition set of data were collected at an adjacent peat plateau during the 2009 growing season with the use of gas chamber CO_2 measurements on manipulated plots, thus targeting the photosynthetic rates of specific plant groups. Differences in meteorological conditions between the two years are not expected to result in differences in the carbon flux, as the 2009 experiments were controlled over varying light levels. A detailed plant cover dataset was obtained during the 2012 field season during peak biomass, to quantify the presence of different plant groups.

6.2 Summary of Results – Chapter 4

During the 2007 study period, the study location was found to be a strong sink for CO_2 throughout the growing season and into September, by sequestering a total of 26.96 $\mu mol/m^2/s$, when annual respiration rates are included. The meteorological conditions between onshore and

offshore wind regimes were significantly different, as temperature was 4.15 °C higher for offshore on average during the season. The energy balance differed as well, as offshore regimes were characterized by higher Q_G, higher Q_E and lower Q_H when all were normalized by Q*. These differences, also found by Rouse and Bello (1985) were reflected in the CO_2 flux and its partitioning between the two regimes. The onshore regimes were consistently characterized by strong carbon sequestration rates for all months of the season, with a seasonal average of -3 $\mu mol/m^2/s$, which is 27 % stronger than the values for offshore (-2.2 $\mu mol/m^2/s$). Due to offshore's constantly higher temperatures, ER was always higher for that wind regime. Although offshore GPP rates were higher when normalized to PAR, ER/PAR was significantly higher, thereby reducing the offshore GPP influence in the carbon sequestration process. However, when normalized to temperature, onshore GPP is stronger, which is associated with more frequent clear sky conditions when winds originate from over Hudson Bay, resulting in high PAR conditions that allow for higher rates of GPP. Although under a warming climate is it expected that the sea-breeze effect will strengthen as a result of increasing land-surface warming as opposed to sea-surface warming and thus producing more onshore winds, observed data indicates otherwise. This suggests that increasing global air temperature as a result of increasing greenhouse gas emissions have had a measurable influence on large scale synoptic events that favour the production of offshore regimes. This proposition requires further investigation, possibly through the application of a North American Regional Reanalysis dataset. Thus, the presence of ice on Hudson Bay and cold open water help create more stable atmospheric conditions associated with high pressure systems, which has a profound effect on the carbon dynamics of the adjacent HBL.

6.3 Summary of Results – Chapter 5

The photosynthesis light response curves revealed large differences in the rate of carbon sequestration in accordance with different plant cover. It was found that the peat plateau had higher rate of photosynthesis for a given light level than the polygon top. The peat plateau is comprised of small vascular and non-vascular plants, in addition to shrubs and scattered trees, whereas the polygon top is mainly comprised of small vascular and non-vascular species, associated with well-drained environments. In addition, the manipulated plots showed that when vascular species were removed, the photosynthetic rate becomes almost negligible. In addition, the herb cloudberry plays an integral role in the strong photosynthetic uptake within peat plateau environments. Its presence notably increased the carbon sequestration rate, whereas other vascular plants did not have such a significant influence. Although the presence of vascular plants within an environment increases the rate of photosynthesis, there needs to be a balance between vascular and non-vascular species. The latter are able to photosynthesize early in the season when other plants are still dormant. In addition, mosses are able to modify the chemistry of the soil, thus favouring their presence and inhibiting decomposition through structural support. This is important for the maintenance of peatlands, which may become carbon sources under increasing decomposition rates.

6.4 Synthesis and Future Studies

The dynamic interaction between atmospheric, physiological and terrain factors has to be considered when assessing the role peatlands play in the global carbon budget. The positive

feedback processes related to the warming of the atmosphere are closely related to the plant composition and hydrological regimes of northern environments. Small plant stature often results in evenly and completely snow-covered ground, which maintains a high albedo and low energy regime. Taller shrubs and trees remain uncovered and reduce the albedo of the ecosystem, resulting in the absorption of more energy. The hydrological regime within peatland environments is an important factor in carbon emissions. Peatlands are maintained through the preservation of high water table, which creates anaerobic soil conditions, consequently favouring organic matter accumulation. The advective influence of Hudson Bay is observed through the comparison of onshore and offshore wind regimes. The former regimes favour the maintenance of arctic-like conditions through cool air temperatures, and subdued ground heat flux and evaporation. This helps maintain high water table and prolonged permafrost conditions, inhibiting the rate of carbon emissions. The presence of non-vascular vegetation that is more difficult to decompose than vascular vegetation helps maintain and promoted peat accumulation, despite the fact that vascular plants are better photosynthesizers. Thus, a fine balance has to be maintained among the hydrology, vegetation and atmospheric dynamics in order to preserve northern wetlands as peat-accumulating ecosystems, thereby offsetting growing global carbon emissions.

In order to build upon the presented analyses, other key measurements can be added to the methods. A detailed dataset of the seasonal variation of the water table would reveal the active layer growth and contraction under shifting wind regimes, temperatures, and precipitation patterns. This, coupled with eddy covariance flux data, will reveal how changing water table is related to the carbon dynamics of a northern wetland. In addition, placing an eddy covariance system on a different peatland ecosystem, such as a fen, would provide comparison data on the

internal workings of different ecosystems present within the Hudson Bay Lowlands. Multi-year analysis will greatly improve the characterization of Hudson Bay's influence on the surround ecosystems, as ice cover, temperature, moisture and growing season length will influence on the carbon flux over the growing season.

7.0 REFERENCES

ACIA (2005) *Arctic Climate Impact Assessment*. Cambridge University Press. New York.

Armentano TV, Menges ES (1986) Patterns of change in the carbon balance of organic soil-wetlands of the temperate zone. *Journal of Ecology*, **74**:755-774.

Arya, SP (2001). *Introduction to Micrometeoroly*. San Diego: Academic Press.

Aubinet M, Gerelle A, Ibrom A et al (2000) Estimates of the annual net carbon and water exchanges of forests: The EUROFLUX methodology. *Advances in Ecological Research*, **30**, 113-175.

Aubry LM, Rockwell RF, Cooch EG, et al (2013) Climate change, phenology, and habitat degradation: drivers of gosling body condition and juvenile survival in lesser snow geese. *Global Change Biology*, **19**, 149-160.

Aurela M, Laurila T, Tuovinen JP (2002) Annual CO_2 balance of a subarctic fen in northern Europe: Importance of the wintertime efflux. *Journal of Geophysical Research*, **107**, 17-1 – 17-12.

Aurela M, Laurila T, Tuovinen JP (2004) The timing of snow melt controls the annual CO_2 balance in a subarctic fen. *Geophysical Research Letters*, **31**, GL20315.

Aurela M, Riutta T, Laurila T et al (2007) CO2 exchange of a sedge fen in southern Finland – the impact of a drought period. *Tellus*, **59B**, 826-837.

Baldocchi D, Falge E, Gu L, et al (2001) FLUXNET: A new tool to study temporal and spatial variability of ecosystem-scale carbon dioxide, water vapour, and energy flux densities. Bulletin of the American Meteorological Society, 82, 2415-2434.

Baldocchi DD (2003) Assessing the eddy covariance technique for evaluating carbon dioxide exchange rates for ecosystems: past, present and future. *Global Change Biology*, **9**, 479-492.

Barber DG, Asplin MG, Raddatz RL et al (2012) Change and variability in sea ice during the 2007-2008 Canadian International Polar Year program. *Climatic Change*, **115**, 115-133.

Bello R, Smith JD (1990) The effect of weather variability on the energy balance of a lake in the Hudson Bay. *Arctic and Alpine Research*, **22**, 98-107.

Berg FE, Hillman KM, Dial R, DeRuwe A (2009) Recent woody invasions of wetlands on the Kenai Peninsula Lowlands, south-central Alaska: a major regime shift after 18000 years wet Sphagnum-sedge peat recruitment. *Canadian Journal of Forest Research*, **39**, 2033-2046.

Billings WD, Luken JO, Mortensen DA, Peterson KM (1982) Arctic tundra: A source or a sink for atmospheric carbon dioxide in a changing environment? *Oecologia*, **53**, 7-11.

Bonan, G (2008) *Ecological Climatology: Concepts and Applications*. New York: Cambridge.

Borges AV, Delille B, Frankignoulle M (2005) Budgeting sinks and sources of CO_2 in the coastal ocean: Diversity of ecosystem counts. *Geophysical Research Letters*, **32**.

Briffa KR, Jones PD, Schewingruber FH, Shiyatov SG, Cook ER (1995) Unusual twentieth-century summer warmth in a 1000-year temperature record from Siberia. *Nature*, **376**, 156-159.

Bryson RA (1966) Air masses, streamlines, and the Boreal Forest. *Geographic Bulletin*, **8**, 228-269.

Buber J, Crill P, Mosedale A et al (2003) Peatland responses to varying interannual moisture conditions as measured by automatic CO_2 chambers. *Global Biogeochemical Cycles*, **17**, GB1946.

Burba G, Anderson D (2010) *A Brief Practical Guide to Eddy Covariance Flux Measurements*.LI-COR Inc, Lincoln, Nebraska.

Burton KL, Rouse WR, Boudreau LD (1996) Factors affecting the summer carbon dioxide budget of subarctic wetland tundra. *Climate Research*, **6**:203-213.

Burton KL, Rouse WR, Boudreau LD (1996) Factors affecting the summer carbon dioxide budget of subarctic wetland tundra. *Climate Research*, **6**:203-213.

Cai T, Flanagan LB, Syed KH (2010) Warmer and drier conditions stimulate respiration more than photosynthesis in a boreal peatland ecosystem: Analysis of automatic chambers and eddy covariance measurements. *Plant, Cell and Environment*, **33**, 394-407.

Cai W, Dai J, Wang Y (2006) Air sea exchange of carbon dioxide in ocean margins: A province-based synthesis. *Geophysical Research Letters*, **33**.

Callaghan TV, Bergholm F, Christensen TR, Jonasson C, Kokfelt C, Johansson M (2010) A new climate era in the sub-Arctic: accelerating climate changes and multiple impacts. *Geophysical Research Letters*, **37**, L14705.

Callaghan TV, Bjorn LO, Chernov Y et al (2004) Effects of changes in climate on landscape and regional processes, and feedbacks to the climate system. *Ambio*, **33**, 459-468.

Cess RD, Potter GL, Zhang MH et al. (1991) Interpretation of snow-climate feedback as produced by 17 general circulation models. *Science*, **253**, 888-892.

Chapin III FS, McGuire AD, Randerson J, et al (2000) Arctic and Boreal ecosystems of western North America as components of the climate system. *Global Change Biology*, **6**, 211-223.

Chapin III FS, Strum M, Serreze MC, et al (2005) Role of land-surface changes in Arctic summer warming. *Science*, **310**, 657-660.

Chapman WL, Walsh JE (1993) Recent variations of sea ice and air temperature in high latitudes. *Bulletin of the American Meteorological Society*, **74**, 33-47.

Chen W, Li J, Zhang Y et al (2009) Relating biomass and leaf area index to non-destructive measurements in order to monitor changes in arctic vegetation. *Arctic*, **62**, 281-294.

Chivers MR, Turetsky MR, Waddington JM et al (2009) Effects of experimental water table and temperature manipulations on ecosystem CO_2 fluxes in an Alaskan rich fen. *Ecosystems*, **12**, 1329-1342.

Ciais P, Peylin P, Bousquet P (2000) Regional biospheric carbon fluxes as inferred from atmospheric CO_2 measurements. *Ecological Applications*, **10**, 1574-1589.

Clymo RS, Turunen J, Tolonen K (1998) Carbon accumulation in peatland. *OIKOS*, **81**, 368-388.

Corradi C, Kolle O, Walter K, Zimov SA, Schulze ED (2005) Carbon dioxide and methane exchange of a north-yeast Siberian tussock tundra. *Global Change Biology*, **11**, 1910-1925.

Danielson EW (1969) MSc Thesis: *The Surface Heat Budget of Hudson Bay*. Montreal: McGill University.

Danielson Jr. ER (1971) Hudson Bay ice conditions. *Arctic*, **24**, 90-107.

Derocher AE, Lunn NJ, Stirling I (2004) Polar bears in a warming climate. *Integrative and Comparative Biology*, **43**, 163-176.

Desjardins RL, MacPherson JI, Schuepp PH, Hayhoe HN (1994) Airborne flux measurements of CO_2, sensible and latent heat over the Hudson Bay Lowland. *Journal of Geophysical Research*, **99**:1551-1561.

Desjardins RL, MacPherson JI, Schuepp PH, Karanja F (1989) An evaluation of aircraft flux measurements of CO_2, water vapour and sensible heat. *Boundary-Layer Meteorology*, **11**, 147-154.

Dorrepaal E, Toet S, van Logtestijn RSP et al (2009) Carbon respiration from subsurface peat accelerated by climate warming in the subarctic. *Nature*, **460**, 616-620.

Dredge LA, Mott RJ (2003) Holocene pollen records and peatland development, northeastern Manitoba. Geographic Phisique et Quarternaire, 57, 7-19.

Eaton AK, Rouse WR, Lafleur PM, Marsh, P, Blanken PD (2001) Surface energy balance of the western and central Canadian subarctic: variations in the energy balance among five major terrain types. *Journal of Climate*, **14**, 3692-3703.

Else BGT, Papakyriakou TN, Granskog MA, Yackel JJ (2008) Observations of sea surface fCO_2 distributions and estimated air-sea CO_2 fluxes in the Hudson Bay region (Canada) during the open water season. *Journal of Geophysical Research*, **113**:1-12.

Environment Canada (2013) National Climate Data and Information Archive. Churchill Airport, 1953-2012.

Etkin DA (1991) Break-up in Hudson Bay: Its sensitivity to air temperatures and implications for climate warming. *Climatological Bulletin*, **25**:21-34.

Eugster W, Rouse WR, Pielke Sr RA, McFadden JP, Baldocchi DD, Kittel TGF, Chapin III FS, Liston GE, Vidale PL, Vaganov E, Chambers S (2000) Land-atmosphere energy exchange in Arctic tundra and boreal forest: available data and feedbacks to climate. *Global Change Biology*, **6**:84-115.

Euskirchen ES, McGuire AD, Kicklighter DW et al (2006) Importance of recent shifts in soil thermal dynamics on growing season length, productivity, and carbon sequestration in terrestrial high-latitude ecosystems. *Global Change Biology*, **12**, 731-750.

Falge E, Baldocchi D, Olson R et al (2001) Gap filling strategies for defensible annual sums of net ecosystem exchange. *Agricultural and Forest Meteorology*, **107**, 43-69.

Finn D, Lamb B, Leclerc MY, Horst TW (1996) Experimental evaluation of analytical and Langrarian surface-layer flux footprint models. *Boundary-Layer Meteorology*, **80**, 283-308.

Finnigan JJ, Clement R, Mahli T, Leuning R, Cleugh HA (2003) A re-evaluation of long term flux measurement techniques: Part 1: Averaging and coordinate rotation. *Boundary-Layer Meteorology*, **107**, 1-48.

Foken T (2006) 50 years of the Monin-Obukhov similarity theory.*Boundary-Layer Meteorology*, **119**, 431-447.

Foken T (2008) *Micro-meteorology*. Berlin: Springer.

Foken T, Gockede M, Mauder M, Mahrt L, Amiro BD, Munger JW (2004) Post-field quality control, in: *Handbook of Micrometeorology*. Kluwer Academic Publishers, Dordrecht.

Foken T, Oncley SP (1995) Results of the workshop 'Instrumental and methodical problems of land surface flux measurements. *Bulletin of the American Meteorological Society*, **76**, 1191-1193.

Foken T, Wichura B (1996) Tools for quality assessment of surface-based flux measurements. *Agricultural and Forest Meteorology*, **78**, 83-105.

Foley JA, Kutzback JE, Cooe MT, Levis S (1994) Feedbacks between climate and boreal forest during the Holocene epoch. *Nature*, **371**, 52-54.

Gagnon AS, Gough WL (2005) Trends in the dates of ice freeze-up and breakup over Hudson Bay, Canada. *Arctic*, **58**, 370-382.

Gaines SD, Denny MW (1993) The largest, smallest, highest, lowest, longest and shortest – extremes in ecology. *Ecology*, **74**, 1677-1692.

Garratt JR (1992) *The Atmospheric Boundary Layer*. Cambridge: Cambridge University Press.

Gauci R, Otrysko B, Catford JG, Lapointe L (2009) Carbon allocation during fruiting in Rubus chamaemorus. *Annals of Botany*, **104**, 703-713.

Gockede M, Rebmann C, Foken T (2004) A combination of quality assessment tools for eddy covariance measurements with footprint modeling for the characterization of complex sites. *Agricultural and Forest Meteorology*, **127**, 175-188.

Gorham E (1991) Northern Peatlands: Role in the carbon cycle and probable responses to climatic warming. *Ecological Applications*, **1**, 182-195.

Gough WA, Cornwel AR, Tsuji LJS (2004) Trends in seasonal sea ice in southwestern Hudson Bay. *Arctic*, **57**:299-305.

Gough WA, Leung A (2002) Nature and fate of Hudson Bay permafrost. *Regional Environmental Change*, **2**, 177-184.

Greenpeace (2007) Climate Change. Retrieved from <http://web.archive.org/web/20120114155032/http:/www.greenpeace.org/canada/en/campaigns/tarsands/archive/threats/climatechange/> on July 1, 2013.

Griffis TJ, Rouse WR, Waddington J M (2000). Interannual variability of net ecosystem CO_2 exchange at a subarctic fen. *Global Biogeochemical Cycles,* **14**, 1109–1121.

Groendahl L, Friborg T, Soegaard H (2007) Temperature and snow-melt controls on interannual variability in carbon exchange in the high Arctic. *Theoretical and Applied Climatology*, **88**, 111-125.

Grogan P, Chapin FS (2000) Initial effects of experimental warming on above- and belowground components of net ecosystem CO2 exchange in arctic tundra. *Oecologia*, **125**, 512-520.

Groisman PY, Koknaeva VV, Belokrylova TA, Karl TR (1991) Overcoming biases of precipitation: A history of the USSR experience. *Bulletin of the American Meteorological Society*, **72**, 1725-1733.

Hamilton JD, Kelly, CA, Rudd, JWM, Hesslein RH, Roulet NT (1994) Flux to the atmosphere of CH_4 and CO_2 from wetland ponds on the Hudson Bay lowlands (HBLs). *Journal of Geophysical Research*, **99**, 1495-1510.

Hare FK, Montgomery MR (1949a) Ice, open water, and winter climate in the eastern Arctic of North America: Part I. *Arctic*, **2**:78-89.

Hare FK, Montgomery MR (1949b) Ice, open water, and winter climate in the eastern Arctic of North America: Part II. *Arctic*, **2**:149-164.

Hayward PM, Clymo RD (1983) Profiles of water content and pore size in Sphagnum and peat, and their relation to peat bog ecology. *Proceedings of the Royal Society of London*, **215**, 299-325.

Heimann M, Reichstein M (2008) Terrestrial ecosystem carbon dynamics and climate feedbacks. *Nature*, **451**, 289-292.

Henry M (2011) Sea ice trends in Canada. *Statistics Canada – EnviroSats*, **5**, 3-13.

Hinzman LD, Bettez ND, Bolton WR et al (2005) Evidence and implications of recent climate change in northern Alaska and other arctic regions. *Climatic Change*, **75**, 251-298.

Hinzmann LD, Goering DJ, Kane DL (1998) A distributed thermal model for calculating soil temperature profiles and depth of thaw in permafrost regions. *Journal of Geophysical Research: Atmospheres*, **103**, 28975-28991.

Hobbie SE, Trumbore SE (2000) Controls over carbon storage and turnover in high-latitude soils. *Global Change Biology*, **6**, 196-210.

Hoccheim KP, Barber DG (2010) Atmospheric forcing of sea ice in Hudson Bay during the fall period, 1980-2005. *Journal of Geophysical Research*, **115**, JC5334.

Hoccheim KP, Lukovich JV, Barber DG (2011) Atmospheric forcing of sea ice in Hudson Bay during the spring period, 1980-2005. *Journal of Marine Systems*, **88**, 476-487.

Horst TW, Weil JC (1992) Footprint estimation for scalar flux measurements in the atmospheric surface-layer. *Boundary-Layer Meteorology*, **59**, 279-296.

Intergovernmental Panel on Climate Change [Field, C.B., V. Barros, T.F. Stocker, D. Qin, D.J. Dokken, K.L. Ebi, M.D. Mastrandrea, K.J. Mach, G.-K. Plattner, S.K. Allen, M. Tignor, and P.M. Midgley (eds.)]. Cambridge University Press, Cambridge, UK, and New York, NY, USA, 582 pp.

IPCC (2012) *Managing the Risks of Extreme Events and Disasters to Advance Climate Change Adaptation. A Special Report of Working Groups I and II of the*

Intergovernmental Panel on Climate Change [Field, C.B., V. Barros, T.F. Stocker, D. Qin, D.J. Dokken, K.L. Ebi, M.D. Mastrandrea, K.J. Mach, G.-K. Plattner, S.K. Allen, M. Tignor, and P.M. Midgley (eds.)]. Cambridge University Press, Cambridge, UK, and New York, NY, USA, 582 pp.

IPCC (2007) *Climate Change 2007: The Physical Science Basis. Contribution of Working Group I to the Fourth Assessment Report of the Intergovernmental Panel on Climate Change*. New York: Cambridge University Press.

Joiner DW, Lafleur PM, McCaughey JH, Bartlett PA (1999) Interannual variability in carbon dioxide exchanges at a boreal wetland in the BOREAS northern study area. *Journal of Geophysical Research*, **104**, 27663-27672.

Kaimal JC, Finnigan J (1994) *Atmospheric boundary layer flows: their structure and measurement*. Oxford, New York, 289 pp.

Keeling CD, Chin JPS, Whorf TP (1996) Increased activity of northern vegetation inferred from atmospheric CO2 measurements. *Nature*, **382**, 146-149.

Kellner E (2001) Surface energy fluxes and control of evapotranspiration from a Swedish *Sphagnum* mire. *Agricultural and Forest Meteorology*, **110**, 101-123.

Keyser AR, Kimball JS, Nemani RR, Running SW (2000) Simulating the effects of climatic change on the carbon balance of North American high-latitude forests. *Global Change Biology*, **6**, 185-195.

Kwon HJ, Oechel WC, Zulueta RC, Hastings SJ (2006) Effects of climate variability on carbon sequestration among adjacent wet sedge tundra and moist tundra ecosystems. *Journal of Geophysical Research*, **111**, 1-18.

Lafleur P, Rouse WR, Hardill SG (1987) Components of the surface radiation balance of Subarctic wetland terrain units during the snow-free season. *Arctic and Alpine Research*, **19**:53-63.

Lafleur PM, Humphreys ER (2007) Spring warming and carbon dioxide exchange over low Arctic tundra in central Canada. *Global Change Biology*, **14**, 740-756.

Lafleur PM, Humphreys ER, St. Louis VL, and others (2012) Variation in peak growing season net ecosystem production across the Canadian Arctic. *Environmental Science and Ecology*, **46**, 7971-7977.

Lafleur PM, McCaughey JH, Joiner DW et al (1997) Seasonal trends in energy, water, and carbon dioxide fluxes at a northern boreal wetland. *Journal of Geophysical Research – Atmospheres*, **102**-29009-29020.

Lafleur PM, Roulet NT (1992) A comparison of evaporation rates frpm two fens of the Hudson Bay Lowland. *Aquatic Botany*, **44**, 59-69.

Law B, Verma S (2004) Introduction, in: *Handbook of Mictometeorology*. Kluwer Academic Publishers, Dordrecht.

Lee XH, Finnigan J, U KTP (2004) Coordinate systems and flux bias error, in: *Handbook of Mictometeorology*. Kluwer Academic Publishers, Dordrecht.

Lloyd J, Taylor JA (1994) On the temperature dependence of soil respiration. *Functional Ecology*, **8**, 315-323.

Lund M, Lafleur PM, Roulet NT et al (2010) Variability in exchange of CO_2 across 12 northern peatland and tundra sites. *Global Change Biology*, **16**, 2436-2448.

Luo Y (2005) Terrestrial carbon-cycle feedback to climate warming. *Annual Review of Ecology, Evolution and Systematics*, **38**, 683-712.

Mauder M, Foken T (2006) Impact of post-field data processing on eddy covariance flux estimates and energy balance closure. *Meteorologische Zeitschrift*, **15**, 597-609.

McGuire AD, Clein JS, Melillo JM et al (2000) Modelling carbon responses of tundra ecosystems to historial and projected climate: sensitivity of pan-Arctic carbon storage to temporal and spatial variation in climate. *Global Change Biology*, **6**, 141-159.

McKane RB, Rastetter EB, Shaver GR et al (1997) Climatic effects on tundra carbon storage inferred from experimental data and a model. *Ecology*, **78**, 1170-1187.

McMillen RT (1988) An eddy correlation technique with extended applicability to non-simple terrain. *Boundary-Layer Meteorology*, **43**, 231-245.

Moncrieff JB, Clement R, Finnigan J, Meyers T (2004) Averaging, detrending and filtering of eddy covariance time series, in: *Handbook of Mictometeorology*. Kluwer Academic Publishers, Dordrecht.

Moncrieff JB, Malhi Y, Leuning R (1996) The propagation of errors in long-term measurements of land-atmosphere fluxes of carbon and water. *Global Change Biology*, **2**, 231-240.

Moncrieff JB, Massheder JM, DeBruin H et al (1997) A system to measure fluxes of momentum, sensible heat, water vapour and carbon dioxide. *Journal of Hydrology*, **188-189**, 589-611.

Monin AS, ObukhovAM (1954) Basic laws of turbulent mixing in the atmosphere near the ground. *Trudy. Geofiz. Inst. AN SSSR*, **24**(151), 163-187.

Monteith JL, Unsworth MH (1990) *Principles of Environmental Physics*. Elsevier, New York.

Moore CJ (1986) Frequency response corrections for eddy correlation systems. *Boundary-Layer Meteorology*, **37**, 17-35.

Moore TR, Bubier JL, Bledzky L (2007) Litter decomposition in temperate peatland ecosystems: the effect of substrate and site. *Ecosystems*, **10**, 949-963.

Moore TR, Knowles R (1989) The influence of water table levels on methane and carbon dioxide emissions from peatland soils. *Canadian Journal of Soil Science*, **69**, 33-38.

Myneni RB, Keeling CD, Tucker CJ et al (1997) Increased plant growth in the northern high latitudes from 1981-1991. *Nature*, **386**, 698-702.

Nelson FE, Shiklomanov NI, Mueller GR, et al (1997) Estimating active-layer thickness over a large region: Kuparuk River Basin, Alaska, USA. *Arctic and Alpine Research*, **29**, 367-378.

Nykanen H, Alm J, Lang K et al (1995) Emissions of CH_4, N_2O and CO_2 from a virgin fen and a fen drained for grassland in Finland. *Journal of Biogeography*, **22**, 351-357.

Oechel WC, Collins NJ (1976) Comparative CO2 exchange patterns in mosses from two tundra habitats at Barrow, Alaska. *Canadian Journal of Botany*, **54**, 1355-1369.

Oke TR (1987). *Boundary Layer Climates*. London: Routledge.

Parkinson CL, Cavalieri DJ, Gloersen P, Zwally HJ, Comisso JC (1999) Arctic sea ice extents, areas and trends. *Journal of Geophysical Research*, **104C**:20837-20856.

Parmentier FJW, van der Molen MK, van Huissteden J et al (2011) Longer growing seasons do not appear to increase net carbon uptake in Northeastern Siberian tundra. *Journal of Geophysical Research: Biogeosciences,* **116**, JG1653.

Pasquill F (1972) Some aspects of boundary layer description. *Quarterly Journal of the Royal Meteorological Society*, **98**, 469-494.

Randerson JT, Field CB, Fung IY, Tans PP (1999) Increases in early season net ecosystem uptake explain the seasonal cycle of atmospheric CO_2 at high northern latitudes. *Geophysical Research Letters*, **26**, 2765-2768.

Rayner PJ, Scholze M, Knorr W et al (2005). Two decades of terrestrial carbon fluxes from a carbon cucle data assimilation system (CCDAS). *Global Biogeochemical Cycles*, **19**, GB2026.

Reichstein M, Falge E, Baldocchi D et al (2005) On the separation of net ecosystem exchange into assimilation and ecosystem respiration: review and improved algorithm. *Global Change Biology*, **11**, 1424-1439.

Reynolds O (1895) On the dynamical theory of incompressible viscous fluids and the determination of the criterion. *Philosophical Transactions of the Royal Society*, **A186,** 123-164.

Richardson LF (1920) The supply of energy from and to atmospheric eddies. *Proceedings of the Royal Society of London. Series A, Containing Papers of a Mathematical and Physical Character*, **97**(686), 354-373.

Rizzo R, Wiken E (1992) Assessing the sensitivity of Canada's ecosystems to climatic change. *Climatic Change*, **21**, 35-55.

Roulet N (1990) Focus: aspect s of the physical geography of wetlands. *The Canadian Geographer*, **34**, 79-88.

Roulet NT, Crill PM, Comer NT, Dove A, Bourbonniere RA (1997) CO_2 and CH_4 flux between a boreal beaver pond and the atmosphere. *Journal of Geophysical Research*, **102,D12**:29313-29319.

Roulet NT, Lafleur PM, Richard PJH, Moore TR, Humphreys ER, Bubier J (2007) Contemporary carbon balance and late Holocene carbon accumulation in a northern peatland. *Global Change Biology*, **13**, 397-411.

Rouse W. R. and R.L. Bello (1985). Impact of Hudson Bay on the energy balance in the Hudson Bay Lowlands and the potential for climatic modification. *Atmosphere-Ocean*, **23**: 375-392.

Rouse WR (1991) Impacts of Hudson Bay on the terrestrial climate of the Hudson Bay Lowlands. *Arctic and Alpine Research*, **23**:24-30.

Rouse WR (2000) The energy and water balance of high-latitude wetlands: control and extrapolation. *Global Change Biology*, **6**, 59-68.

Rouse WR, Bello RL, D'Sourza A, et al, (2002) The annual carbon budget for fen and forest in a wetland at Arctic treeline. *Arctic*, **55**, 229-237.

Rouse WR, Carlson DW, Weick EJ (1992) Impacts of summer warming on the energy and water balance of wetland tundra. *Climatic Change*, **22**, 305-326.

Rouse WR, Hardill SG, Lafleur P (1987) Energy balance in the coastal environment of James Bay and Hudsob Bay during the growing season. *Journal of Climatology*, **7**, 165-179.

Sakai R, Fitzjarrald D, Moore KE (2001) Importance of low-frequency contributions to eddy fluxes observed over rough surfaces. *Journal of Applied Meteorology*, **87**, 179-200.

Scheupp PH, Lecrec MY, MacPherson JI, Desjadins RL (1990) Footprint prediction of scalar fluxes from analytical solutions of the diffusion equation. *Boundary-Layer Meteorology*, **50**, 355-373.

Schlesinger ME, Mitchell JFB (1987) Climate model simulations of the equilibrium climatic response to increased carbon dioxide. *Reviews of Geophysics*, **25**:760-798.

Schmid HP (1997) Experimental design for flux measurements: Matching scales of observations and fluxes. *Agricultural and Forest Meteorology*, **87**, 179-200.

Schmid HP (2002) Footprint modeling for vegetation-atmosphere exchange studies: A review and perspective. *Agricultural and Forest Meteorology*, **113**, 159-183.

Schmid HP, Oke TR (1990) A model to estimate the source area contributing to turbulent exchange in the surface layer over patchy terrain. *Quarterly Journal of the Royal Meteorological Society*, **116**, 965-988.

Schreader C (1995) Summertime carbon dioxide exchange over a subarctic sedge wetland. M.Sc. thesis. Department of Geography, McMaster University, Hamilton, Ontario, 101 pp.

Schuur EAG, Bockheim J, Canadell JP, et al (2008) Vulnerability of permafrost carbon to climate change: implications for the global carbon cycle. *BioScience*, **58**, 701-714.

Serreze MC, Walsh JE, Chapin III FS et al (2000) Observational evidence of recent change in the northern high-latitude environment. *Climatic Change*, **45**, 159-207.

Shurpali NJ, Verma SB, Kim J, Askebauer TJ (1995) Carbon dioxide exchange in a peatland ecosystem. *Journal of Geophysical Research*, **100**, 14319-14326.

Silvola J, Alm J, Ahlholm U, Nykanen H, Martikainen PJ (1996) CO_2 fluxes from peat inn boreal mires under varying temperature and moisture conditions. *Journal of Ecology*, **84**, 219-228.

Smith DM (1998) Recent increase in the length of the melt season of perennial Arctic sea ice. *Geophysical Research Letters*, **25**:655-658.

Smith LC, MacDonald GM, Velichko AA, Beilman DW, Borisova OK, Kremenetski KV, Sheng Y (2004) Siberian peatlands a net carbon sink and global methane source since the early Holocene. *Science*, **303**, 353:356.

Stella GF, Stein S, Dixon TH, et al (2007) Observation of glacial isostatic adjustment in "stable" North America with GPS. *Geophysical Research Letters*, **34**, 1-6.

Swystun K (2011) *CO_2 exchange in a subarctic sedge fen in the Hudson Bay Lowland during two consecutive growing seasons*. M.Sc. thesis, Department of Environment and Geography, University of Manitoba, Winnipeg, Manitoba, 97 pp.

Tanner CB, Thurtell GW (1969) *Anemoclinometer measurements of Reynolds stress and heat transport in the atmospheric surface layer*. University of Wisconsin Tech. Report, 82 pp.

Tans PP, Fung IY, Takahashi T (1990) Observational constraints on the global atmospheric CO_2 budget. *Science*, **247**, 1431-1438.

Tarnocai C (2006) The effect of climate change on the carbon in Canadian peatlands. *Global and Planetary Change*, **53**, 222-232.

van Breeman N (1995) How Sphagnum bogs down other plants. *Trends in Ecology and Evolution*, **10**, 270-275.

Verhoeven JTA, Liefveld LM (1997) The ecological significance of organochemical compounds in *Sphagnum*. *Royal Botanical Society of Netherlands*, **46**, 117-130.

Vesala T, Kljun N, Rannik U, Rinne J, Sogachev A, Markkanen T, Sabelfeld K, Foken T, Lecrec MY (2008) Flux and concentration footprint modeling: State of the art. *Environmental Pollution*, **152**, 653-666.

Vitt DH, Wieder RK, Scott KD, Faller S (2009) Decomposition and peat accumulation in rich fens of boreal Alberta, Canada. *Ecosystems*, **12**, 260-373.

Vourlitis GL, Oechel WC (1999) Eddy covariance measurements of CO_2 and energy fluxes of an Alaska tussock tundra ecosystem. *Ecology*, **80**, 686-701.

Vourlitis GL, Oechel WC (1999) Eddy covariance measurements of CO_2 and energy fluxes of an Alaska tussock tundra ecosystem. *Ecology*, **80**, 686-701.

Waddington JM, Roulet NT (1996) Atmosphere-wetland carbon exchanges: Scale dependency of CO_2 and CH_4 exchange on the developmental topography of a peatland. *Global Biogeochemical Cycles*, **10**, 233-245.

Webb EK, Pearman GI, Leuning R (1980) Correction of flux measurements for density effects due to heat and water vapour transfer. *Quarterly Journal of Royal Meteorological Society*, **106**, 85-100.

Wilczak JM, Oncley SP, Stage SA (2001) Sonic anemometer tilt correction algorithms. *Boundary-Layer Meteorology*, **99**, 127-150.

Woo MK (2012) *Permafrost Hydrology*. Springer, London.

Woo MK, Lewkowicz AG, Rouse WR (1992) Response to the Canadian permafrost environment to climatic change. *Physical Geography*, **134**:287-317.

Zimov SA, Davidov SP, Zimova GM, et al (1999) Contribution of disturbance to high-latitude amplification of atmospheric CO_2. *Science*, **284**, 1973-1976.

Zimov SA, Davydov SP, Zimova GM et al (2006) Permafrost carbon: Stock and decomposability of a globally significant carbon pool. *Geophysical Research Letters*, **33**, L20502.